Project - Task
2301/D1 0100/00

Final Technical Report in the Subject

DAMAGE IN COMPOSITES AND OTHER ADVANCED MATERIALS TREATED BY PERCOLATION THEORY

Grant No. AFOSR - 89- 0374

by

R. Englman, Z. Jaeger and M. Murat

Soreq Nuclear Research Center

Yavne 81800, ISRAEL

Program Managers:

(1) **Dr. Spencer T. Wu**
Air Force Office of Scientific Research
Bolling Air Force Base, DC 20332-6448

(2) **Dr. Arnold H. Mayer**
Assistant for Research & Technology
Vehicle Subsystems Division
Flight Dynamics Directorate
Wright Laboratory
Wright-Patterson Air-Force Base
Ohio 45433 - 6553

UNCLASSIFIED

AFOSR-TR-95

0607

SECURITY CLASSIFICATION OF THIS PAGE

REPORT DOCUMENTA

1a. REPORT SECURITY CLASSIFICATION UNCLASSIFIED	1b. RE
2a. SECURITY CLASSIFICATION AUTHORITY	3. DISTRIBUTION / AVAILABILITY OF REPORT Approved for public release; distribution unlimited.
2b. DECLASSIFICATION / DOWNGRADING SCHEDULE	
4. PERFORMING ORGANIZATION REPORT NUMBER(S)	5. MONITORING ORGANIZATION REPORT NUMBER(S)
6a. NAME OF PERFORMING ORGANIZATION SOREQ Nuclear Research Center 6b. OFFICE SYMBOL (If applicable)	7a. NAME OF MONITORING ORGANIZATION European Office of Aerospace Research and Development (EOARD)
6c. ADDRESS (City, State, and ZIP Code) Dept. of Physics and Applied Mathematics Yavne 81800 ISRAEL	7b. ADDRESS (City, State, and ZIP Code) Box 14 FPO N.Y. 09510-0200
8a. NAME OF FUNDING / SPONSORING ORGANIZATION AFOSR 8b. OFFICE SYMBOL (If applicable) NA	9. PROCUREMENT INSTRUMENT IDENTIFICATION NUMBER AFOSR-89-0374
8c. ADDRESS (City, State, and ZIP Code) Bolling AFB, DC 20332-6448 AFOSR/NA 110 Duncan Ave St B115	10. SOURCE OF FUNDING NUMBERS PROGRAM ELEMENT NO. 61102F; PROJECT NO. 2301/D1; TASK NO. 0100/00; WORK UNIT ACCESSION NO

11. TITLE (Include Security Classification)
Damage in Composites and Other Advanced Materials Treated by Percolation Theory. (Unclassified)

12. PERSONAL AUTHOR(S)
R. Englman, Z. Jaeger and M. Murat

13a. TYPE OF REPORT	13b. TIME COVERED	14. DATE OF REPORT (Year, Month, Day)	15. PAGE COUNT
Final Technical	From 15 Apr. 91 To 14 Apr. 94	1995, April 5	17

16. SUPPLEMENTARY NOTATION

17. COSATI CODES		
FIELD	GROUP	SUB-GROUP

18. SUBJECT TERMS (Continue on reverse if necessary and identify by block number)
See attached page.

19. ABSTRACT (Continue on reverse if necessary and identify by block number)
See attached page.

20. DISTRIBUTION / AVAILABILITY OF ABSTRACT ☒ UNCLASSIFIED/UNLIMITED ☐ SAME AS RPT. ☐ DTIC USERS	21. ABSTRACT SECURITY CLASSIFICATION (U)
22a. NAME OF RESPONSIBLE INDIVIDUAL Dr. Spencer Wu	22b. TELEPHONE (Include Area Code) 202-767-6962 22c. OFFICE SYMBOL NA

DD FORM 1473, 84 MAR 83 APR edition may be used until exhausted. All other editions are obsolete.

SECURITY CLASSIFICATION OF THIS PAGE

UNCLASSIFIED

18. Subject Terms

Anisotropic percolation, universal exponents, impacted composites, ballistic limit, scaling laws, fracture, fragment size and shape distribution, finite size scaling, maximum entropy, mechanical modeling, fiber reinforcement.

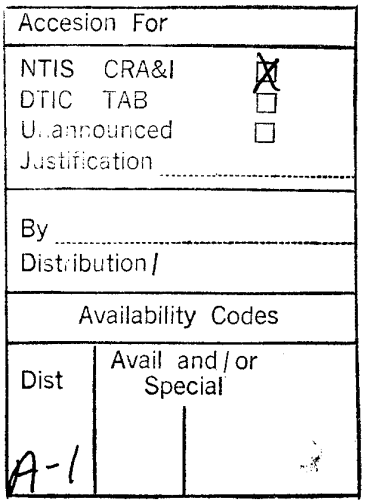

19. Abstract

We have performed detailed theoretical and numerical investigations concerning the nature of regions that arise when energy is quickly deposited in a small domain, i.e., by impact or explosion. Such situations naturally lead to inhomogeneous, spatially dependent probability of microfracturing which is diminishing with the distance from the center of the zone where the energy was released. The appearance of critical boundaries of fragmentation and of connected fracture is a direct consequence of this decaying field of crack probabilities.

Within the fragmentation envelope, the various regions are distinguished by their distributions of fragment sizes. In particular, in the narrow region in which fragmentation just begins to occur (and outside which only connected cracks and sporadic small fragments prevail), the fractal form of the distribution is found to be $N \sim 1/s^{\tau}$, where s is the fragment volume and τ is the critical exponent. (For the two dimensional case, s is the fragment area. The value of τ varies with the dimension of the space.)

In a composite target, the crack probability field is inherently anisotropic. Generalization of the classical percolation model to this case resulted with the same functional form as mentioned above, but with a small shift in the value of τ. Size and shape distributions of the fragments in the 2D case were calculated and submitted to the American partner about a year before the experiments began.

The experimental program, supervised by Dr. A. H. Mayer, Wright Laboratories, Wright Patterson AFB, consisted of firing 1/2" diameter spherical steel projectiles at carbon-fiber epoxy-matrix composite plates, made of 32 plies. Projectile velocity was measured ahead of the target as well as behind it. Large diameter rigid plastic cylinders with axes coincident with the shotline were lined with adhesive paper and placed perpendicular to the target plate from both sides. The fragments ejected from the target are catched on the adhesive paper and photographed. Each experiment was theoretically evaluated by the Israeli group.

Taking the well recognized view that near the ballistic limit, terminal behavior tends to be probabilistic rather than deterministic, we defined the ballistic limit as the smallest velocity at which the front side fragmented zone (the crater) first overlaps with the back side one (the spalled zone). That is to say, for velocities smaller than the ballistic one, these two fragmented zones are separated by an intact layer of the original target material and therefore the projectile is not able to penetrate. On the other hand, when the ballistic limit is approached from below, global fragmentation is just achieved. As was explained before, the fractal form of the size distribution is thus expected.

When the experimental results were analyzed by the Israeli group using image processing techniques, it turned out that in all cases the fragment size distribution is indeed characterized by the above mentioned functional form. Moreover, the experimental exponent came out to be close to the theorerical one (however, subject to deviations due to the finiteness of the samples), especially for velocities near the ballistic limit. Away from this limit, the distribution changes (sharpens) from the critical one and a shift in the experimental exponent is noted (at higher strain rates, the relative

number of small particles increases). A microscopically based critical transition manifestation of the ballistic limit is thus established (at least for brittle materials).

Additional research efforts during these years have been directed to the following subjects:

a) Fragment distributions in a rock were obtained from a 2D and 3D crack percolation model that included a crack probability p decaying with distance from the center of the explosive as inverse power law. The mean size of the fragments peaks sharply near the radial distance r_c, at which the crack density becomes critical. The diggable amount of fragments around a borehole in 3D exceeds (by several tens of percent) the volume contained inside a sphere of radius r_c.

b) The fracture process in a composite of short stiff fibers in a softer matrix was simulated. The simulation revealed different fracture behavior as a function of fiber content and length. Effective Young's modulus, fracture stress and the strain at maximum stress as a function of the volume fraction and aspect ratio of fibers were evaluated.

c) Single fiber fragmentation was analyzed using maximum entropy principle. Theoretical predictions fit quantitatively to experimental ones by imposing two constraints.

d) A non-linear transport equation was derived for crack population behavior and damage induced by blast in a medium surrounding a charged borehole. The damage is defined as the effective volume associated with the cracks. Intensive cracking (large damage) appears near the borehole and close to the free surface (spalling). The effects of the initial crack distribution, sample size and pulse shape on the damage were numerically investigated.

TABLE OF CONTENTS

PART 1

ADMINISTRATIVE

Statement of Work

In our previous research, we have applied percolation theory, Information theory and fractal analysis to granular or porous solids, such as rocks and concrete, in order to understand basic issues of damage growth and fragmentation processes. The purpose of this investigation is to extend our former work to advanced materials (such as carbon-fiber epoxy-matrix laminates) that are likewise heterogeneous but also anisotropic.

In practice, it is necessary to determine the critical points P_c of the anisotropic system together with the universal exponents. Moreover, for fragmentation problems this is not enough and a description of the system further away from the critical point is required for the appropriate size (and shape) distributions of the fragments.

The Soreq group will take its share in the experimental work in ballistics carried out at Wright Laboratories, by proposing discriminating experiments and by interpreting the results in the light of models developed at Soreq. The interpretation will be aimed at establishing correlation between the energy level of impact and the critical densities. In addition, determining the statistics for fragment sizes and comparing them to the theoretical predictions.

Status of Research

A mini workshop on "Fracture and Fragmentation" under high strain rate loading in impacted composites was organized in June 1991 at CRREL by Dr. P.K. Dutta and Dr. A.H. Mayer (Wright-Patterson A.F.B.). Experimental results and methods were presented by the other participants, while the Soreq group contributed a theoretical lecture on "Application of Percolation Theory to Fragmentation of Materials".

The experimental program was determined as a result of this workshop. It was planned to perform a series of ballistic impact experiments on plates having the same size and support with a projectile having the same nature (size and material). Impact speeds as well as rebound velocities (residual ones in the case of perforation) are also measured in each experiment in order to determine the energy (momentum) absorbed in the target. The weight of the target is measured before and after the hit. The weight loss is a measure of the total ejecta mass.

The composite debris generated by the impact are caught at their point of impact with the duct wall which is covered with adhesive paper. The population of fragments from each experiment is photographed and scanned and a digitized image is

formed. Fragment size histograms were obtained by image processing techniques. Since losing fragments (either in the collection procedure or due to low resolution and ambiguity due to interference of shades with fragments' edges) results in a biased fragment distribution, the Soreq group was actively involved in this section of the experimental program, as well as in the image processing and the final analysis.

These well controlled impact experiments are tedious and time consuming. The first set of photographs from each of the nine impacts on 0°-90° composite plates arrived at Soreq in early summer 1993. Meanwhile, (during 1992 and the first half of 1993) theoretical models and tools to deal with different aspects of the problem were prepared at Soreq. (List of articles 1-5). Especially noteworthy is the calculation of fragment size and shape distribution in 2D anisotropic percolation (Part 3, annual report for the period April 15, 1991-April 14, 1992) which predicts that the slope of the number of fragments versus fragment size (in log-log presentation) is $\tau = 2.1$ (Fig. 1, p. 13, above mentioned annual report). This value is not far away from the isotropic percolation values, i.e., $\tau = 2.05$ (2D) and $\tau = 2.2$ (3D). Moreover, all these theoretical predictions came out very close to the experimental slope: $\tau = 2.1$ (0°/90°) (Table 1,a, Part 3, this report). A similar result, $\tau = 2.2$, was accepted from the set of impact experiments on the 0°/45° composites (Table 1,b). More evidence has been accumulated since then (Part 4) pointing to the conclusion that the Ballistic Limit is a critical point in phase transition. Consequently, the power laws with universal exponents, which are well known in the theory of critical phenomena, may have an equivalent form also in ballistics.

The percolation program was also extended to cover fragmentation processes in three dimensional anisotropic and heterogeneous systems. A new entity, the relative excess shattered volume (RESV) was defined. This quantity is related to the total mass of material that is fragmented within the shattered zone. Using scaling arguments, we expressed RESV in terms of the rate of decay of the crack formation probability as a function of the distance from the region of energy deposit. Simulations in 3D situations show that RESV increases as the rate of decay becomes milder. In two dimensions, RESV is practically independent of the rate of decay of crack formation probabilities.

We have also treated observationally obtained distributions of fragment sizes and showed that to derive conservation laws for the fragmentation process one has to compute the information entropy S and then obtain the changes in S when the conserved quantities are varied by varying the experimental conditions. The criterion for the existence of conservation laws is the equality between the S-derivative and the Lagrange multiplier in the Maximum Entropy distribution, coupled to the non-vanishing of the determinant formed out of the second derivatives of S. Application of

the method to ballistically created rock pieces indicates conservation of the average of log (fragment-size) in the break-up process.

Another topic treated is the distribution of broken bonds (as function of their length l) in a random 2D network, fragmented by pulling. The obtained distribution is in the form of a product of a prior distribution and an exponential function (the constraint factor of Maximum Entropy) whose exponent is linear in l. This is yet another case of the constraint factor being a simple function of the variable.

Our research, in addition, included approaches to composite materials other than the statistical ones. We modeled the fiber-reinforced materials using a triangular lattice of springs with bond-bending forces between them. This model has the advantage of being able to deal with the complex situations of broken fibers, matrix cracks and fiber matrix debonding. Such situations arise during the fracture process of (continuous or discontinuous) fiber-reinforced composites. We first showed that the equations of equilibrium for the lattice sites reduce to equation of isotropic elasticity in the continuum limit. We then used the model to simulate both the elastic and the fracture behaviour of composites. Our research focused on the influence of fiber volume fraction and fiber aspect ratio on the elastic moduli and the fracture strength of the composite. The results were compared with other theoretical approaches and with experiments.

An attempt to model the damage growth and accumulation was also accomplished. A non-linear transport equation was derived for crack population behavior and damage induced by blast in a medium surrounding a charged borehole. The damage is defined as the effective volume associated with the cracks. Intensive cracking (large damage) appears near the borehole and close to the free surface (spalling). The effects of the initial crack distribution, sample size and pulse shape on the damage were numerically investigated.

Details of Work Performed

A major objective of the present research has been to generalize the percolation model to deal with the fragmentation process in highly anisotropic materials such as fiber composite laminates, which include layers of uniaxial high strength fibers in a much weaker matrix. To that end, we developed a code that assigned different crack formation probabilities in different spatial directions. The code was applied to analyze the size and shape distributions of the fragments formed on lattices of varying anisotropy. A fragment is defined as a section of the lattice isolated from the rest by a continuous path of cracks. Any "fragment" that touches the external boundary is not considered in the distribution. In an anisotropic system, the percolation threshold is given by the line $P_X + P_y = 1$. We have studied several cases

on the threshold line as well as a few cases further away from it. A typical case (P_X = 0.7, P_y = 0.3) is shown in Fig. 1 (page 13, Part 3, annual report for the period April 15, 1991-April 14, 1992). The plot of the number of fragments n(s) versus their size s on double logarithmic scale is a straight line over at least 3 decades (i.e., between s = 5 and s = 5000). The slope that gives the exponent of the power law decay is about 2.1 which is not far from the value τ = 187/191 = 2.055 for ordinary (isotropic) percolation. This power law is very accurate for all (P_X, P_y) couples on the threshold line within some range. Outside this range there are deviations for very small fragments ("dust") as well as for very large ones.

It was found that in isotropic systems the aspect ratio of fragments was lower than 3.5, while it could go as high as 20 in highly anisotropic cases. Photographs of fragments collected in the preliminary experiment performed by P. Dutta at CRREL were analyzed using image processing techniques. The distribution of fragment sizes and shapes were compared with those obtained from the simulations. The aspect ratio distribution from the experimental fragmentation was found to have a width of about 8, implying a rather high degree of anisotropy.

Percolation theory has been recognized as a statistical physics model for critical phenomena. By applying it to fracture and fragmentation problems, we were able to show that fragmentation occurs whenever the density of the microcracks reaches its critical value. That is to say, when the probability p of creating a microcrack achieves its critical value p_c. At and near this point, the number n of fragments (clusters) having size s (per site) behaves as $n \propto 1/s^{\tau}$, where the critical exponent τ has the value τ = 2.05 for a two dimensional isotropic system and τ = 2.2 for a three dimensional isotropic one. As was described above, we found the value τ = 2.1 for an anisotropic two dimensional system (having different crack probabilities in the x and y orthogonal directions). These are the statistical physics predicted results for the fragment size distribution at the critical point, which is identified as the ballistic limit (see Part 4).

The experimental program performed at W.P.A.F.B. is briefly described in Part 4. Additional details relating to the image analysis procedure are given in Part 3. Consider the trend of the damage and the energy transfer ratio, defined here to be the ratio of imparted to initial projectile energies, as the projectile velocity (or energy) is increased. At very low velocities, the projectile experiences a perfect, loss-free rebound from the panel and the transfer ratio remains at zero. As the velocity is increased beyond the damage threshold, a crater is produced in the panel, causing the transfer ratio to increase. With higher impact velocities, incipient spall first appears and the transfer ratio further increases. Below the ballistic limit, it is expected that the spalled fragmented zone at the backside of the sample and the shattered and

penetrated zone in the front side (the crater) are separated by an intact or delaminated layer of the material which is strong enough to prevent the projectile from perforating the target. In the limit (in fact, the ballistic limit) this intact layer becomes very thin and the two damage zones will touch each other. That is to say, the sample will then become disintegrated throughout its thickness.

Our experimental investigation provides quantitative evidence that the ballistic limit represents a critical phenomenon. This evidence comes from the size distribution of the ejecta produced near the ballistic limit. The distribution density function for fragments of area s was found to decrease with s raised to a negative power. Results for several impact velocities for 0°-90° fiber orientation are presented in Table 1,a. Similar results for 0°-45° are given in Table 1,b (Part 3). The experimental exponents $\tau = 2.1$ (0°-90°) and $\tau = 2.2$ (0°-45°) are very close to the values found theoretically for fragment sizes.

Impact loading or other localized energy deposition mechanisms (i.e. explosion and laser irradiation) lead to spatially dependent, inhomogeneous probability of microfracturing. A three dimensional percolation simulation of fragmentation has been performed for the first time (at this stage only for isotropic microfracturing.) The characteristic (average) fragment size as a function of the radius from the point at which the energy was released was obtained in two and three dimensions. Close to the impact point fine fragments are obtained, but their size increased up to a maximum just short of the distance R_c^{II} from the center, which is defined as the position at which the crack formation probability achieves the critical value p_c^{II} for fragmentation. The distance R_c is also meaningful for estimating quantitatively the total amount of shattered material. In a naive picture, the volume (surface in 2D) of the broken material is just equal to $4/3\pi(R_c^{II})^2$ in 2D). Deviations from these values have been calculated for various energy deposition configurations and were found to be the more in access of the naive values the shallower is the decrease of the microcracing probability with the distance from the center. (Part 2).

Fragmentation is a complex phenomenon. Its outcome, the fragment distribution, is expected to reflect this complexity. The Maximum Entropy (ME) approach has been used in the past to impose regularities on the distribution. In this work we set out to uncover regularities from the data. The key to this effort are the derivatives of the entropy with respect to the invariants. The procedure leads to a "Thermodynamics" of the fragment - (or any other) data. Application has been made to relatively simple case of ballistic fragmentation of rock targets, where only one invariant <logs> is in evidence. For future uses of the procedure, when more than one invariant is expected, further development of the method is needed to make it practical. This appears possible. (Part 5).

A priori - constraint function decomposition of distributions has been also carried out in this work for the broken bonds in a disordered network at the moment of its falling to pieces. The aim was to see whether the constraint function is simple, as anticipated in the ME treatment. This was found. Additional interest is attached to possible changes in the distribution as the fragmentation threshold is approached. (Part 5).

The transport equation approach to crack population growth (Part 6) is only one of the possible treatments of a complicated stochastic problem: to us it appears neither less nor more justified than any other, and for a space and time-dependent description it may be uniquely workable. There are, admittedly, a great number of free parameters in the approach, whose values are not easily fixed in any concrete situation. Our aim was to elucidate the wide range of phenomena that can occur with some (not unphysical) choice of the parameters. Yet more parameters can be varied (as the crack velocity or introducing inhomogenity in the initial crack distribution).

Although the results presented in his work are related to the specific samples defined in Part 6, it is possible to reach some conclusions, which seem to present the general behavior of damage in systems.

(a) In a given sample, a pressure wave creates a spall zone, if the ratio σ_c/σ_t is larger than some threshold value.

(b) For a given pressure wave in a given medium, the damage peak in the spall zone increases for $R_0 \leq R^*_0$ and decreases for $R_0 \leq R^*_0$. For sufficiently large size of the sample R_0, the spall does not exist. (In the case of Sec. 4, the threshold is $R^*_0 = 4.4$).

(c) For a given pressure wave in a given medium, the damage peak and the width of the inner damage zone increases with the sample radius R_0.

(d) For a given pressure wave and sample size R_0, if $\alpha \geq \alpha^*$ is a sufficiently small number, the damage peak and the width of the inner damage zone and the spall region are independent of the α value. In the limit, as $\alpha \rightarrow 0$, the peak of the damage near the center reaches a minimal value, and the peak of the spall attains a maximal one.

(e) For a given pressure wave and sample size R_0, if $\alpha > \alpha^*$, where α^* is sufficiently large number, the spall zone does not exist.

(f) A pressure wave and a sample of radius R_0 are given. For $\delta > \delta^*$, is a sufficiently large number, the spall zone does not exist and the damage peak of the inner damage zone increases with the δ value. In the limit, $\delta \rightarrow \infty$, the damage achieves a maximal value.

Participating Personnel

Robert Englman (Prof.); B.Sc., A.R.C.S. (in Mathematics) in 1954 and Ph.D. (Theoretical Physics) in 1957 at London. Thesis title "Extension of the theory of the mean-free-path effects in metals".

Zeev Jaeger (Dr.); M.Sc. in Chemistry, Physics as major subjects and Mathematics and Applied Mathematics as subsidiary subjects in 1967 at the Hebrew University in Jerusalem, Ph.d. in Physics in 1973 at the Hebrew University, Jerusalem with the thesis title. "Charge-transfer states and their physical application in crystals of transition metals".

Raphael Ruppin (Dr.); M.Sc. in Physics at the Hebrew University of Jerusalem in 1964 and Ph.D. in Theoretical Solid State Physics from the Hebrew University in 1969 with the thesis title "Size dependent elementary excitations in solids".

Miriam Lemanska (Dr.); M.Sc. in Mathematics in 1952 at the Lodz University in Mathematics and Ph.D. in Nuclear Sciences in 1967 at the Technion, Haifa in the subject "Perturbation theory in fast reactors".

Michael Murat (Dr.); B.Sc. in Chemistry in 1977 from the Technion, Haifa, then M.Sc. in Physical Chemistry in 1978 from the Technion, Haifa with a thesis on "The triplet state of the biexciton" and Ph.D. in Physics in 1987 at the Tel Aviv University with a thesis entitled "The structure and physical properties of porous materials".

Micha Anholt (Mr.); B.Sc. in Physics (1989) from Tel Aviv University. Studying towards M.Sc. in Physics of Condensed Matter.

Interactions

Prof. T.J. Ahrens, Dept of Geology and Astrophysics, California Institute of Technology, Pasadena. CA, Discussions with Z. Jaeger July 1991, June 1992.

Prof. H.D. Wagner, Department of Materials and Interf, The Weizmann Institute of Science, Rehovot 76100, Israel. Discussion with M. Murat throughout the year.

Dr. E. Schulz & Dr. A. Hampe, Federal Institute for Materials Research and Testing (B.A.M.) D-1000, Berlin 45, Germany. Correspondence during the year and discussions with R. Englman and M. Murat in Israel, June 1992.

Prof. S.L. Phoenix, Dept. of Theoretical and Applied Mechanics Cornell Univ., Ithaca, N.Y. Discussions with Z. Jaeger at Cornell.

Dr. J. Karger-Kocsis, Institute for composite materials, D-6750 Kaiserslautern, Germany. Correspondence during the year and discussions with R. Englman and M. Murat in Israel, June 1992.

Prof. S.M. Wiederhorn, National Institute of Standards and Technology. Several discussions with Z. Jaeger 1992-1993.

Dr. F. Allahdadi, Space Kinetic & Impact Debris Group, Space Technical Center Philips Laboratories, Albuquerque, N.M. Presentation by Z. Jaeger and discussion, 1993.

Dr. D.E. Grady, Experimental Impact Physics Div. 1433, Sandia N.L., Albuquerque, N.M. Correspondence and discussions 1992-1995.

James F. O'Bryon, Deputy Director, Operational Test and Evaluation, Live Fire Testing, Office of the Secretary of Defense DDOT & E/LFT, The Pentagon. A few discussions on damage in composites and vulnerability of flying structures made of composites, Jerusalem, Israel, May 1955.

List of Articles

1. R. Englman and Z. Jaeger, "Percolation Theory of Fragmentation", an invited lecture presented at the International Symposium on Intense Dynamic Loading and its Effects, Chengdu, China, June 9-12 (1992) pp. 425-430.
2. M. Murat, M. Anholt and H.D. Wagner, "Fracture Behaviour of Short-Fiber Reinforced Materials". J. Mater. Res. 7, 3120-3131 (Nov. 1992).
3. R. Englman, "Information-Entropy Distribution for Sequential Fragmentation in Single Fibers", Int. Conf. on "Microphenomena in Advanced Composites", G. Marom and H.D. Wagner (Edits) Herzlia, Israel, June 28-July 1, (1992).
4. M. Anholt, R. Englman and Z. Jaeger, "Percolation Approach to Locally Caused Fragmentation", Centre de Physique des Houches Workshop on Fragmentation Phenomena, 12-17 April 1993, Editor: D. Beysens.
5. Z. Jaeger, M. Anholt and A.H. Mayer", Impact of Fiber Composite Laminate Plates: A Percolation View of Perforation and Spallation" in "Dynamic Response of Composite Structures", D. Hui and G. Anderson (Edits), New Orleans, LA, August 30-Sept. 1, 1993.
6. A.H. Mayer, Z. Jaeger and R. Englman, "The Ballistic Limit of Laminated Carbon Fiber Epoxy Plates as a Critical Point in Phase Transition", a post deadline paper (TB60) in the 15th International Symposium on Ballistics, Jerusalem, Israel, 21-24 May 1995. M. Mayseless and S.R. Bodner (Edits.).
7. R. Englman, "Maximum Entropy Principles in Fragmentation Data" in "High Pressure Shock Compression in Solids II". Editors: L. Davison, D.E. Grady and M. Shahimpoor, Springer-Verlag, N.Y. (1994).
8. M. Lemanska, R. Englman and Z. Jaeger, "Transport Treatment of Crack Population in Finite Medium Part II: Damage Behavior in Different Zones". Submitted for publication.

Patents and Inventions

None

Statement to Program Manager

Achievements

The first summer of research began with presentations of earlier achievements which were presented by the participants of the mini workshop on composites' impact problems. As a result of the preliminary impact experiment, the lectures and the discussions during the workshop, the directions of research during the year were agreed upon.

During the second year percolation model was generalized to anisotropic two dimensional case as well as to the nonhomogeneous and anisotropic three dimensional one. Shape and size distributions of fragments in the 2D case were calculated and compared at first with data deduced by image processing techniques from results achieved by the preliminary experiment. A series of very well controlled impact experiments with different velocities on 0°/90° composite plates were performed at W.P.A.F.B. and analyzed several months after the annual report for the second year, (including the theoretical percolative values) was submitted. It was found that the distribution density function for fragments of area s decreases with s raised to a negative power. Moreover, the value of the experimental negative power at the ballistic limit was indistinguishable from the theoretically predicted one. Later on a second series of similar experiments was done on 0°/45° composite plates and the analysis gave again very similar results. **The evidence accumulated show that we have succeeded in uncovering the physical meaning of the perforation threshold (the Ballistic Limit): it represents a critical phenomenon. Moreover, Percolation theory could provide an adequate description of the fragmentation process.** The identification of the ballistic limit velocity V_c with a critical point lays open the field of ballistics to the theoretical apparatus of critical processes and its scaling laws. In addition, it has also been shown that much insight into the complicated process of fragmentation can be achieved by using the Maximum Entropy Principle.

Future Research Envisaged

The fragmentation process is clearly related to the damage accumulated in the impacted composite at and above the Ballistic Limit. It is expected that scaling laws which hold at the critical point of the phase transition will also hold around it. New hitherto unknown scaling laws for damage would be theoretically identified and experimentally confirmed. Such relations are relevant to vulnerability considerations of flying systems.

It is suggested to repeat the experiments with velocities near and around the ballistic limit. It is recommended to use better techniques of photographing and

higher resolution equipment for image processing in order to receive more reliable experimental fragment size distributions (fragment size should span two or three orders of magnitude). It is suggested that a series of well controlled impact experiments would be repeated with different target thicknesses, and different sizes and shapes of projectiles. (Control on the strain rate could be achieved by changing the sphere to a long cylinder). Larger scale experiments should also be accomplished. Ejecta at the front side has to be measured and analyzed along the same lines that ejecta from the backside was studied. It is also recommended to trace back spacial effects in damage and fragmentation by identifying the places from where the fragments and their velocities came from.

PART 2

PERCOLATION APPROACH TO LOCALLY CAUSED FRAGMENTATION

Micha Anholt, Robert Englman and Zeev Jaeger

Department of Physics and Applied Mathematics
Soreq Nuclear Research Center
Yavne 70600, Israel

ABSTRACT: The paper starts with a survey of the variety of fragmentations, with emphasis on the factors which determine whether the size distribution will be monotonic, decreasing with size or peaked. We consider cases of loading that are local and uniform, fast and slow; confined or locked-in situations and excess-energy redistributions that are channel-specific or statistical. Fragment distributions in a rock were obtained from a 2D and 3D crack coalescence (percolation) model, that included a crack formation probability p decaying with the distance from an explosive bore-hole as an inverse power law. The mean size of the fragments peaks sharply near that radial distance r_c at which the crack density is becomes critical. In this neighbourhood the spread and the height of the mean fragment-size peak follow scaling-laws appropriate to space-varying p. The digable amount of fragments around a borehole in three dimensions exceeds (by several tens of percents) the volume contained inside a sphere of radius r_c .

Introductory Overview

The subject of fragmentation is exceedingly ramified and calls for classification. This is attempted here from several viewpoints.

First we make some rather obvious classifications related to the mode of loading or of energy input. This can be done in a manner affecting the medium uniformly(such as occurs when one bends a bar) or in a local manner (which is the case treated in the following sections in this paper). In the former the stress in the medium essentially scans the medium for its weakest points (and is strain controlled), while in the latter fracture may occur at the point where stress is applied and propagates from that point. The speed of the loading has essentially two consequences on fragmentation: It affects characteristic particle sizes [1,2,3] , in the sense that high strain rates produce small-size fragments and tend to act uniformly through the medium. The number-distribution of fragment-sizes found experimentally, or predicted theoretically often peaks at a finite, nonzero size, the weight-weighted distribution (important in technology) almost invariably does so. This statement holds for one-time, sudden loading; sequential breakage favours small sized fragments whose distribution has some inverse power law form (fractality [4]). An essentially theoretical postulate affects directly the predicted distribution. If one assumes that the loading energy is a priori equally likely distributed among all *bonds* between particles, then a peaked distribution is expected; on the other hand, if all *fragments* are estimated to be a priori on equal footing, then a monotonic distribution (decreasing at larger sizes) results. Both cases are quoted in a review [3]; however, it is not clear which choice fits which factual circumstance. Competition for the available energy by different modes has remarkable consequences in molecular physics (*e.g.,* photofragmentation and predissociation [5]) and presumably in nuclear multi-fragmentation. When excitation is brought about locally the

spread of excitation energy in time and space is a subject that has been researched especially since the 70's. In one extreme there is the possibility of a fast redistribution of the excitation-energy among all modes democratically (this is the case of thermalization in the 'statistical', high density-of-state limit) which tends to result in the simultaneous production of many molecular fragments. Alternatively, one has situations (for harmonically bonded particles) that the mode with the highest frequency takes up most of the energy and breaks preferentially. At the other extreme the energy becomes channelled to a special, localized (highly non-harmonic) mode, which is the one that breaks first, while the other modes are only moderately excited. A further classification depends on whether fragmentation occurs when the matter is in a confined, locked-in situation or it is free. (Rock blasting and spacecraft breaking up are representative instances for the two cases.) There are indications that the latter gets fragmented by a percolation process. This means that cracks are formed fairly rapidly and uniformly in the system and when these coalesce the fragments fly apart without further interaction with each other. The coalescence is a percolation process. The fragment size distribution of space debris appears to arise under such circumstances [3].

Background

Rock blasting for the purpose of mining is carried out by exploding point-like or cylindrical charges in bore-holes. As a consequence, cracks are created whose density near the borehole is large and there the rock breaks into small fragments (the crushed zone). As one moves away from the centre the crack-density decreases and larger fragments start to dominate (the fragmented zone), until one reaches region where the 'infinite-fragment' contains mainly isolated cracks (the cracked region), ending in intact, uncracked recesses.

The Simulational Scheme

In this work the statistics of the fragment in obtained and analyzed in the framework of a percolation model, that extends to three dimensions the earlier computations of Murat *et al.* [6]. The rock is modelled by a cubic lattice(or by a square lattice in 2D) and planar crack plaquettes are formed on the faces of the cells of linear size a, (representing the granular composition of the rock) with a probability which decreases with the distance r from the centre according to

$$p(r) = (r_0/r)^{\alpha} \qquad ; \qquad (r > r_0). \tag{1}$$

r_0 is the borehole radius, $\alpha = 0.2$–0.4.

We expect from percolation theory for infinite homeogeneous structures [7] that at distances below the value where $p(r) = p_{c1}$ (the standard critical percolation probability; for numerical values of this and other critical parameters in 2D and 3D, see table I) there will be a connected cluster of cracks across which (for example) fluid can percolate throughout the inside volume. However, as shown in Ref. [8], fragmentation will not occur inside all this volume, but only within a smaller volume defined by the critical fragmentation radius r_c at which

$$p(r_c) = p_{c2} \qquad (> p_{c1}).$$

see Figure 1. At distances less than r_c fragmentation will be intensive and the mean fragment size will be small, approaching the minimal size a (the 'grain' dimension). For distances beyond r_c one encounters the infinite fragment plus some small fragments embedded in it. Due to considerations that are both practical and theoretical, we exclude henceforth the infinite fragment from summation over fragments. Then at $r > r_c$ the mean fragment size will decrease, once again approaching a, since at low crack densities fragments formed out of more than the minimal crack number

(4 in 2D ,6 in 3D) are extremely unlikely. Mean fragment size S_{av} as function of the radius are shown in Figures 2,3. Computations were performed on lattices of sizes up to $(150a)^3$ - in 3D and $(2000a)^2$ in 2D, sufficiently large to neutralize any edge or finite size effects. There were between 50 (in 3D) and 2000 (in 2D) realizations for each set of parameters. The exponent α in (1) was taken to vary between 0.2–0.4,as already remarked; the borehole-variation is discussed below.

Scaling

Since the total lattice size is large enough not to affect the results (as is apparent in Figure 1), there remain only two length variables: the borehole radius r_0 and the cell size a. In making the model apply to an actual blast, we assign to the borehole radius a value that corresponds to the actual situation , r_c is then obtained (at least roughly) from the outcome and will be, if the model is anything like right, of the order of r_0, independent of a. However the average size S_{av} in Figures 2,3 and the width of the distribution are given in units of a and the effect upon these of increasing r_0 is equivalent to a corresponding decrease in a. This circumstance is useful since we have varied the borehole radius r_0 and computed changes in the location of the maximum of S_{av} and in the width w of the peak in the S_{av} versus r curve(Figure 4). It is apparent that the location of the S_{av}-maximum scales linearly with the borehole size, which is reasonable since its value is close to (though not quite) r_c and this scales linearly with r_0. In the same figure the width shows a milder variation with r_0 which is linear with r_0 for large boreholes and something like $r_0^{0.5}$ for small boreholes. Recalling our previous remark regarding reciprocity between r_0 and a we can formalize this as $w/a \propto a^{-0.5}$ for large a, or equivalently $w \propto a^{0.5}$. To discuss quantitatively behaviors of S_{av} and of w in the critical regime, namely around $r = r_c$, we recall that in a lattice with uniform occupation probability both

the maximum fragment size and the width will be of the order of the size L of the lattice. For a non-uniform probability the spatial variation of $p(r)$ around r_c will provide the appropriate size scale and it has been shown [6,9] that the correct scaling is with

$$L_{eff} \approx (r_c/\alpha p_{c2})^{\nu/(1+\nu)}. \tag{2}$$

We shall now relate the average size of the fragments near r_c to the maximum fragment size S_{max} utilizing the result [3]: $n_s \propto s^{-\tau}$, where n_s is the average number per site of fragments having size s. (We assume the statistical isotropy of fragments though the model does not warrant this.) Then

$$S_{av}/a^d = \int_1^{S_{max}/a^d} ds\, n_s s^2 \Big/ \int_1^{S_{max}/a^d} ds\, n_s s$$

$$= (S_{max}/a^d)^{3-\tau}\left(\frac{\tau-2}{3-\tau}\right) \tag{3}$$

$$\propto (L_{eff}/a)^{(3-\tau)d} \simeq (r_c/p_c\alpha a)^{d(3-\tau)\nu/(1+\nu)}$$

Using the values in Table I this leads to the following scaling between S_{av}(near $r = r_c$) and a

$$S_{av} \propto a^{.97} \qquad \text{in 2D}$$

$$S_{av} \propto a^{1.86} \qquad \text{in 3D}$$

Let it be remarked that away from r_c on both sides S_{av} varies with a^d. Our numerical results confirm this. To calculate the width w of the S_{av} peak around r_c we remark that this is related to the fractal dimension by

$$\begin{aligned} \frac{w}{a} &= \left(\frac{S_{max}}{a^d}\right)^{1/D} \\ &= (L_{eff}/a)^{\alpha\nu/[D(1+\nu)]} \end{aligned} \tag{4}$$

From the first line we obtain $w = (S_{max})^{1/D} a^{(1-2/D)}$ and from the second line

$$w \propto a^{.40} \qquad 2D$$

$$w \propto a^{.43} \qquad 3D$$

which may be compared with the exponent 0.5 estimated from computation.. Numerical comparison (Table II) shows that there is a constant factor of 4 between the two members of Eq. (5) in both 2D and 3D. (Presumably this means that the definition of the width is not clear cut) Figure 5 exhibits the probability p_∞ that a site belongs to the infinite fragment as fuction of the distance from the centre. The objective is to quantify what part of the rock can be mined or digged out, with the understanding that the infinite fragment is not digable. In the uppper curve the isolated or embedded fragments are counted as part of the infinite fragment and the approach to unity is faster than when the embedded fragments are presumed digable (the lower curve). Estimation of digability is the subject of the following section.

The Excess Digable Fraction (EDF).

Digable broken pieces appear beyond r_c because fragments have finite size on the scale of the basic crack size a, and are not infinitesimal, point like. Likewise, unbroken pieces belonging to the infinite fragment appear inside r_c. Both effects represent fluctuations from an 'ideal' situation in which the radius $r = r_c$ defines a sharp boundary between fragmented and unbroken (though, possibly, cracked) regions. Both small and large sized fluctuations exist and are apparent in Figure 1 ; however statistically the most important ones are the large sized ones. The digable volumes as function of fragments-volume are shown in Figures 6-8 for 3D simulations with the charge having either spherical or cylindrical geometries. Parameters are marked in the figures. The horizontal line represents the ideal situation where $r = r_c$ (written as R_c in the drawing) is a sharp boundary. We now define the excess digable fraction (EDF) as the relative difference between the computed digable volume and

the ideal one. The excess fraction is also the difference between averaged volume of broken pieces (including those that extrude beyond r_c) and the averaged volume of the unfragmented pieces (including the intrusions), all this divided by the volume contained within r_c. Figure 9 represents the results of our computation in 2D and in 3D (with two types of charges). Now in two dimensions on a square, where the opened and closed plaquettes are self-dual (with $p_{c2} = 0.5$ for either), fragments and unbroken pieces behave identically and one expects that to within random statistical error there will be no net excess fraction. In three dimensions EDF will have the form

$$\text{EDF} \propto (L_{eff})^{\rho} r_c^{-3} \propto \alpha^{-\rho\nu/(1+\nu)}\, p_c^{[3-\rho\nu/(1+\nu)]/\alpha}. \tag{5}$$

We have used here $r_c = r_0/p_c^{1/\alpha}$ and have inserted in the exponent the parameter ρ whose value is between 1 and 3, due to our uncertainty as to the shape of the extracted volume (whether it is similar to a sphere , $\rho = 3$, or to a flat piece lying on the hull at $\rho = 1$). In any case, due to both factors in EDF, this decreases with increasing value of the exponent. In our simulations a positive EDF is found in 3D and a power law dependence in the form $EDF = 0.05\alpha^{-1.9}$. Contrasting this are the two dimensional results in Figure 9 which show that EDF is negative and so small as to be zero within the statistical errors of our data. The dependence on α is also negligibly small. These agree with the analysis of the 2D situation given above.

Conclusion

Our model of fragmentation based on the coalescence of randomly created cracks needs a good deal of experimental confirmation, especially when applied to a confined geometry (as in solid rock). However, in fast processes which characterize blasting there is some justification for the model, including the neglect of correlations in crack development. Though our results are based on a special form [Eq.(1)] of crack generation probability, there are several generally valid features which could could be useful in the design of post-blast mining operation (quarrying). Examples are the rather sharp maxima in fragment sizes near r_c, the advantages we have found in having sharply decaying probabilities (α large)relative to flat ones (α small), and finally our finding that there are different digable volumes in different dimensions.

REFERENCES

1. D. E. Grady, *J. Appl. Phys.* **53** (1982) 322.

2. R. Englman, N. Rivier and Z. Jaeger, *Phil. Mag. B* **56** (1988) 751.

3. R. Englman *J. Phys.: Condens. Matter* **3** (1991) 1019.

4. D. L. Turcotte, *J. Geophys. Res.* **91** (1986) 1921.

5. K.P. Lawley, *Photodissociation and Fragmentation* , (Advances in Chemical Physics) (1985, Wiley, Chichester).

6. M. Murat, A. Aharony and Z. Jaeger, "Fragmentation in a Percolation Model with Radially Decaying Crack Concentration " in Fragmentation Form and Flow in Fractured Media, R. Englman and Z. Jaeger, Eds. (1986 Israel Phys. soc. Jerusalem)p.182

7. D. Stauffer, *Introduction to Percolation Theory*, Taylor and Francis, London, (1985).

8. A. Aharony, A. Levi, R. Englman and Z. Jaeger , "Percolation Model Calculation of Fragment Properties" in Fragmentation,etc. (ibid)p.112

9. B. Sapoval, M. Rosso and J. F. Gouyet, *J. Phys. Lett. (Paris)* **46** (1985) L149.

Table I

Values of parameters used in our computation(symbols explained in text). Critical exponents and concentrations rely on Ref [7].

	2D	3D
d	2	3
D	1.9	2.5
$3-\tau$	0.9	0.8
ν	1.33	0.9
p_{c1}	0.5	0.249
p_{c2}	0.5	0.751

Table II

Maximum value of average size S_{av} near r_c and width w of the distribution of average sizes as function of distance from the borehole obtained from our computation (expressed in units of the cell dimension a).

	2D	3D
$(S_{av}/a^d)^*$	960	38
$4(S_{av}/a^d)^{1/D}$	148	17.1
$(w/a)^*$	150	17

* From computation

FIGURE CAPTIONS

Figure 1: One realization on a square lattice. Different clusters are marked by different grey shades. The black lines represent the cracks opened cracks.

Figure 2: S_{av} as function of r for a square lattice of linear size $2000a$, borehole radius $100a$, $\alpha = 0.35$. Results were averaged over 50 realizations.

Figure 3: S_{av} as function of r for a cubic lattice of linear size $150a$, borehole radius $10a$, $\alpha = 0.2$. Results were averaged over 200 realizations.

Figure 4: Location of maximum of S_{av} and width of $S_{av}(r)$ at half maximum for a square lattice with $\alpha = 0.35$ and $Size/r_0 = 20$.

Figure 5: The p_∞ as function of r for a cubic lattice of linear size $100a$, borehole radius $5a$, $\alpha = 0.3$. Results were averaged over 50 realizations. Note that when only digable fragments are considered p_∞ reaches 1 at the maximum r the digable zone reached in the simulations performed. However when all fragments are considered p_∞ approaches 1 asimptoticaly since the probability of fragment formation is small but not zero even beyond the digable zone.

Figure 6: Digable 'volume'(area) in two dimensional blasting on a square lattice for lattice of linear size $1000a$, borehole radius $50a$, $\alpha = 0.35$. Results were averaged over 50 realizations.

Figure 7: Digable volume in cylindrical blasting on a cubic lattice for lattice of linear size $100a$, borehole radius $10a$, $\alpha = 0.35$. Results were averaged over 200 realizations.

Figure 8: Digable volume in spherical blasting on a cubic lattice for lattice of linear size $100a$, borehole radius $10a$, $\alpha = 0.4$. Results were averaged over 200

realizations.

Figure 9: The excess digable fraction for the three types of charges discussed previously. The borehole was chosen as $5a$ in all cases.

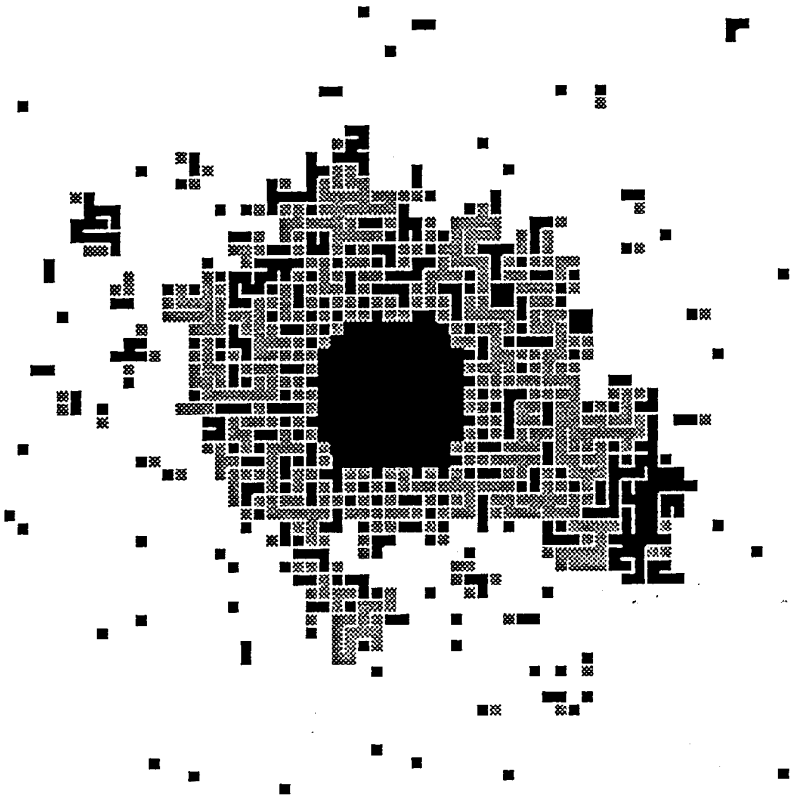

Figure 1

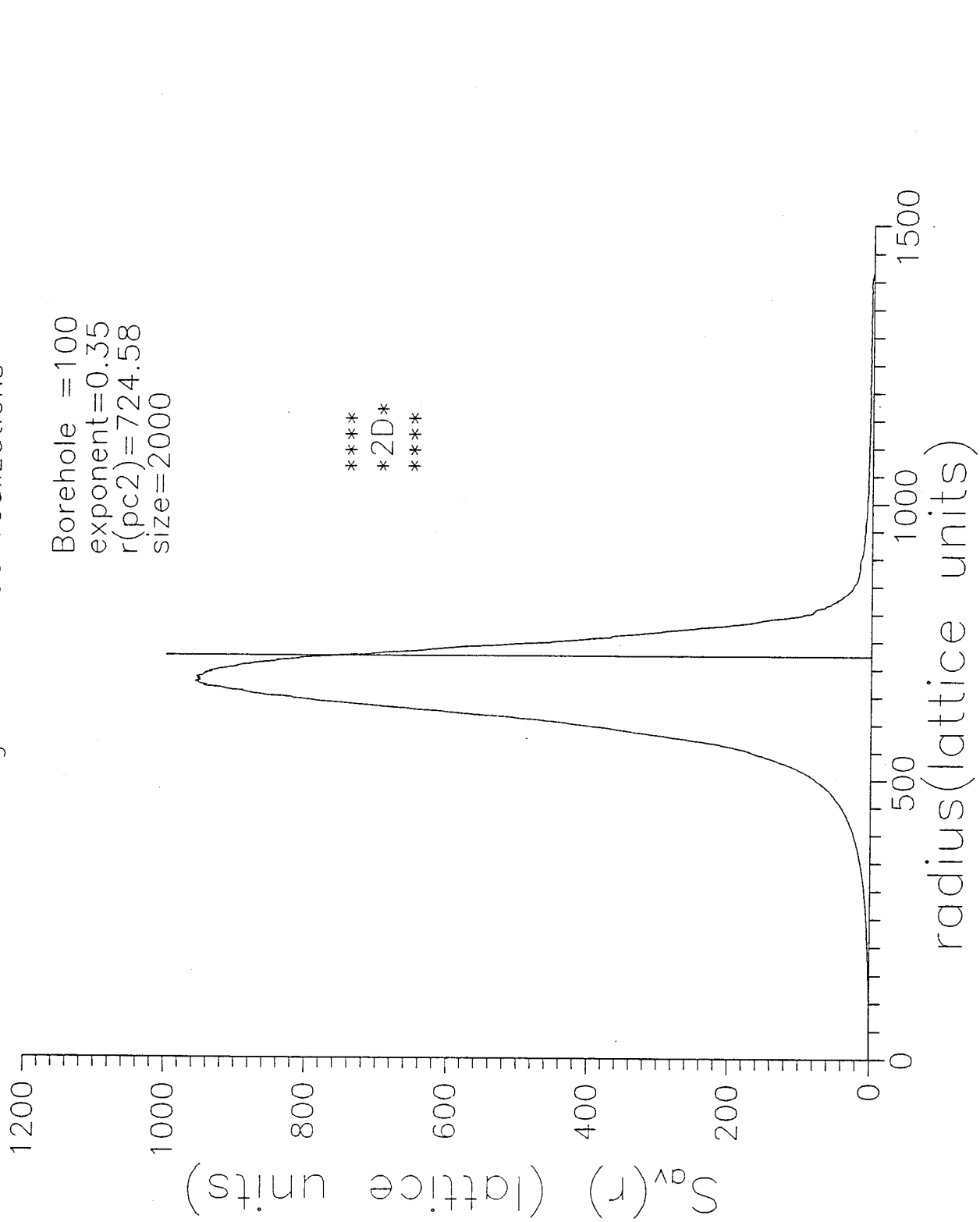
Cluster size vs. distance from origin
Average over 50 realizations
Borehole =100
exponent=0.35
r(pc2)=724.58
size=2000
****
2D
****
$S_{av}(r)$ (lattice units)
radius(lattice units)
0
200
400
600
800
1000
1200
500
1000
1500

Figure 2

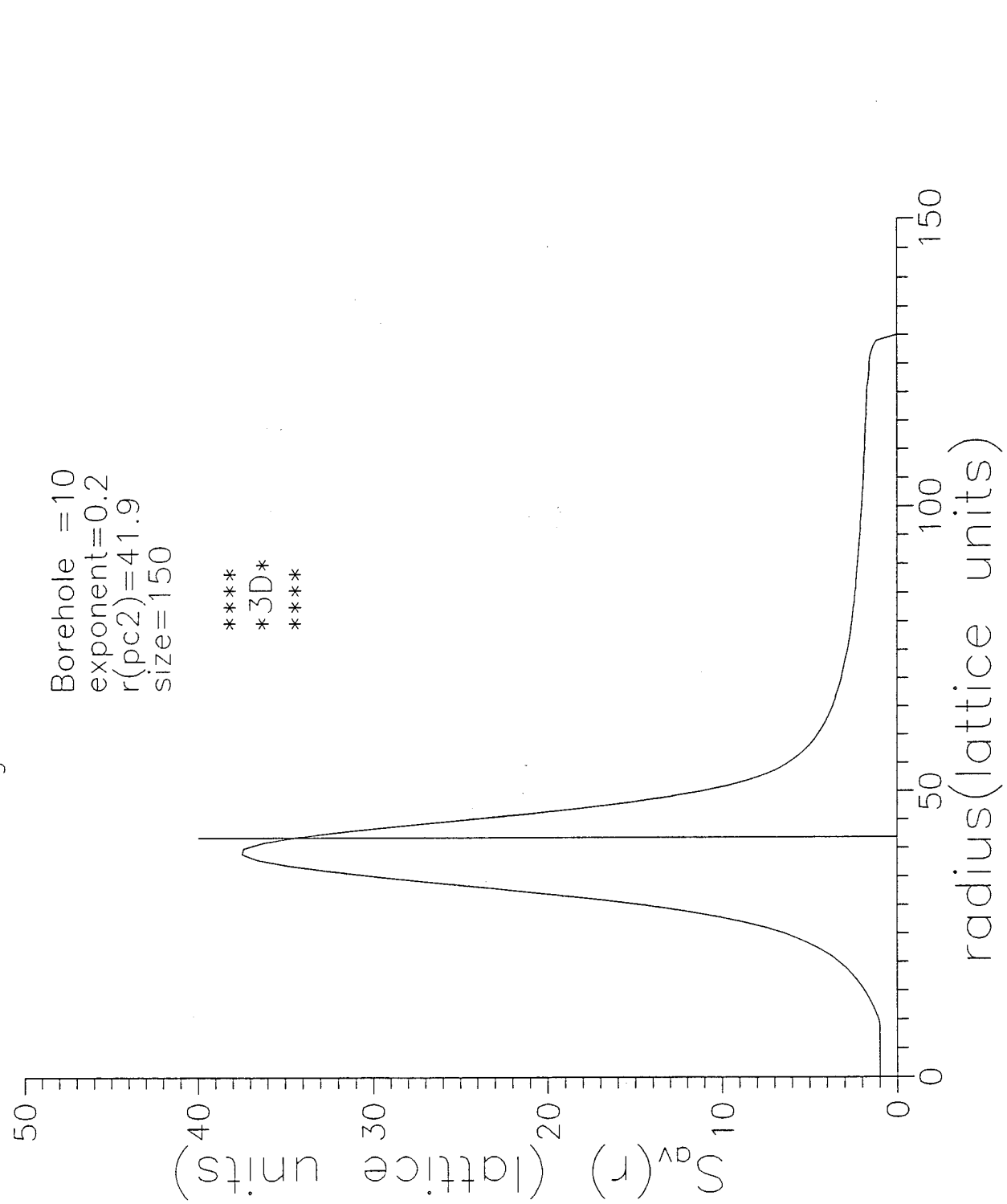
Cluster size vs. distance from origin
Average over 200 realizations
Borehole =10
exponent=0.2
r(pc2)=41.9
size=150
****
3D
****
$S_{av}(r)$ (lattice units)
radius(lattice units)
0
10
20
30
40
50
0
50
100
150

Figure 3

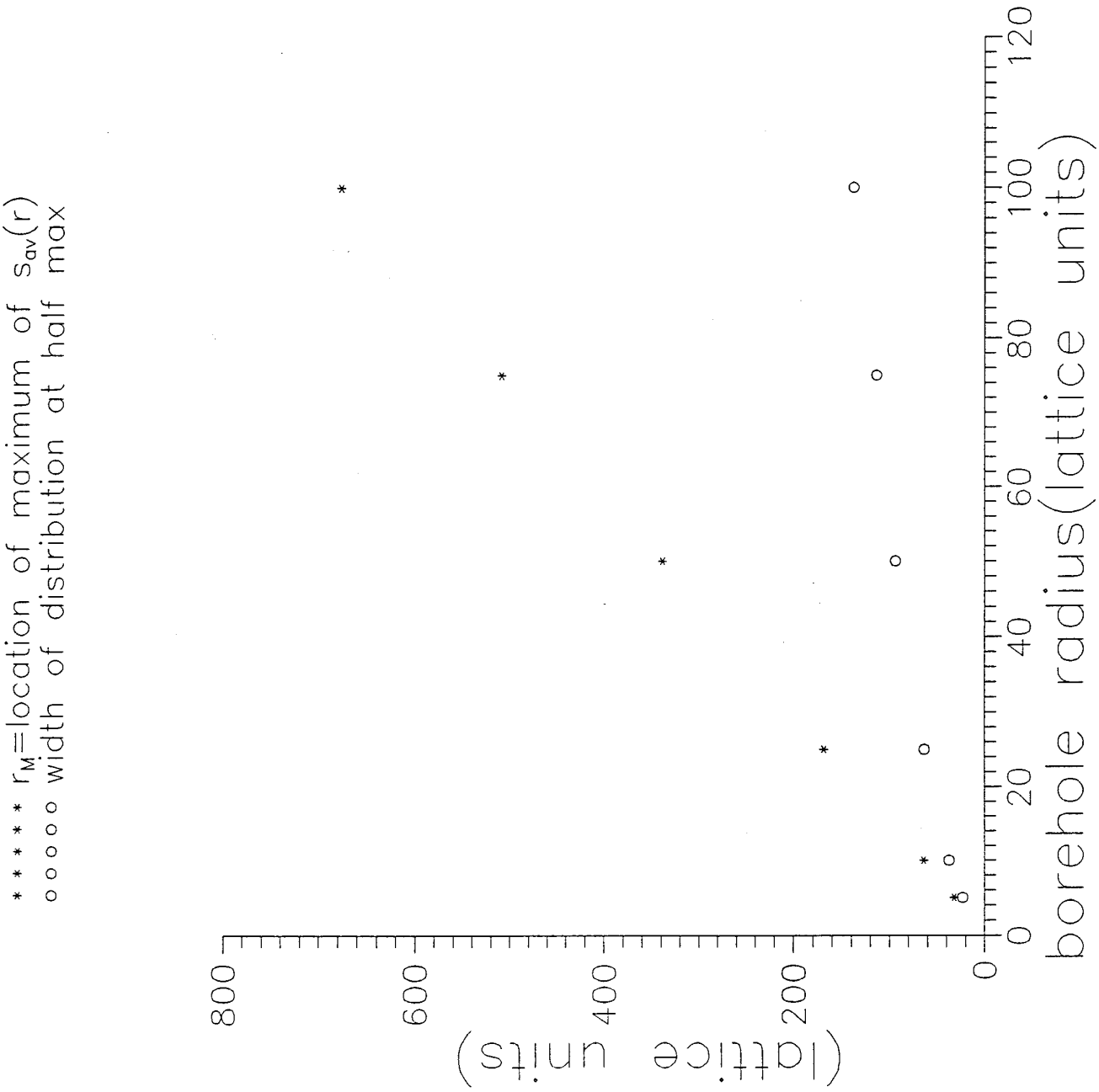
* * * * * r_M=location of maximum of $s_{av}(r)$
o o o o o width of distribution at half max
(lattice units)
0
200
400
600
800
0
20
40
60
80
100
120
borehole radius(lattice units)

Figure 4

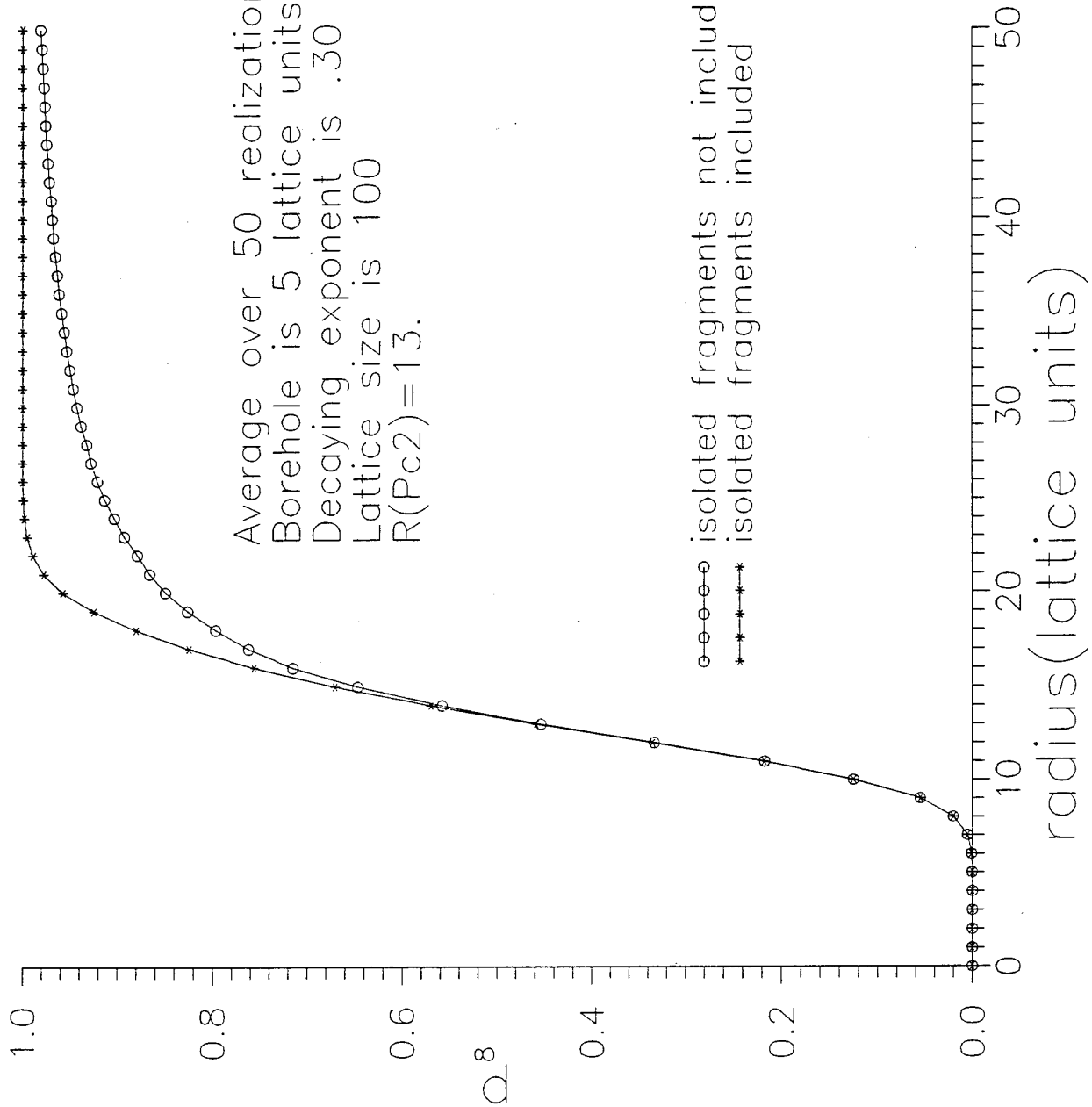
Average over 50 realizations
Borehole is 5 lattice units
Decaying exponent is .30
Lattice size is 100
R(Pc2)=13.
isolated fragments not included
isolated fragments included
Ω^8
radius(lattice units)
0.0
0.2
0.4
0.6
0.8
1.0
0
10
20
30
40
50

Figure 5

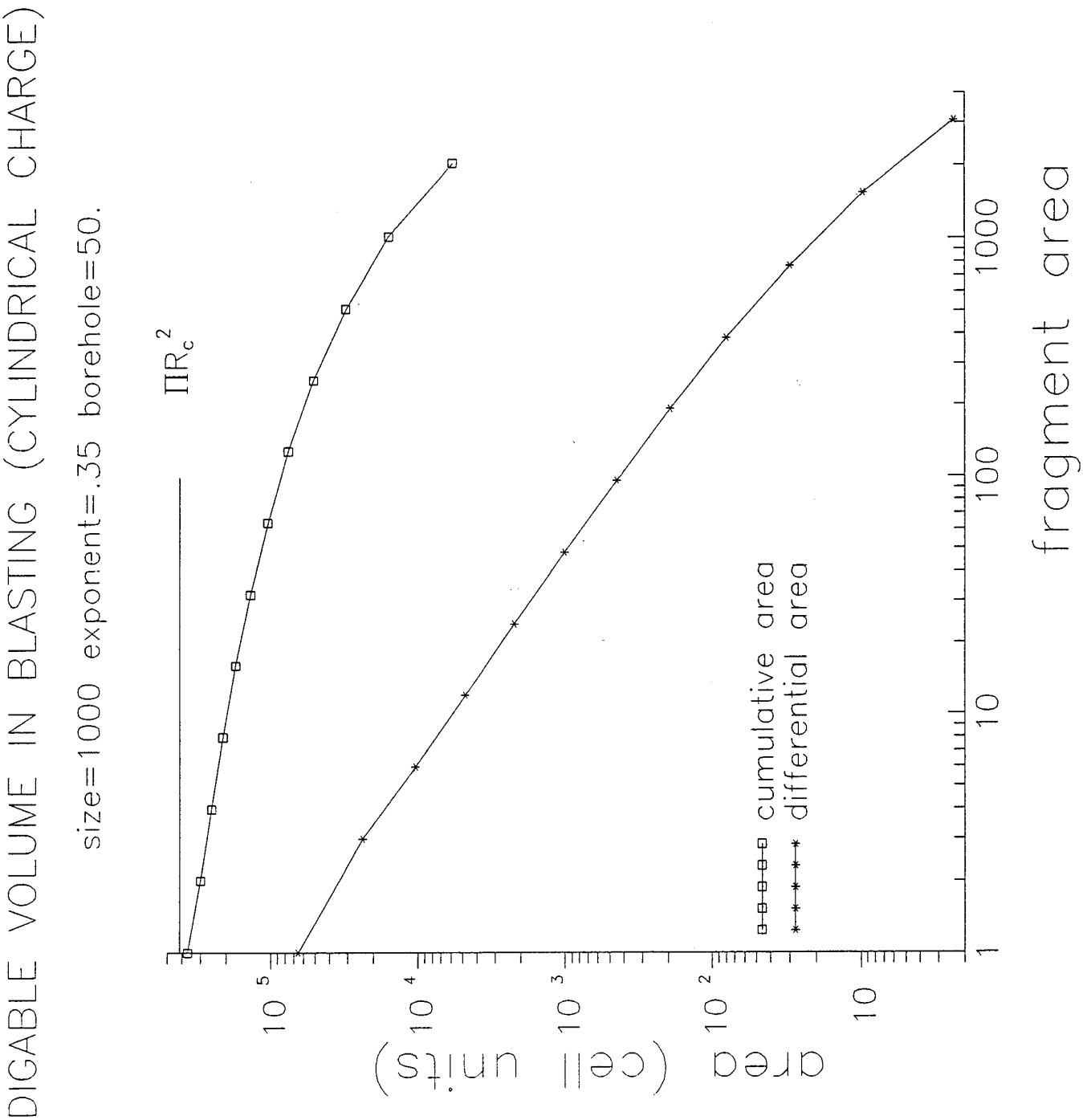
DIGABLE VOLUME IN BLASTING (CYLINDRICAL CHARGE)
size=1000 exponent=.35 borehole=50.
ΠR_c^2
area (cell units)
10^5
10^4
10^3
10^2
10
1
10
100
1000
fragment area
cumulative area
differential area

Figure 6

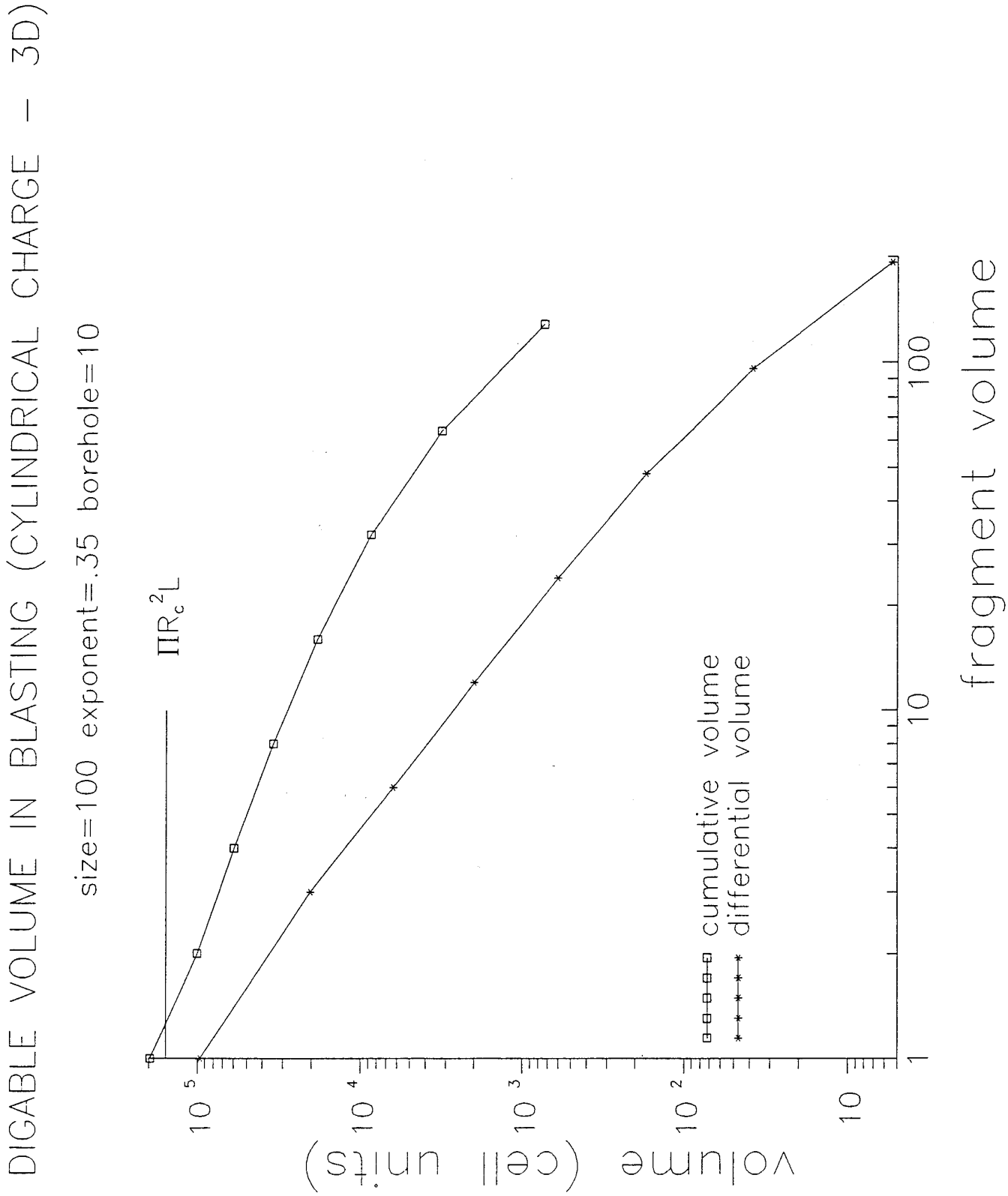
DIGABLE VOLUME IN BLASTING (CYLINDRICAL CHARGE - 3D)
size=100 exponent=.35 borehole=10
$\Pi R_c^2 L$
volume (cell units)
10^5
10^4
10^3
10^2
10
1
10
100
fragment volume
cumulative volume
differential volume

Figure 7

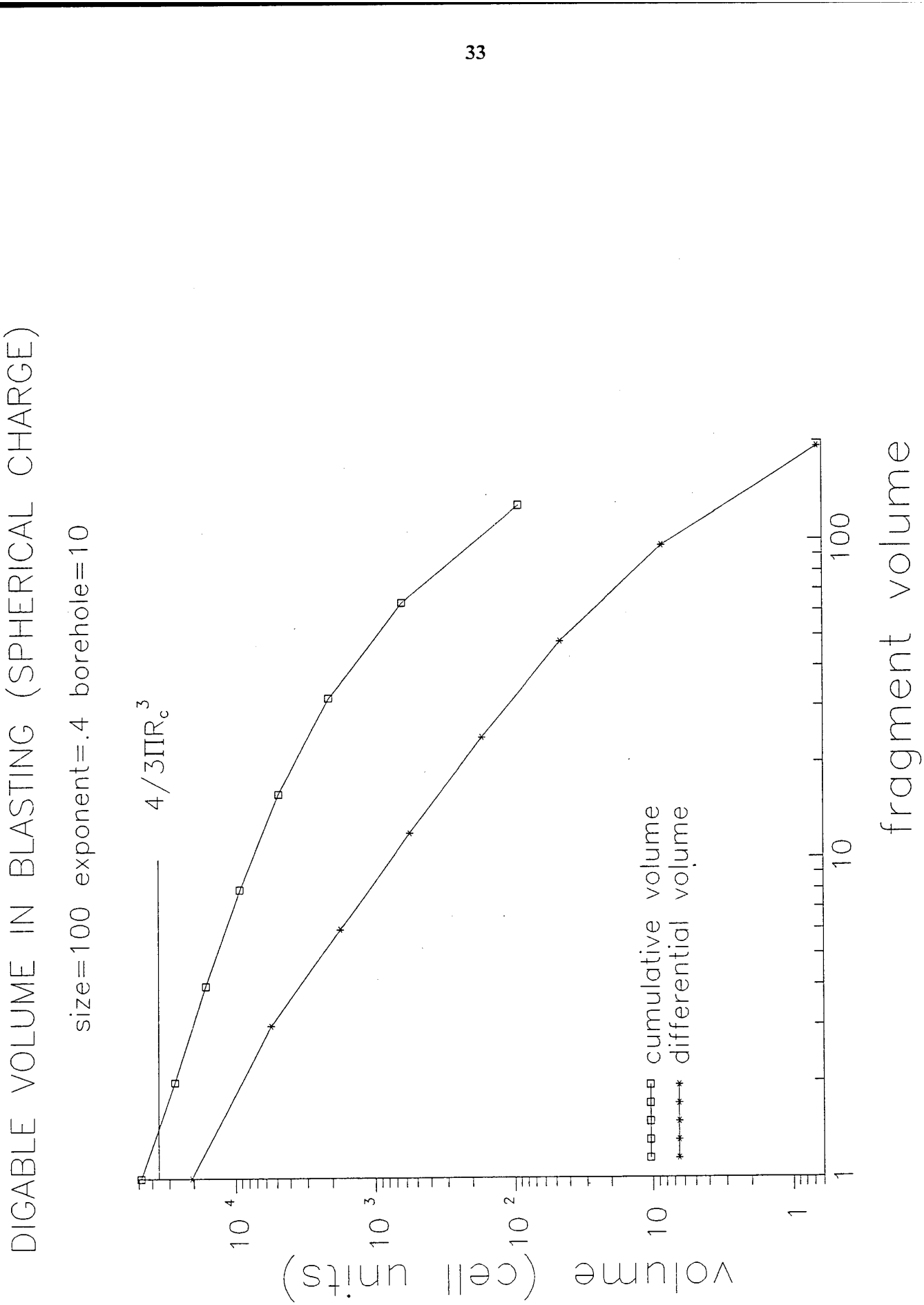
DIGABLE VOLUME IN BLASTING (SPHERICAL CHARGE)
size=100 exponent=.4 borehole=10
4/3ΠR_c^3
cumulative volume
differential volume
volume (cell units)
fragment volume
10^4
10^3
10^2
10
1
1
10
100

Figure 8

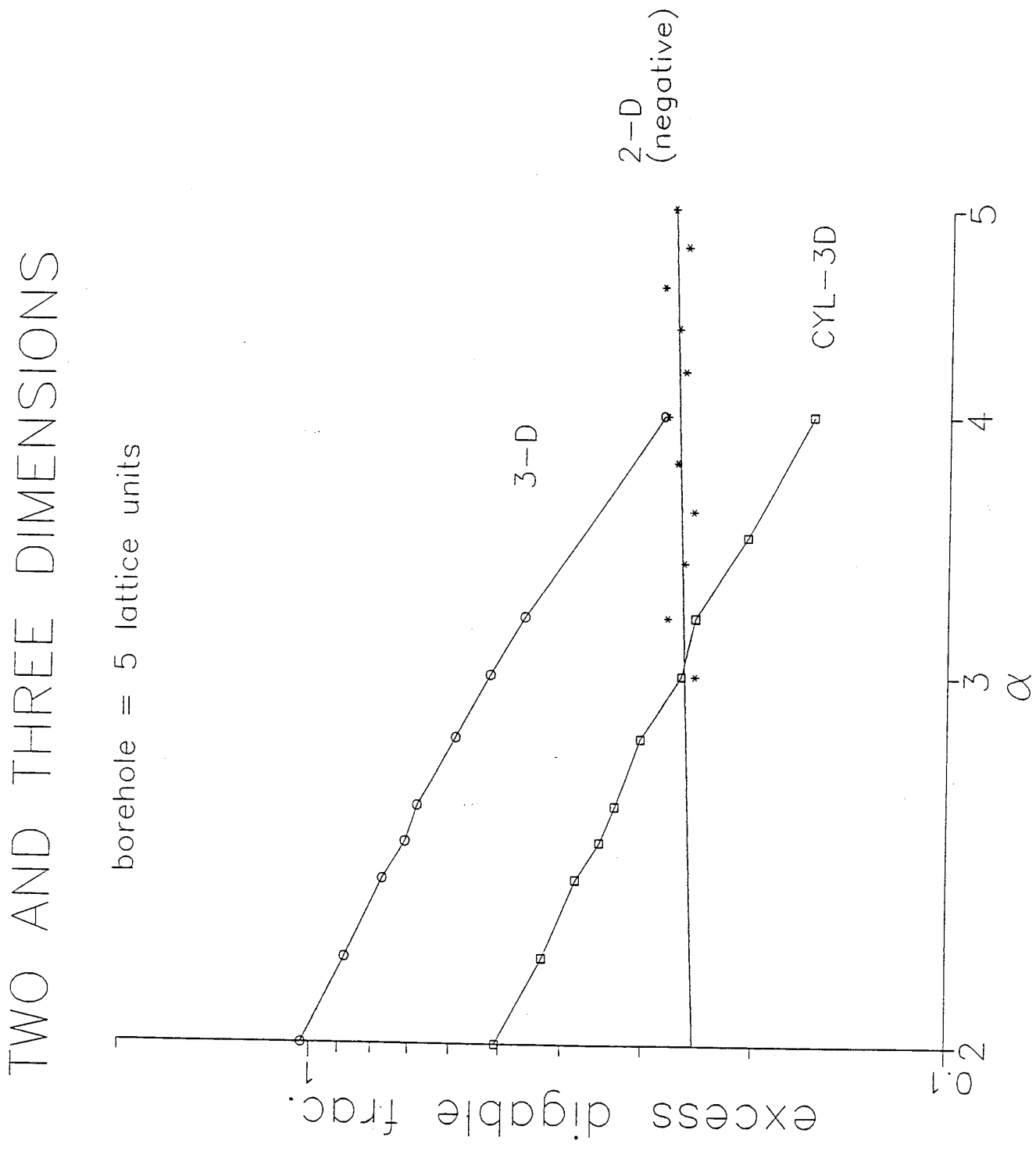
TWO AND THREE DIMENSIONS
borehole = 5 lattice units
excess diggable frac.
1
0.1
2
3
4
5
α
3-D
2-D
(negative)
CYL-3D

Figure 9

PART 3

Impact of Fiber Composite Laminate Plates: A Percolation View of Perforation and Spallation

Zeev Jaeger[1], Micha Anholt[1], and Arnold H. Mayer[2]
1 Soreq Nuclear Research Centre, Yavne, Israel
2 Wright Laboratory, WPAFB, OH

Abstract

In a series of impact experiments on composite plates which were aimed at testing the conjecture that the perforation threshold represented a critical phenomenon and that Percolation Theory could eventually provide an adequate description of the spallation or fragmentation process accompanying the perforation of anisotropic layered materials, the fragments emerging from a 0/90 layup fiber epoxy plate target were collected and photographed. Image analysis techniques were used to deduce the size distribution of the backside fragments. It was found that the number N of fragments having area S may be represented as a power law $N \sim 1 / S^{J}$. The average exponent for the experiments which were performed at nine different values of impact velocity over the range from 300 to 6000 fps had the value $J = 2.17 \pm 18\ \%$, which lies between the previously predicted theoretical values from Percolation Theory of $J(2D) = 2.05$ and $J(3D) = 2.2$. For the velocity $V_1 = 397$ fps which is close to the perforation threshold velocity, J had the value 2.03, which is surprisingly close to the two dimensional Critical Percolation Limit.

Introduction

The mechanical properties of a composite are severely degraded by impact induced damage. A significant fraction of the projectile kinetic energy is channelled into rival modes of damage, i.e. delamination, fiber fracture, matrix cracking and fragmentation. Some disintegration appears around and inside the penetration hole, and at the backside of the target spall is produced even at velocities less than the ballistic limit. More energy is consumed above this limit, as intense fragmentation emerges from the target. This process may be studied quantitatively by measuring the fragment size distribution.

Under a short impulse of pressure, a situation typical of either an impact or an explosion is created. The stress acts in a local way and is "unable" to scan the medium for its weakest points. Therefore, many cracks grow simultaneously and independently in different regions of the target. These conditions lead to the well known result (4) that the average fragment size becomes smaller the higher the strain rate.

Moreover, they provide the physical justification for using percolation theory in predicting fragment size distributions. (2,3)

Percolation theory (1) has been recognized as a statistical physics model for critical phenomena. By applying it to fracture and fragmentation problems we were able to show that fragmentation (as well as the coalescence of many microcracks forming a macroscopic fracture) is a critical phenomenon. Fragmentation occurs whenever the density of cracks reaches its critical value. That is to say, that when the probability, p, of creating a microcrack achieves the critical value, p_c. For crack densities higher than p_c, the critical density of microcracks, the number of small particles in the population grow at the expense of the reduction of the number of large ones. Consequently, the total surface area of the fragments is growing. It is therfore, expected, that the minimal surface energy required for fragmentation is received at p_c (below p_c a complete shattering of the finite macroscopic piece of material is not possible).

Coming back to impact physics, the determination of the limit velocity below which perforation of a given target by a given projectile is not possible continues to be of much interest. Even the definition of the ballistic limit (5) (the critical value of striking velocity at which the probability of perforation is 50%) suggests that stochastic mechansms are at play. Below the ballistic limit, it is expected that the spalled fragmented zone at the backside of the sample and the shattered and penetrated zone in the front side will be well separated by a zone of delaminated material strong enough to prevent the projectile from perforating the target. In the limit as this intact zone becomes very thin, these two zones will touch each other, and the sample will then become disintegrated throughout its thickness. It is of interest to inquire whether the critical condition for fragmentation supplied by percolation theory is able to yield additional information about the ballistic limit and the physical conditions of its occurrence.

Image Analysis

The population of fragments from each experiment was collected on the inner surface of a cylindrical sheet of paper coated with a sticky adhesive. After the experiment, the cylinder was rolled flat and photographed. Such a procedure has to be carried out with caution in order to avoid any optical noise resulting from shadows, unequal illumination or spurious particles.

The photographs were scanned and a digitized image was obtained. The next step is the division of the digital image into clusters of material (fragments) and the background. This procedure is not easy when the gray levels of the fragments and local background overlap. Also, it is not easy to distinguish two fragments partially overlapping each other. Special data treatments were adopted to reduce distortion and deterioration of the information recorded in the digital picture, which was scanned by a 512 X 512 black and white scanner. Higher resolution of the original photograph, of course, will result in higher final resolution and consequently more data on possible lost information with regard to the very fine fragments.

The measured fragment size histograms vary continuously in an irregular way. In order to overcome the effects of random fluctuations, the results were accumulated in bins having unequal width. Each bin further along on the size axis was made twice as large as the preceding one. The total number N of occurences in a bin was divided by the bin width, to obtain the average distribution density of size S. A linear least squares fit of log N against log S was performed in order to deduce the parameters of the expected power law relationship.The results are presented in Figure 1. The slopes and intercepts of the linear fits are presented in Table 1 for each velocity.

The role of strain rate in controlling fragmentation was recognized by Grady [3] in the early eighties. The highest strain-rate found during an impact may be estimated by the ratio of the projectile to its radius, $de/dt \sim V_p / R_p$. Strain rates at the backface may be estimated by multiplying this value by some attenuation function for the particle velocity. In any case, it is expected that the higher the impact energy is, the smaller will be the average fragment size. It is not surprising therefore that the trend of intercepts in Table 1 really represents the fraction of fine particles in the distribution. The behavior of the slopes needs further consideration. The mass of a fractal structure having a length L (L>>1) is given by $M(L) \sim A L^D$ where D is the fractal dimension. At the critical point, $p = p_c$, the value of D is known. For homogeneous percolation in the plane, D = 1.9 (2D). In three dimensional space D = 2.5 (3D). An additional result of percolation theory [1] is that the number n_s of clusters having s sites (per site) is given by $n_s \sim 1 / S^{\tau}$, where $\tau = (d+D) / D$, and where the exponent τ has the value $\tau = 2.05$ in two dimensions and J= 2.2 in three dimensions (d=3). All the slopes in Table 1 are around these values with an error not exceeding about 20%. Furthermore, in the introduction, a possible relation between the perforation threshold and critical fragmentation was conjectured. The lowest velocity in Table 1 is not far from the perforation threshold found experimentally [6], namely V_0 = 375 fps. The slope of the corresponding fragment size distribution is extremely close to the theoretical value of J for the two dimensional case. If the fragments of the impacted composite plate have a fixed thickness (as would be the case if it they resulted from the fragmentation of previously delaminated plies), then the measured area distributions would represent, in fact, two dimensional mass distributions. In a laminated material with planar weaknesses between the plies, such a hypothesis appears plausible. In general isotropic solids, a true three dimensional behaviour is expected with $\tau = 2.2$. It is interesting to check whether fragment size distributions from impacted brittle soldis also behave in the same way near the perforation limit. More work is needed in order to correlate other statistical Physics features either with dynamical predictions or with experimental data.

References

(1) D. E. Grady, J. Appl. Phys. 53,322 (1982)

(2) R. Englman, N. Rivier and Z. Jaeger Phil. Mag B56, 751 (1988)

(3) M. Anholt, R. Englman and Z. Jaeger, "Percolation Approach to Locally Caused Fragmentation", Centre de Physique, Les-Houches, France, D. Beysems et. al. Eds, April 12-17 1993

(4) D. Stauffer "Introduction to Percolation Theory", Taylor and Francis, London 1985

(5) J. A. Zukas, "Penetration and Perforation of Solids", chap.5 in "Impact Dynamics", J. A. Zukas, T. Nicholas, L. B. Gresczuk and D.R. Curran Eds, Wiley N.Y. (1982)

(6) G. J. Czarnecki, "A Preliminary Investigation of Dual Mode Fracture Sustained by Graphite/Epoxy Laminates Impacted by High Velocity Spherical Metallic Projectiles" MS Thesis, University of Dayton, OH (1992)

No.	Velocity (ft/sec)	Slope	Intercept
1	397	-2.03	1.88
2	696	-1.94	2.28
3	697	-1.86	2.02
4	994	-1.58	1.83
5	1981	-2.29	2.70
6	3200	-2.47	2.77
7	3691	-2.62	2.77
8	4954	-2.57	2.99
9	5877	-2.58	3.00

Table 1,a: Number n(s) of fragments having area s is a power law: $n(s) = A\ s^{-\tau}$. Slopes and intercepts of the least square best line: Log n versus Log s, for 9 impact velocities on (0°/90°) (fiber oriented) composite. Slope extrapolated to near the ballistic limit equals to -2.1.

No.	Velocity (ft/sec)	Slope	Intercept
1	398	2.28	316
2	1092	2.15	49
3	1967	2.45	792
4	2008	2.40	580
5	3148	2.69	861
6	4159	2.63	817
7	4902	2.87	1472
8	5939	2.66	1181

Table 1,b: Number n(s) of fragments having area s is a power law: $n(s) = A\ s^{-\tau}$. Slopes and intercepts of the least square best line: Log n versus Log s, for 9 impact velocities on (0°/45°) (fiber oriented) composite. Slope extrapolated to near the ballistic limit equals to -2.2.

PART 4

15th International Symposium on Ballistics, Jerusalem, Israel 21-24 May 1995
Post deadline paper

THE BALLISTIC LIMIT OF LAMINATED CARBON FIBER EPOXY PLATES AS A CRITICAL POINT IN PHASE TRANSITION

A. H. Mayer
Assistant for Research & Technology
Vehicle Subsystems Division
Flight Dynamics Directorate
Wright Laboratory
Wright Patterson Air Force Base, OH 45433, USA

Z. Jaeger and R. Englman
Applied Physics & Mathematics Department
SOREQ Nuclear Research Centre
Yavne, Israel 81800

From steel ball impact on laminated composite (carbon fiber reinforced epoxy matrix) plates we have obtained the hole and delamination areas, total ejecta masses and ratio of residual-to-initial velocities as functions of V_1-V_c, the initial velocity (V_1) less the threshold penetration velocity (V_c, the ballistic limit). The power-law nature of the dependencies and the observed exponents, both below and above V_c, indicate that plate penetration occurs as phase transition whose critical point is V_c. We found that the energy absorption displays cusp-like behavior and projectile velocity ratio variation approaches universal power-law dependence typical of the order parameter. Confirmation of a critical behavior is that the ejecta masses distribute close to the inverse 2.2 power of the size, as in a percolation process.

I. BRIEF SUMMARY OF CRITICAL PHENOMENA

Examples of critical continuous phase transitions (Ma 1976, Callen 1985) include the phase change from liquid to a vapor at the critical pressure and temperature, and the vanishing of the magnetization of a ferromagnetic material at zero magnetic field as its temperature is raised past the Curie Temperature. In the case of the former, it has been observed that large fluctuations of density develop which increase with approach to the critical temperature. The fluctuation phenomenon may be observed visually as the appearance of a critical opalescence or opaque cloudiness of the fluid at the critical point itself. The opalescence is due to the presence of bubbles of almost all sizes in the liquid that scatter light of all wavelengths. This broad range of sizes requires the dependence of the distribution on a power law of the distance from the critical point and, indeed, around the critical point, the difference between the mean densities of liquid and vapor have been measured to vary as a power law function of the temperature interval to the critical temperature, with a non-integral value for the exponent of the temperature difference variable. The magnetization has a similar behavior, with the quite astonishing similarity that the exponents of the power law variations with the temperature of these two phenomena are almost indistinguishable to within experimental accuracy (Goldenfeld 1992). The density difference and the

magnetization thus vary with temperature difference from the critical temperature as follows: $\rho_f - \rho_g = C\,(T - T_c)^{0.357\pm0.006}$, $M = C'(T - T_c)^{0.311\pm0.005}$.

The above facts lead to the following general statements:

i) Fluctuations of properties increase in the vicinity of the critical point. The spatial extent of the fluctuations are quantified by a reference length (correlation length) ξ.

ii) A quantity called an order parameter exists which is non-zero on one side of the critical point and vanishes on the other side. The magnetization is such an order parameter for the Curie Point of ferromagnetic phenomena. The liquid-vapor density difference plays the role of order parameter for fluid systems.

iii) Material properties obey power laws with respect to the distance from the critical point. The specific heat at constant volume is singular at the critical point and displays a cusp-like variation on either side of the critical point.

iv) The exponents in the power law dependence of various thermodynamic quantities on the temperature difference to the critical temperature have been conventionally given certain lower case Greek letters, as follows. The order parameter: $M \propto (T_c - T)^{\beta}$, The specific heat at constant volume: $C_V \propto |T_c - T|^{-\alpha}$, The correlation length: $\xi \propto |T_c - T|^{-\nu}$. Experimentally determined values for these exponents for various systems were published in the literature (Goldenfeld 1992).

v) The critical (universal) exponents are interrelated by algebraic relationships of the following typical forms. As a consequence of these relations, only two of the critical exponents are independent, the remaining ones being deducible from these two. As examples we cite the Rushbrooke relation: $\alpha + 2\beta + \gamma = 2$ and Widom relation: $\gamma = \beta(\delta - 1)$ where δ is another critical exponent.

vi) Mean Field Theory has not been successful in exactly predicting the critical exponents. Accepted modern computational approaches for computing the critical exponents utilize the methods of the Percolation Theory or the Renormalization Group Theory (Creswick et al. 1992). For the Ising Model universality Class of Phase Transitions, renormalization group techniques give the following values for the critical exponents: β = 0.325, α = 0.125 while three dimensional Percolation Theory for a cubic lattice gives: β = 0.4038. Results of various types of theoretical computations for the critical exponents are summarized in the literature (Stauffer 1985).

II. DESCRIPTION OF THE EXPERIMENTAL PROGRAM

The experimental program consisted of firing one-half inch diameter spherical steel projectiles at carbon fiber epoxy matrix composite plates which were clamped between steel plates containing a 3 inch diameter circular hole with the design impact point located at its center. The composite target plates were 32 plies thick, Stacking arrangements consisting of combinations of 0, 90° and ±45° fiber orientations and also in balanced spiral staircase layups in which the fiber direction increased in increments of 90, 45, 22.5 or 11.25 degrees from ply to ply. Ten inch diameter plastic cylinders with axes coincident with the shotline were lined with adhesive paper and placed flush with the front and rear target support plates in order to catch spall fragments emanating from the target plate. Circular end plates containing a small central hole to permit uninterrupted passage of the projectile were also covered with adhesive paper to catch fragments travelling with velocity vectors contained within a small cone of the axis. The population of fragments from each experiment was photographed and scanned in order to form a digitized image. Fragment size histograms were obtained by using image processing techniques.

Projectile velocity was measured ahead of the target plate by means of a set of fine trip wires of known separation distance and by noting the instants of the break of electrical continuity and behind the target by two sets of induction coils of known location along the pipe axis which were wrapped around the outer cylindrical surface of the plastic pipe. Thus the energy imparted by the projectile to the target material could be computed (Fig. 1). Some experiments were performed without the adhesive paper and the loose fragments collected in the plastic pipe were swept together and weighed and compared with the weight loss of the target plates (Fig. 2). A single set of plates consisting of plates which had been penetrated at different velocities were stained with Gold Chloride, pyrolyzed in an air oven, deplied with a scalpel, mounted on a rigid backing and subjected to a measurement of the areas of the penetration hole and of the envelope of the surrounding gold-stained delaminated area. This was done with the aid of automatic image analysis equipment. It was thus possible to obtain the shapes and distribution of hole and delaminated areas on each ply of panels penetrated at different velocities over the range of 200 to 6000 feet per second (Lair 1991, Samad 1994).

III. THE BALLISTIC LIMIT AND CRITICAL PHASE TRANSITIONS

In ballistic impact the projectile closing velocity rather than the temperature plays the role of marker for the critical point of impact phenomena. We have therefore a ballistic limit velocity or penetration threshold velocity rather than a critical temperature, and closeness to the critical state is measured as a difference between the initial projectile velocity and that at the ballistic limit. (To emphasize the critical nature of the ballistic limit we prefer the notion V_c over the conventional one V_{50}) An explanation of the similarity between the initial projectile velocity and the temperature will be presented further on in this paper.

While critical points are a phenomenon of systems in thermodynamic equilibrium, most ballistic impact phenomena are considered to be dynamic phenomena which produce material states that are both irreversible and far from equilibrium. Certainly, gross states of fracture and fragmentation do not appear to have ever been observed to reheal themselves back into an unflawed continuum state. However, "reversibility" is not a necessary condition for phase transition (though critical fluctuations are, as a rule). An example for "irreversible" phase transition is a percolative process which is describable as one with an infinitely large activation energy in the reverse direction. More common phase changes, like in ferromagnetism or the Ising model, have microscopic (single site) activation energies that are of the order of the transition temperature.

Consider the trend of the damage and the energy transfer ratio, defined here to be the ratio of imparted to initial projectile energies, as the projectile velocity (or energy) is increased. At very low velocities, the projectile experiences a perfect, loss-free rebound from the panel and the transfer ratio remains at zero. As the velocity is increased beyond the damage threshold, a crater is produced in the panel, causing the transfer ratio to increase. With higher impact velocities, incipient spall first appears and the transfer ratio further increases. Below the ballistic limit, it is expected that the spalled fragmented zone at the backside of the sample and the shattered and penetrated zone in the front side (the crater) will be separated by an intact or delaminated layer of the material which is strong enough to prevent the projectile from perforating the target. In the limit (in fact, the ballistic limit) this intact layer becomes very thin and the two damaged zones will touch each other. That is to say, the sample will then become disintegrated throughout its thickness.

Percolation theory has been recognized as a statistical physics model for critical phenomena. By applying it to fracture and fragmentation problems, we were able to show that fragmentation occurs whenever the density of the microcracks reaches its critical value. That is to say, when the probability p of creating a microcrack achieves its critical value p_c. At and near this point, the number n of fragments (clusters) having size s (per site) behaves as $n \propto 1/s^{\tau}$, where the critical exponent τ has the value $\tau = 2.05$ for a two dimensional isotropic system and $\tau = 2.2$ for a three dimensional isotropic one. We have found (Murat and Anholt 1992) the value $\tau = 2.1$ for an anisotropic two dimensional system (having different crack probabilities in the x and y orthogonal directions). This is, therefore, the statistical physics predicted result for the fragment size distribution at the critical point, which is identified as the ballistic limit.

According to the U.S. Navy definition (Zukas 1982) of the ballistic limit, the residual velocity of the projectile is practically zero, thus producing a transfer ratio of unity. Any motion of the target is quickly damped out by the frictional resistance to motion presented by the internal fracture (Tamilvanan 1991). Beyond the ballistic limit, the energy transfer ratio decreased sharply because the projectile acquires an increasing residual velocity relative to its initial value. At intermediate velocities above the ballistic limit, the transfer ratio levels off to a small value which depends on and increases with the thickness of the target panel. In the present experiments which were conducted with 32 ply thick plates, the ratio corresponding to this plateau attained the value 0.2. At much higher velocities, the energy transferred divided by one half the projectile mass (E_m) varies as $E_m = CV_i^n$ [V_i = input velocity in ft/s $C = 1.33 \times 10^{-3}$ and $n = 1.49$ (Altamirano 1990)]. This causes the transfer ratio to decrease to zero asymptotically and inversely as the square root of the velocity. The variation of the transfer ratio around the ballistic limit (velocity or energy) gives it a cusp-like appearance centered at the ballistic limit (Figure 3). The first derivative of the transfer ratio increases to a finite bound from below at the ballistic limit, and experiences a discontinuity with a change in sign there to a finite negative bound from above, after which it increases rapidly to zero. The transfer ratio derivative at the ballistic limit resembles the behavior of the specific heat of a fluid at its liquid-vapor critical point

IV. EXPERIMENTAL SIZE DISTRIBUTION OF COMPOSITE FRAGMENTS

Our experimental investigation provides quantitative evidence that the ballistic limit represents a critical phenomenon. This evidence comes from the size distribution of the ejecta produced near the ballistic limit. The distribution density function for fragments of area s was found to decrease with s raised to a negative power. Results for several impact velocities for 0-90° fiber orientation are presented in Table 1. The experimental exponents are very close to the values found theoretically for fragment sizes obtained from two dimensional bond percolation on a square anisotropic lattice ($\tau = 2.1$) or percolation on a three dimensional lattice ($\tau = 2.2$) at the percolation limit (Jaeger, Mayer et al. 1993).

We interpret our results by supposing that the ejecta originate mainly from the target region adjacent to the projectile at the moment of passage. There and then, fracture conditions appropriate to the percolation limit obtain, which are reflected in the debris size distribution. Subsequently and elsewhere in the target, the crack density may exceed the percolation limit; the resulting fragments are not ejected and are not collected on the adhesive paper.

Similar conditions apply to other forms of fragmentation, when the target is not confined and lie probably behind the $s^{-2.2}$ law that appears to hold over several decades

of s in the space debris distribution (Englman 1991). Below the ballistic limit, the fragmenting materials of, and near, the projectile are confined by the target and the fragmentation occurs beyond the critical fragmentation limit (above p_c). For velocities above the ballistic limit (and p above p_c) it is expected to find many more fine particles (and less larger ones) in the distribution. These Percolation theory outcomes agree with the dynamical considerations relating the average fragment size with the strain-rate (Grady 1982).

V. ORDER PARAMETER & CRITICAL EXPONENTS

Critical phenomena may be characterized by an order parameter, which is zero on one side of the critical point but takes on a continuous range of non-zero values above the critical point. The order parameter either grows or decreases in accordance with the asymptotic power law form of the scaling hypothesis near the critical point with an exponent β. For critical phenomena belonging to the Ising Model class $\beta = 0.325$. For percolation on a cubic lattice $\beta = 0.4038$. For ballistic impact and penetration phenomena various parameters at first thought might be considered to be candidates for order parameters, namely final projectile velocity, the mass of spall or ejecta expelled from behind the target, and perhaps the volume of the hole punched out by the projectile. The degree of success with which each one of these was found to qualify by virtue of its exponent is discussed below. A numerical technique has been developed for simultaneously extracting the limiting exponent and the ballistic limit from the experimental data (Mayer, unpublished).

(a) Velocities Above the Ballistic Limit.

For data which were obtained with identical, quality controlled, fabricated panels, the residual energy fraction or square of the ratio of residual to initial the velocity was found to vary with distance to the ballistic limit raised to the 0.649 power. Thus, the velocity ratio will vary with one-half this exponent, or the 0.3245 power, which agrees closely with the critical exponent 0.312 of the order parameter for the Ising Model class in the two experimental examples discussed earlier which also belong to this class. The best simultaneous estimate of the V_c, the ballistic limit velocity was found to be 348 ft/s. The evolution of ejecta mass with velocity in the form of the scaling hypothesis yielded a value of 351 ft/s for the V_c and a value of 0.743 for the critical exponent. The ejecta mass and hole area depend on various factors of the observed energy and impact velocity. As shown in Table 2, ejecta mass and hole area exponents appear to be aberrant and display considerable variability. Velocity ratios show much less dispersion and approach the theoretical values for the order parameter to a satisfactory degree. Critical exponents for impact above the ballistic limit are recorded in Table 2.

(b) Velocities Below the Ballistic Limit

Here, analysis of data for rebound velocity and decreasing part of the delaminated area yielded exponents of 0.4467 and 0.8387 respectively. The exponent of the velocity ratio appears to be within 12% of the universal exponent for the order parameter as determined from the Percolation theory. We cannot relate the exponent of the delaminated area variation to any theory at this time. The results are presented in Table 2.

(c) Analysis

Denoting impact and residual quantities by 1 and 2 (respectively) and the absorbed energy by E_A, and its dimensionless form by $E_A^* = E_A / E_1$.

$$E_A = E_1 - E_2 = E_1\left\{1 - \left(\frac{V_2}{V_1}\right)^2\right\}$$

By the scaling hypothesis, and as confirmed experimentally near the $V_{50} \equiv V_c$,

$$\frac{V_2}{V_1} = C\left(\frac{V_1 - V_{50}}{V_{50}}\right)^{\beta} = CV_1^{*\beta}$$

Taking the derivative

$$\frac{dE_A^*}{dV_1^*} = \frac{dE_A^*}{d(V_2/V_1)} \times \frac{d(V_2/V_1)}{dV_1^*} = -2\beta C\frac{V_2}{V_1}V_1^{*\beta-1} = -2\beta C^2 V_1^{*2\beta-1} = C_2 V_1^{*-\alpha}$$

with α denoting the exponent of the specific heat C_V, is equal to $\alpha = -(2\beta - 1)$ by the Rushbrooke relation $\alpha + 2\beta + \gamma = 2$ provided $\gamma=1$, as in mean field theory. Notice that α yields the expected cusp like singularity. In the 3D Ising model and from experiments in many materials $\alpha \sim 0.110$. From our velocity ratio measurements $\alpha = 0.1218$ (Table 2). The fragment number data in Table 1 provide a further way to obtain critical exponents, through the susceptibility (χ) exponent γ. χ is identifiable with the second moment of s over sn(s) for all fragments up to fragment sizes of the correlation length ξ.

$\chi = \frac{\sum s^3 n(s)}{\sum sn(s)}$ for $s<\xi$. Since $\chi \propto \xi^{(4-\tau)}$ and $\xi \propto |T_c - T|^{-\nu}$, where $\nu = 0.89$ (in 3D), we obtain from $\gamma = (4-\tau)\nu$ and $\tau = 2.1$ (see Table 1) the value $\gamma = 1.69$. ($\gamma = 1.73$ in 3D percolation). The Widom scaling relation with $\delta = 4.8$ (from the 3D Ising model) gives $\beta = .44$ which agrees closely with several entries in Table 2, obtained directly from dynamic data (not from fragment distribution). α can now be derived from the Rushbrooke relation (without resorting to the mean field theory value for γ) to find $\alpha = -.44$, similar to the fragment mass entry, though differing from others. The exponent for 0/45 are gotten with a similar analysis.

VI. CONCLUSION

Though the exponents in Tables 1 and 2, both those directly observed and those calculated from models, show variations, they bear out the phase transition picture of plate penetration. Notably, the exponent β for the velocity ratio agrees in several cases with experimental and theoretical values for the order parameter in diverse thermodynamic systems.

In a brittle material like the epoxy matrix, a natural cause for the phase transition is the coalescence of microcracks coming from the crater and spall regions. It has been argued previously (Englman 1991, Anholt et al 1993) that in solids that are not confined, at the moment of fragmentation the crack densities attain their critical level. In impact this happens at the ballistic limit. The identification of the ballistic limit velocity V_c with a critical point lays open the field of ballistics to the theoretical apparatus of critical processes, including renormalization and finite size scaling.

VII. ACKNOWLEDGEMENTS

This work was supported in part by the U.S. Air Force Office of Scientific Research, under Contract No. 89-0374. We thank Prof. S. Alexander for a discussion. Further thanks are due to M. Anholt and S. Shwartzberg for image processing. We also acknowledge technical contributions to this work through experimental measurements

made at WPAFB, OH by Prof. D. Hui, University of New Orleans, and his students, M. Altamirano, J. Lair, S. Maryala, M. Samad and V. Tamilvanan.

REFERENCES

1. Altamirano, M. M.Sc Dissertation, University of New Orleans, LA, August 1990.
2. Anholt, M., Englman, R., Jaeger, Z., "Percolation Approach to Locally Caused Fragmentation", Centre de Physique des Houches Workshop on Fragmentation Phenomena, 12-17 April 1993, Editor: D. Beysems.
3. Callen, H. B., "Thermodynamics and an Introduction to Thermostatistics", John Wiley and Sons, Inc., New York, NY, 1985.
4. Creswick, R. J., Farach, H. A., Poole, Jr., C. P., "Introduction to Renormalization Group Methods in Physics", John Wiley & Sons, Inc., New York, 1992.
5. Englman, R., J. Phys. Condensed Matter 3 (1991) 1019.
6. Goldenfeld, Nigel, "Lectures on Phase Transitions and the Renormalization Group", Addison-Wesley Publishing Company, Reading, MA, 1992.
7. Grady, D. E., J. Appl. Phys., 53, 322 (1982).
8. Jaeger, Z., Mayer, A. H., Anholt, M., Samad, M., Applicability of Percolation Theory to Prediction of Ballistic Limits of Carbon Fiber Epoxy Composite Plates, Composites Engineering Conference, New Orleans, LA, 1993.
9. Ma, Shang-keng, "Modern Theory of Critical Phenomena", Addison-Wesley Publishing Company, Redwood City, CA, 1976.
10. Samad, M., M.Sc Dissertation, University of New Orleans, LA, August 1994.
11. Stauffer, D., "Introduction to Percolation Theory", Taylor and Francis, London 1985.
12. Tamilvanan, V.J, M.Sc Dissertation, University of New Orleans, LA, August 1991.
13. Zukas, J. A, "Penetration and Perforation of Solids", Chap. 5 in "Impact Dynamics", J. A. Zukas and T. Nicolas (Edits.), John Wiley & Sons, Inc., NY, 1982.
14. Lair, J. Unpublished results, 1991.
15. M. Murat and M. Anholt, "Fragment size and shape distributions in 2D anisotropic percolation", in "Damage in Composite and Other Advanced Materials Treated by Percolation Theory", R. Englman, Z. Jaeger and M. Murat, Annual Technical Report, Grant AFOSR-89-0374, July 1992.

No.	Velocity (ft/sec)	Slope	Intercept
1	397	-2.03	1.88
2	696	-1.94	2.28
3	697	-1.86	2.02
4	994	-1.58	1.83
5	1981	-2.29	2.70
6	3200	-2.47	2.77
7	3691	-2.62	2.77
8	4954	-2.57	2.99
9	5877	-2.58	3.00

Table 1: Number n(s) of fragments having Area s is a power law: $n(s) = A\, s^{-\tau}$. Slopes and intercepts of the least square best line: Log n versus Log s, for 9 impact velocities on 0-90° (fiber oriented) composite. Slope extrapolated to near the ballistic limit equals to -2.1

Balanced Layup	0/90	0/90	0/90	0/45	0/45	0/45	0/90/45/-45	0/90/45/-45	0/90/45/-45	0/90	0/45
Measured Quantity	Vel Ratio	Vel Ratio	Delam Area	Vel Ratio	Vel Ratio	Frag Mass	Vel Ratio	Frag Mass	Hole Area	Size Dist.	Size Dist.
Parameter Type	Order	Order	Unknown	Order	Order	Order	Order	Order	Order	Order	Order
Relation to V50	Below	Above	Below	Below	Above	Above	Above	Above	Above	Above	Above
Value of V50, ft/s	335	335	335	350	376	348	348	351	350	366	375
Exponent β	0.4391	0.3316	----	0.3368	0.3160	0.2608	0.3245	0.743	0.425	+0.44*	+0.42*
Exponent α	0.1218	0.3368	----	0.3264	0.368	0.4784	0.3510	-0.486	0.150	-0.58*	-0.44*
Exponent τ										2.1	2.2
Exponent			0.8387							----	----
Quality of Data	High	High	Medium	High	Medium	Medium	Medium	Low	High	High	High

* See discussion in Section V(c).

Table 2
Summary of Ballistic limit and critical exponents values deduced from measurements.

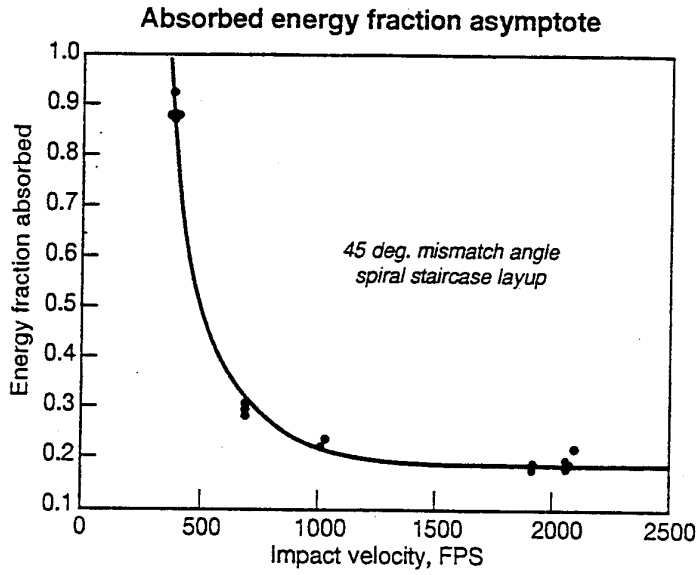

Fig 1. Energy Fraction Absorbed Versus Impact Velocity

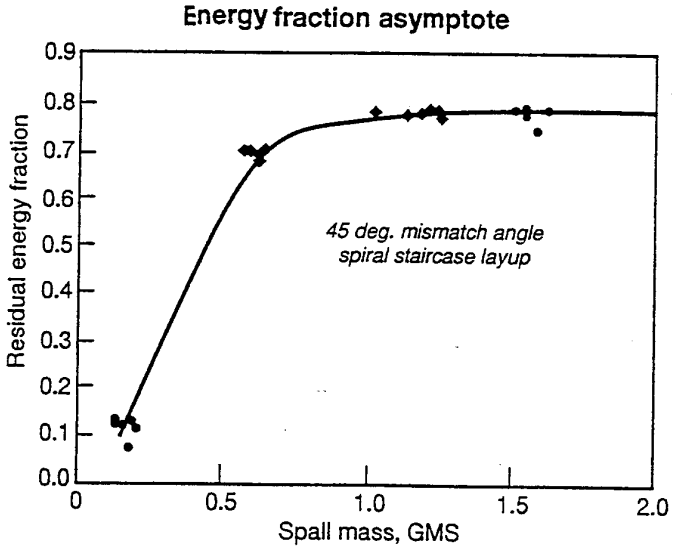

Fig 2. Residual Energy Fraction Versus the Spalled Mass.

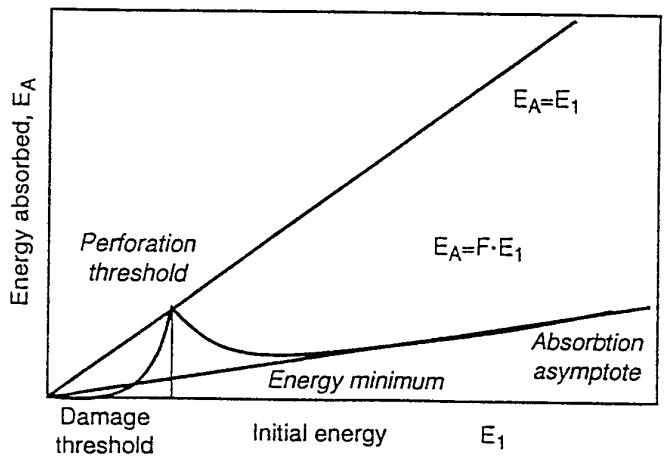

Fig 3. Absorbed Energy vs. Initial One.

PART 5

MAXIMUM ENTROPY PRINCIPLES IN FRAGMENTATION DATA ANALYSIS

R. Englman

Soreq N.R.C., Yavne 70600

Israel

Abstract

As a first topic the article treats observationally obtained distributions of fragment sizes and shows that to derive conservation laws for the fragmentation process one has to compute the information entropy S and then obtain the changes in S when the conserved quantities are varied by varying the experimental conditions. The criterion for the existence of conservation laws is the equality between the S-derivative and the Lagrange multiplier in the Maximum Entropy distribution, coupled to the non-vanishing of the determinant formed out of the second derivatives of S. Application of the method to ballistically created rock pieces indicates conservation of the average of log (fragment-size) in the break-up process.

The other topic is the distribution of broken bonds (as function of their length l) in a random 2D network, fragmented by pulling. (The numerical simulation was performed by Dr. M. Lemanska). The obtained distribution is in the form of a product of a prior distribution and an exponential function (the constraint factor of Maximum Entropy) whose exponent is linear in l. This is yet another case of the constraint factor being a simple function of the variable.

1. Introduction

It is widely thought that probability theory, laws of inference and predictive procedures are among the most debated of disciplines. They have been such since the days of the Bernoullis and have remained such up to the present in terms of fundamentals, in spite of remarkable technical advances in the use and manipulation of the rules [1-3]. Thus the acharned controversy between frequentists and Bayesians continues anabated, with each side holding to its position tenaciously.

The use of Maximum Entropy (ME) as a predictive tool shares the trait of being disputed in principle and effective in practice [2]. The formal apparatus of the method is briefly set out in Appendix 1. Stated in verbal language, the method predicts that the "best" probability p(s) for the occurrence of the value s for a variable is obtained by maximizing the information entropy, subject to constraints (see appendices and the next section for quantitative definitions). The method has been used in a wide range of subjects, e.g. statistical mechanics, molecular biology, pattern recognition.

The present author has applied the method to distribution of sizes obtained by a variety of fragmentation processes, where the issue was: supposing you know the constraints (regularities, conservation laws) on the distribution, what p(s) do you anticipate [4,5].

In this article we address ourselves to two issues of principle in the use of the ME method: First, given an empirical distribution p(s) what can you say about the regularities (constraints, laws) that underlie the processes which have led to the distribution. Secondly, we treat the question of priors (probabilities or weight that are attached to each event before receiving experimental information). Both subjects will be treated from the viewpoint of fragmentation, though their implications are far wider.

2. Deductions of and from Maximum Entropy

In this section we shall pose and discuss the following two questions (application will be given in section 3 and particular instances will be worked out in Appendix 2):

(i) If our fragmentation experiments have resulted in a distribution of sizes s in the form p(s), is there a way to establish that p(s) is a distribution with maximum entropy?

(ii) What information can be gleaned from a ME distribution?

The immediate answer to question (i) is in the negative: there is no way of learning from a single, experimentally derived distribution whether or not it is in accordance with ME. For suppose that experiments provide a set of numbers, e.g. by sorting about 10^4 fragments into $10^{1.5}$ bins representing sizes. Writing

$$\log p(s) = -g(s) - Q \tag{1}$$

(where Q is a normalizing constant) this has the "appearance" of a ME distribution, especially if g(s) has a simple form, like being linear in s, namely

$$g(s) = Gs. \tag{2}$$

It then appears natural to conclude that G is the Lagrange multiplier and <s> is the invariant for the distribution. However, this is illusory. To see this, we note that we can rewrite (2) as

$$g(s) = G_s = G_1(s-as^2) + G_2s^2 \quad (G_2 = aG_1)$$

$$= G_1(s-as^2) + G_2(s^2-bs^3) + G_3s^3 \quad (G_3 = bG_2)$$

and in many other ways that would indicate other invariants and multipliers consistent with the data. Therefore, to summarize, a single set of experiments cannot establish the ME nature of the distribution. To achieve this we have to perform the experiments repeatedly under different experimental conditions that will generate different distributions. The quantities that we wish to vary through varying the experimental conditions are primarily the averages and then the entropy S. The analysis is as follows:

Suppose that we suspect the logarithm of p(s) to be composed of several linearly independent functions $g_i(s)$, $g_r(s)$... $g_R(s)$. (R cannot be larger than the number of bins.)

$$g(s) = \sum_{r=1}^{R} G_r g_r(s) \tag{3}$$

We next compute the entropy and the averages

$$S = -\sum_{s} p(s) \log p(s) \tag{4}$$

$$\langle g_r \rangle = \sum_s p(s) g_r(s) \tag{5}$$

from the distributions that are obtained under several different conditions; in particular, under conditions that the averages $\langle g_r \rangle$ change infinitesimolly so that one can obtain the derivatives of S with respect to $\langle g_r \rangle$. For precision's sake we shall write the derivative in the form customary in Thermodynamics:

$$\left(\frac{\partial s}{\partial \langle g_r \rangle} \right)_{(\langle g_s \rangle,\, s \neq r)} \equiv G_r^* \tag{6}$$

with the averages in the subscript being kept constant.

We now assert and shall presently prove that p(s) is a ME distributions if and only if the entropy derivatives are all equal to the corresponding coefficients in the exponent, or

$$G_r^* = G_r \tag{7}$$

If these quantities are linearly independent functions of the averages, than the averages are invariants for the generation of distributions by experiment. If there are some linear relations between the G_r's, as functions of the means $\langle g_r \rangle$, then the invariant functions are superpositions of the g_r's. The simplest example of this is when, say,

$$(G_2^* =)\ G_2 = G_4\ (= G_4^*)$$

then an invariant function is h(s) where

$$g_2(s) + g_4(s) = h(s) \tag{8}$$

If the equality (7) is not achieved with the chosen set $g_1(s)_1 .. g_R(s)$, then one should choose other sets of g's to see whether (7) holds. Formally, one can expand the logarithm of p(s) in terms of complete sets, whose number of components cannot exceed the number of bins $\sim 10^{1.5}$, [6], but this seems to be prohibitively laborious. Clearly, we do not claim that the observed distributions are necessarily ME distributions.

However, if they are such, then eq. (7), can be proved as follows:

Let the experimental conditions be described by a set of constraints on the functions $g_r(s)$ so that their averages are given and equal to $<g_r>$. The ME distribution is

$$p(s) = e^{-\Sigma G_r g_r(s)} - Q \qquad (9)$$
$$= e^{-g(s)} - Q$$

having simplified by using (3). The normalizing constant is

$$Q = \log \sum_s e^{-g(s)} \qquad (10)$$

In (9) the coefficients G_r are so chosen as to reproduce the averages $<g_r>$. We assume that this can be done uniquely. (If not, we restrict our considerations to regions neighbouring the ME choice for the Lagrange multipliers G_r). A non-ME probability p(s) is represented by the same functions $g_r(s)$ whose averages are fixed by the values $<g_r>$ and an additional function $\delta g(s)$. To maintain values of $<g_r>$ as before the coefficients G_r change to, say, $\tilde{G}_r$. With adaptation of the notation in (3) we write

$$\tilde{g}(s) = \sum_r \tilde{G}_r g_r(s) \qquad (11)$$

and

$$\tilde{p}(s) = e^{-\tilde{g}(s) - \delta g(s) - \tilde{Q}} \qquad (12)$$

$$\tilde{Q} = \log \sum_s e^{-\tilde{g}(s) - \delta g(s)} \qquad (13)$$

Furthermore

$$S = \sum_r G_r <g_r> + Q \qquad \text{(ME)} \qquad (14)$$

$$\tilde{S} = \sum_r \tilde{G}_r <g_r> + <\delta g> + \tilde{Q} \qquad \text{(non–ME)} \qquad (15)$$

Differentiating first the expression (14) for the ME case

$$\frac{\delta S}{\delta <g_r>} \equiv G_r^* = G_r + \sum_m \frac{\partial G_m}{\partial <g_r>} <g_m> + \frac{\partial Q}{\partial <g_r>} \qquad (16)$$

However, from (10)

$$\frac{\partial Q}{\partial <g_r>} = -\sum_m \sum_s g_m(s) \cdot \frac{\partial G_m}{\partial <g_r>} e^{-g(s)} / \sum_s e^{-g(s)} \tag{17}$$

$$= -\sum_m <g_m> \cdot \frac{\partial G_m}{\partial <g_r>} \tag{18}$$

so that the last two terms in (16) cancel and eq. (7) is proven for a ME distribution.

In the entropy derivatives $\delta S/\delta <g_r>$ for a non-ME distribution two terms, corresponding to the last two terms in eq. (16), again cancel but one is left with a further term, as follows:

$$\frac{\delta \tilde{S}}{\delta <g_r>} = \tilde{G}_r + \frac{\partial <\delta g>}{\partial <g_r>} \tag{19}$$

The additional term in (15) can be rewritten as the covariance

$$\mathrm{cov}(g_r(s) - <g_r>, \delta g_{,r}(s) - <\delta g_{,r}>) \tag{20}$$

where the comma notation represents

$$\delta g_{,r}(s) \equiv \partial \delta g(s) / \partial <g_r> \tag{21}$$

and the differential operates on the coefficients $\tilde{G}_m$.

Though we have not been able to prove this rigorously, the cov are extremely unlikely to vanish for all the indexes r. Their vanishing would mean that the coefficients G_r are unaffected by the addition or the new function δg, while still maintaining the averages $<g_r>$.

We have thus shown that the entropy derivatives are equal to the corresponding coefficients in the probability exponent for a ME distribution and fail to be such in a non-ME distribution.

A corollary to the proof answers question (ii), in that the functions $g_r(s)$ for which (7) holds have invariant averages or, in other words, reflect some physical, geometrical, etc. law or constraint. The introduction of entropy-derivatives is a key step in the development.

The second derivatives of the entropy

$$\frac{\delta^2 S}{\delta<g_r>\delta<g_s>} \equiv S_{,rs}$$

are also important. It can be shown that if the determinant formed out of these derivatives vanishes identically as function of the averages, then a smaller number of the functions $g_r(s)$ can be found (by some linear superposition of the original functions) which form invariants. Thus the nonvanishing of the determinant

$$|S_{,rs}| \neq 0$$

is a further condition.

It is now possible to develop "Statistical Dynamical" formulae equivalent to the familiar thermodynamical ones. The conjugate variables in the latter (e.g., p and -v) are replaced by the twin set $\{G_r, <g_r>\}$ and the Legendre - transformed functions are:

$$S(\{<g_r>\}), Q(\{G_r\}) \tag{22}$$

connected by the relation (14) as functions of the averages [7]. Alternatively, as functions of the Lagrange multipliers

$$Q(\{G_r\}) = S[<g_n>(\{G_r\})] - \sum_n <g_n>(\{G_r\})\cdot G_n \tag{23}$$

where, on the right hand side, the averages have been expressed as functions of the multipliers G_r. The relations

$$\frac{\partial Q}{\partial G_r} = - <g_r> \tag{24}$$

complement the derivative relations

$$\frac{\partial S}{\partial <g_r>} = G_r \tag{25}$$

with which we have been busy.

Maxwell's relations take the forms

$$\frac{\partial G_r}{\partial \langle g_m \rangle} = \frac{\partial G_m}{\partial \langle g_r \rangle} \tag{26}$$

$$\frac{\partial \langle g_r \rangle}{\partial G_m} = \frac{\partial \langle g_m \rangle}{\partial G_r} \tag{27}$$

The equivalent of the Gibbs-Duhem relations is given by (17).

It has to be emphasized that the validity of these relations ("Statistical Dynamics") does not depend on an equilibrium (indeed the processes leading to the distributions can take place far from equilibrium), but only on the continuous variation of the data with the parameters of the experiment. (E.g., a continuous change of the outcome of a biased-coin tossing experiment with the height of the toss.) Occasionally continuity does not obtain: then we have the analogy of phase transitions which, however, are not treated here. What is important to note is that we work in a space (or sub-space) of the data base, without direct reference to the physical processes that generate the data.

3. Application in Target Ballistics

In experiments by Matsui et al. [8] projectiles of mild steel and of rocks having velocities between 17 and 270 m/s were made to impact on four kinds of rocks (tuff, basalt, granite and dunite) with various shapes and sizes. The size distributions of fragments were plotted for twenty target samples out of the 60 or so studied. (We emphasize these numbers to focus on our earlier assertion that a statistical analysis requires the availability of sets of data under different conditions, rather than a single set.) Their data are shown in figures 1(a) - 1(d) and a numerical representation is exhibited in Table 1. The authors of Ref. [8] fit their data to an inverse power-law dependence of distribution p on the size s relative to the total target size. In our terminology this has the form

$$p(s) = s^{-1} \exp(-G\log s - Q) \tag{28}$$

where Q is a normalizer, s^{-1} is the prior and G the Lagrange multiplier. In the choice of the prior we have followed Jeffrey's argumentation [9], based on the scale invariance of the distribution. The multipliers G (= α - 1 in the notation of [8]) are given in table 1; they are not constant but depend

mildly (logarithmically) on the kinetic energy of the projectile. For thoroughly fragmented targets G ranges between 1 and 2. (The values of G are close to the fractal exponents of Turcotte [10] found for a wide assortment of fragmentation processes). As shown in the previous section, the verification of (28) being a ME distribution is contingent to satisfying

$$\frac{\partial S}{\partial \langle \log s \rangle} = G \tag{29}$$

To form derivatives from numerical data we require data in which two values of <logs> are close. Inspection of Table 1 shows that there are four pairs of targets in which <logs> fall within .03 of each other. The following table (Table 2) shows that for three pairs (two in tuff and one in granite) equation (29) is satisfied to within ten per cent, while in the remaining pair (in basalt) the discrepancy is large (even the signs of the two members differ).

One might thus conclude that only in tuff and granite is the distribution that of ME, but not in basalt. In fact, however, the discrepancy in the last is due t o another cause: the minimum sizes (the lower cut-off) in B13 and B6 differ (column 4 in Table 2).

Now, the cut-off s_o can be incorporated in the ME formalism by a constraint of the form

$$\int H(s_o - s)\, p(s) ds = 0 \tag{30}$$

where H is the Heaviside step function. (The corresponding Lagrange multiplier is infinite). The differentiation in (29) implies [as in eq. (6)] the constancy of all other invariants (or invariance of s_o). It appears that violation of this requirement has led to the failure of satisfying equation (29).

In summary, then, the experimental data of Mitsui et al. are representable, by eq. (28), as ME distributions with the invariant being < logs>. It is not clear at this stage what it is in the physical process which brings about fragmentation that causes <logs> to be invariant. However, only very recently has a suggestion been made concerning a physical cause for self-similar distribution [11] and apparently much work needs to be done before relations between distributions and their governing processes will be established.

4. Priors and Simple Constraints

A source of difficulty in the use of ME are the priors Π(s) (described formally in Appendix 1). They are weights ascribed a priori (that is to say, without regard to observation) to each event and are analogous to "measure" in set theory. In the words of Skilling [2]: "The prior is the Lebesgue measure associated with [the variable], which must be given before an integral can be defined". An alternative, probabilistic interpretation identifies priors with subjective beliefs as regard to outcome of experiments or with relative reliance attached to different events. Only in quantum mechanics is the choice of priors ('equal weight to all states') incontrovertible, and even there only for discrete Hilbert spaces; whereas for distributions in a classical or in a continuous domain prior choices are flexible. Atempts to find "best" priors were based on invariance principles [9] or the weighting of several expert opinions in view of new evidence [12]. [Bayesians tend to use "priors" in the sense of hypotheses that are already there and need not to be invented, but have to be verified by observation [13]).

A different understanding of priors and indeed of the ME method was provided by Levine and coworkers, mainly in the realm of molecular dynamics [14], and extended recently to classical processes (fragmentation) [15]. In this approach, the factorization of the distribution function P(s) into two factors, as shown in Eq. (A8) of Appendix 1, is based on the philosophical principle that Nature is generally kind enough to make the second exponential factor short and simple. This happens, e.g., in a canonical distribution, where the prior is the multiplicity or statistical weight of the energy shell and the exponent is simply. - (Energy/k_B x temperature). Molecular collision and photofragmentation experiments also lead to simple exponential factors (called also constraint or likelihood factors) [14], provided that the statistical or probabilistic information is condensed in the prior. Then the constraint factor incorporates the characteristics of the process which led to the distribution. This process is almost invariably very complex and it is only through Nature's so far unfathomed benevolence that the experimental data can be approximated by constraint factors that are simple.

Simple exponential factors rule many empirical distributions, e.g., gaussians and log-normal one. They also work for distributions that arise from numerical simulations. E.g. distributions of polygons in cellular networks can be well represented by the product of a probabilistic prior and a simple constraint factor [16,17]. In the following section we employ a ME distribution function, consisting of a prior and a simple constraint factor, to describe the statistics of broken bonds in a simulated Voronoi - network that has been fragmented by the application of tensile forces.

5. Fragmentation in a Disordered Network

To model fracture in granular materials with geometrical disorder a two dimensional model of solids consisting of polygonal grains has been constructed by Voronoi-tessellation [18]. This means that (up to 2000) points were chosen randomly in a plane and, by joining up the perpendicular bisectors of bonds that link neighbouring points, the plane was divided into polygons of different sizes and shapes (Figure 2). The average number of sides of the polygons is 6. A theory of side distribution in 2D and in 3D has been given in [19]. The present, Voronoi-tessellation is a reasonable approximation to disordered multiphase structures containing irregular grains. More precisely, it is deemed superior to alternative models in which disorder enters through randomness of bond strengths in a geometrically regular (e.g. square or triangular) lattice [20,21].

In this simulation fracture is brought about by applying either a fixed stress or a fixed elongation (constant strain) at two parallel edges and calculating the elongation in each bond for a harmonic, central force model of springs.

One or more bonds break when their calculated relative extensions (defined as the ratio of the extension to the original bond length) exceed a certain value. Then the stress or strain is reapplied or is raised until newer bonds breaks (and in fact they do so with greater facility since the broken bonds no longer support the stress). The procedure is repeated until one gets a continuous domain of broken bonds cutting across the sample, which is then considered fractured.

Several parameters of the fracture process are computed, such as:

(a) the least stress or strain which causes fracture (the fracture stress or strain),

(b) the number of bonds that are broken at each stage of the fracture process,

(c) the location of the broken bonds as function of their length,

(d) the distribution of broken bonds as function of their length (Fig. 3) under condition that a fixed elongation ΔL_x (in the x-direction, say) was imposed on two edges.

A simple ME analysis of the data shown in Fig. 3 is as follows:

The distribution $q(\delta l_x)$ of elongations δl_x of bonds in the x-direction ($\| \Delta L_x$) can be obtained from the conservation condition for the elongation component δl_x^i of the i'th bond:

$$\Delta L_x = M^{-1} \sum_i \delta l_x^i \tag{31}$$

where M is the number of instances that the elongation has been applied The ME distribution then follows:

$$g(\delta l_x) = \left(\frac{N}{M \Delta L_x} \right) \exp\left[- \delta l_x / \left(\frac{M}{N} \Delta L_x \right) \right] \tag{32}$$

N being the total number of bonds.

The fracture criterion used in the simulation was for the elongation δl^i of the i-bond of original length l_i

$$\frac{\delta l^i}{l_i} \geq \varepsilon_f (= 0.2) \tag{33}$$

Assuming that the bond-directions between points in a Voronoi-tessellation are isotropic, we can replace the above relation by the following relation (true in the mean) for the elongations in the x-direction

$$\frac{\delta l_x^i}{l_i} \geq \frac{\varepsilon_f}{\sqrt{2}}$$

Then the number of fractured bonds of length l is

$$N_f(l) = N_o(l) \int_{l\varepsilon_f/\sqrt{2}}^{\infty} dx g(x)$$

$$= N_o(l) \exp[- l\varepsilon_f/\sqrt{2}\ (M\Delta L_x/N] \qquad (34)$$

The factor $N_o(l)$ is the number of bonds of length l created originally and is shown in Fig. 3 as the full-lined histogram. $N_o(l)/N_{total}$ serves as the prior for the distribution $N_F(l)/N_{total}$ of broken bonds. The percent of broken bonds [N_F/N_o x 100] is shown in Figure 4 for three simulations in which elongations ΔL_x (~ 0.04) were applied to the end points (numbering about 20) several times (about 5 times) until the bond structure, containing about 800 bonds (N ≈ 800), became fragmented. The least square fits of the data to exponential curves (seen in Fig. 4) were reasonably accurate. In terms of our earlier discussion of the roles of the prior and of the constraint (or likelihood) factor in a ME distribution the present simulations confirm the expectation that the exponent in the constraint factor takes a simple form (linear in the bond lengths l), in spite of the complexity of the fragmentation process.

The fitted exponents in Fig. 4 are about 10 l. Comparing this with the exponent in Eq. (34), using also the appropriate values of the symbols (M,N, ε_f, ΔL_x), the latter predicts a much faster decay (30 l) of the distribution curve.

6. Conclusion

Fragmentation is a complex phenomenon whose outcome, the fragment distribution, is expected to reflect this complexity. The ME approach has been used in the past to impose regularities on the distribution [4,5,14]. In this article we set out to uncover regularities from the data . The key to this effort are the derivatives of the entropy with respect to the invariants. The procedure leads to a "Thermodynamics" of the fragment - (or any other) data. Application has been

made to relatively simple case of ballistic fragmentation of rock targets, where only one invariant <logs> is in evidence. For future uses of the procedure, when more than one invariant is expected, further development of the method is needed to make it practical. This appears possible.

A prior - constraint function decomposition of distributions has been carried out in this article for the broken bonds in a disordered network at the moment of its falling to pieces. The aim was to see whether the constraint function is simple, as anticipated in the ME treatment. This was found. Additional interst is attached to possible changes in the distribution as the fragmentation threshold is approached.

Appendix 1.

The formalism

In deriving the distribution p(s) of fragment sizes s the ME method maximizes the information entropy (or missing information) given by

$$S = -\sum_s p(s) \log p(s) \tag{A1}$$

One allows for R observational inputs or constraints in the form of averages whose values are given:

$$\langle g_r \rangle = \sum_s g_r(s) p(s) \qquad (r=1,...,R) \tag{A2}$$

Then one maximizes with respect to p(s) the quantity

$$S - \sum_r G_r \langle g_r \rangle , \tag{A3}$$

where G_r are Lagrange multipliers, whose role is to ensure that with the solution p(s) the constraints are satisfied. This solution is

$$p(s) = \exp\left[- \sum_r G_r g_r(s) - Q \right] \tag{A4}$$

where Q normalizes p. Exp Q is also the partition function.

When there are "priors" $\Pi(s)$, discussed in section 4 that are not uniform, the previous quantities change in the following way:

$$S = \sum_s \Pi(s) p(s) \log p(s) \tag{A5}$$

$$\langle g_r \rangle = \sum_s \Pi(s) p(s) g_r(s) \tag{A6}$$

and the distribution is

$$P(s) = \Pi(s) p(s) \tag{A7}$$

$$= \Pi(s) \exp\left[- \sum_r G_r \, g_r(s) - Q \right] \tag{A8}$$

Appendix 2

On Gausian Probabilities

These illustrate different cases that are treated in the text in a general manner. (For convenience averages are shown with bars over the variable).

Suppose that we find that the experiments yield a distribution p of a quantity z that can be represented as

$$p(z) = e^{-G_1 z - G_2 z^2 - Q} \tag{A9}$$

Several possibilities arise.

(1) Two constraints (in addition to normalization).

These are on the mean and the variance, in the form

$$g_1 = z, \quad \bar{g}_1 = a$$

$$g_2 = z^2, \quad \bar{g}_2 = \sigma^2$$

Then p in (A9) has the form:

$$p(z) = \frac{1}{\sqrt{2\pi(\sigma^2 - a^2)}} \exp\left[-\frac{1}{2}(z-a)^2/(\sigma^2 - a^2) \right] \tag{A10}$$

From this we find immediately

$$G_1 = -a(\sigma^2 - a^2)^{-1}, \quad G_2 = \frac{1}{2}(\sigma^2 - a^2)^{-1}$$

$$Q = \frac{1}{2}a^2/(\sigma^2 - a^2) + \frac{1}{2}\log[\sigma^2 - a^2)] \tag{A11}$$

The entropy is

$$S = G_1 \bar{z} + G_2 \bar{z^2} + Q$$

$$= \frac{1}{2} + \frac{1}{2}\log\left[(2\pi(\sigma^2 - a^2)\right]$$

The partial derivatives of S with respect to the averages are:

$$\frac{\partial S}{\partial a} \equiv G_1^* = -a/(\sigma^2 - a^2)$$

$$\frac{\partial S}{\partial \sigma^2} \equiv G_2^* = \frac{1}{2}(\sigma^2 - a^2)^{-1}$$

which are respectively equal to G_1 and G_2. This verifies that (A10) is a ME distribution,

(2) <u>One constraint</u>

(2a) $g' = z + z^2$, $g' = a + \sigma^2$

but no constraint on z and z^2 separately.

In (A9) we have now $G_1 = G_2$.

The ME distribution satisfying the one constraint is

$$p(z)\left[2\pi\left(\sigma^2 + a + \frac{1}{4}\right)\right]^{-1/2} \exp\left[-\left(z+\frac{1}{2}\right)^2 / 2\left(\sigma^2+a+\frac{1}{4}\right)\right] \qquad \text{(A12)}$$

from which the coefficient in the exponent is

$$G' = \left[2\left(\sigma^2 + a + \frac{1}{4}\right)\right]^{-1}$$

$$S = \frac{1}{2} + \frac{1}{2}\log\left[2\pi\left(\sigma^2 + a + \frac{1}{4}\right)\right]$$

Differentiating this

$$\frac{\partial S}{\partial \bar{g}'} = G'^* = \left[2\left(\sigma^2 + a + \frac{1}{4}\right)\right]^{-1} = G'$$

so that (A12) is also a ME distribution.

However, (A10) satisfying two constraints has a lower entropy than (A12) satisfying one constraint (since, in general, adding constraints makes the distribution less uniform). Indeed

$$\Delta S_{1,2} \left(\equiv S_{G'} - S_{G_1,G_2}\right) = \frac{1}{2}\log\left[\left(\sigma^2 + a + \frac{1}{4}\right)/(\sigma^2 - a^2)\right] \qquad \text{(A13)}$$

This entropy difference is plotted in Fig. 5 as function of σ for different choices of σ^2 and is seen to be non-negative (for all values of σ that make sense: $a^2 \le \sigma^2$). Note, however, that the entropy difference can be negative for certain choices of the priors, in particular of non-uniform ones)

(2b) $g' = z^2,\ g^{'} = \sigma^2$

without constraining z.

$$p(z) = (2\pi\sigma^2)^{-1/2} \exp\left(-\frac{1}{2}z^2/\sigma^2\right) = \exp(-G'z^2 - Q) \qquad \text{(A14)}$$

$$G' = (2\sigma^2)^{-1},\ Q = \frac{1}{2}\log(2\pi\sigma^2)$$

$$S = \frac{1}{2} + \log(2\pi\sigma^2)$$

$$\frac{\partial S}{\partial \bar{g}'} \equiv G'^{*} = (2\sigma^2)^{-1} = G^{'}$$

demonstrating the ME nature of the distribution (A14). The entropy difference compared to the 2-constraint distribution is again positive:

$$\Delta S = \log(\sigma/\sqrt{\sigma^2 - a^2}) \ge 0$$

(3) We now consider a non-ME (NME) distribution and show inter alia that partial derivatives of the entropy with respect to averages are not, in general, equal to the corresponding coefficient in the exponent of the distribution p, i.e. $G_i^{*} \ne G_i$

(3a) Assume that there is just one constraint.

$$g = z,\ \bar{g} = a$$

and no constraint on z^2. Suppose further that the observation can be represented (somewhat to our surprise) by the distribution

$$p(z) = e^{-Gz - Cz^2 - Q} \qquad \text{(A15)}$$

To satisfy normalization and $\bar{z} = a$, one must have

$$p = (2\pi/C)^{-1/2} \exp[-C(z-a)^2]$$

whence

$$\tilde{G} = 2Ca$$

$$\tilde{Q} = Ca^2 + \frac{1}{2}\log(2\pi/C)$$

$$\tilde{S} = \frac{1}{2} - \log(2\pi/C)$$

$$\tilde{G}^* = \frac{\partial \tilde{S}}{\partial \bar{z}} - \frac{1}{2C}\frac{\partial C}{\partial Q} \qquad \text{(A16)}$$

Since the variation of C with a or z is not prescribed G^* will not in general equal G. Should one find experimentally such dependence of C on a that $G = \bar{G}$ is satisfied, then a new constraint on z^2 has been discovered.

(3b) Constraint on $g = z^2$: $\bar{g} = \sigma^2$, no constraint on z.

Suppose that observations yield the non-ME distribution

$$p = e^{-Az - \tilde{G}z^2 - Q}$$

Satisfaction of the constraint leads to the quadratic in $X \equiv G^{-1}$,

$$\tilde{S} = \frac{1}{2} + \frac{1}{2}\log\left[2\pi\left(\sigma^2 - \frac{1}{4}AX^2\right)\right]$$

$$\bar{G}^* \equiv \frac{d\tilde{S}}{d\sigma^2} = \frac{\partial \tilde{S}}{\partial \sigma^2} + \frac{\partial \tilde{S}}{\partial X}\frac{dX}{d\sigma^2} + \frac{\partial \tilde{S}}{\partial X}\frac{\partial X}{\partial A}\frac{dA}{d\sigma^2} + \frac{\partial S}{\partial A}\frac{dA}{d\sigma^2}$$

$$\neq \bar{G}$$

The last non-equality is again due to the arbitrary dependence of A on the mean σ^2.

Table 1. Analysis of rock fragmentation data [8]. Computed averages are over observed distribution points z_n. $z \equiv s/s_{total}$ is the mass variable normalized to total mass. A prior $\Pi_n = z_n^{-1}$ was used to calculate the cross-entropy $(=\sum_n p_n \log p_n/\pi_n)$. z_o is the minimum normalized size that was sampled.

Sample		$\langle z \rangle \times 10^3$	$\langle \log z \rangle$	Cross-entropy	z_o(minimum size) x 10^3
Tuff	T5	1.642	-6.524	-.280	1.270
	T19	2.610	-6.069	-.246	1.953
	T13	2.533	-6.095	-.283	1.953
	T14	4.245	-5.622	-.226	3.008
	T4	1.760	-6.410	-.328	1.465
	T16	2.474	-6.098	-.278	1.914
	T6	6.518	-5.086	-.362	5.625
	T7	6.820	-5.055	-.307	5.625
Basalt	B16	4.961	-5.452	-.307	3.750
	B13	4.416	-5.650	-.1964	2.851
	B3	2.767	-5.992	-.298	2.187
	B5	4.341	-5.583	-.297	3.281
	B6	4.004	-5.627	-.285	3.125
Granite	I5	4.172	-5.607	-.222	3.047
	I3	4.172	-5.386	-.219	3.789
	I1	3.927	-5.633	-.255	3.047
	K1	3.293	-5.853	-.200	2.344
Dunite	D4	2.564	-6.081	-.263	1.953
	D3	2.302	-6.171	-.272	1.797
	D2	3.536	-5.704	-.324	2.969

Table 2. Entropy derivatives computed from data points [8] for pairs of rocks, compared with corresponding coefficients G[T = tuff, B = basalt, IG = granite]. Also, smallest relative fragment size $z_o(z = s/s_{total}, \bar{x} = <\log z>)$

Rock 1/Rock 2	$dS/d\bar{x}$	G	$z_o(x10^3)$
T19/T13	1.42	1.7/1.4	1.95/1.95
T6/T7	1.94	1.94/1.84	5.6/5.6
B13/B6	- 4	0.87/1.28	2.85/3.1
IG5/IG3	1.25	1.4/1.5	3.05/3.05

Figure Captions

Fig. 1. Fragment size distributions for four target types after high velocity impact obtained by Matsui et al. [8] . In the log-log plots N is the number of fragments per unit volume size s. s_t is the target volume. The different symbols relate to different samples, whose data appear in Table 1.

Fig. 2. Voronoi-tessellation of a plane. (Part of the plane is shown). The lines are perpendicular bisectors of the bonds (not shown), joining neighbouring points (thrown at random). The broken lines are bisectors of those bonds that have been fractured by the application of tensile strain at the boundary points.

Fig. 3. Histogram of broken bonds as function of the original bond length at fracture. The data represent averaging over several runs. The criterion for bond rupture is that the relative elongation $\delta l/l$ of bonds exceeds 0.2. The distribution $N_O(l)$ of original lengths is also shown by broken lines and the percentage of bonds broken $N_F(l)/N_O(l)$ by dotted lines. In our model short bonds have a preference for being broken.

Fig. 4. Fraction of broken bonds (percent of the original number) as function of original bond length at the moment when the network becomes fragmented. Data points from three simulations are shown together with fitted exponentials.

Fig. 5. The entropy difference $\Delta S_{1,2}$ in (A13). It is non-negative since the distribution in (A12) has less constraint (more disordered) than that in (A10).

The three curves are for $\sigma^2 = 1$ (broken line), 5 (full line), 1 (dotted line).

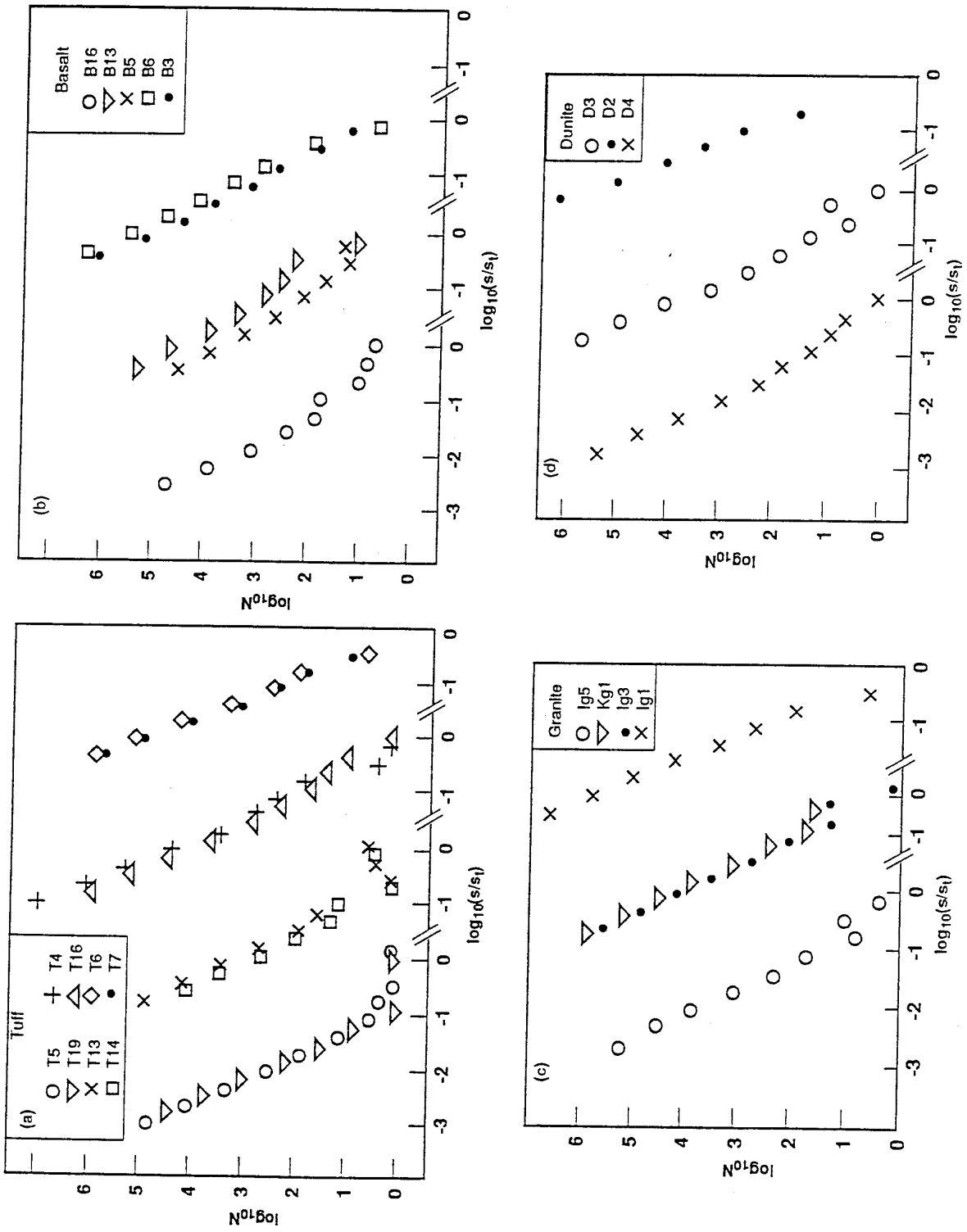
(a)
Tuff
T5
T19
T13
T14
T4
T16
T6
T7
(b)
Basalt
B16
B13
B5
B6
B3
(c)
Granite
Ig5
Kg1
Ig3
Ig1
(d)
Dunite
D3
D2
D4
log10N
log10(s/s1)

Figure 1

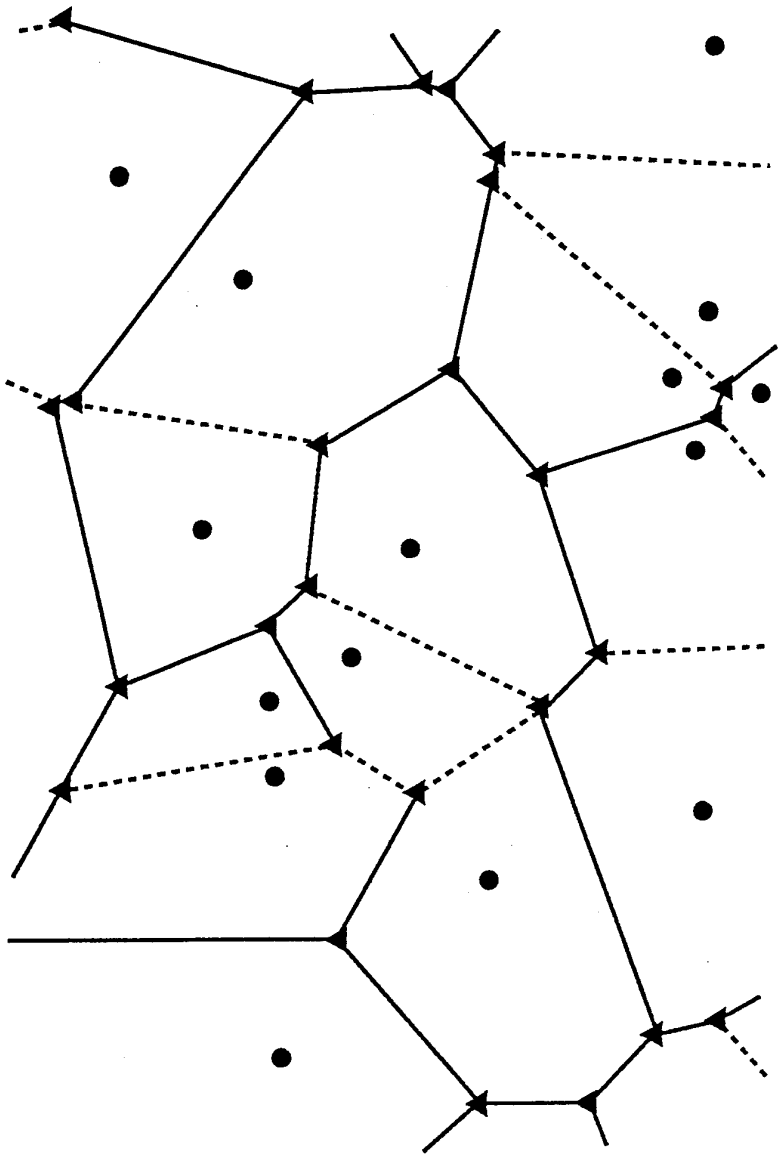

Figure 2

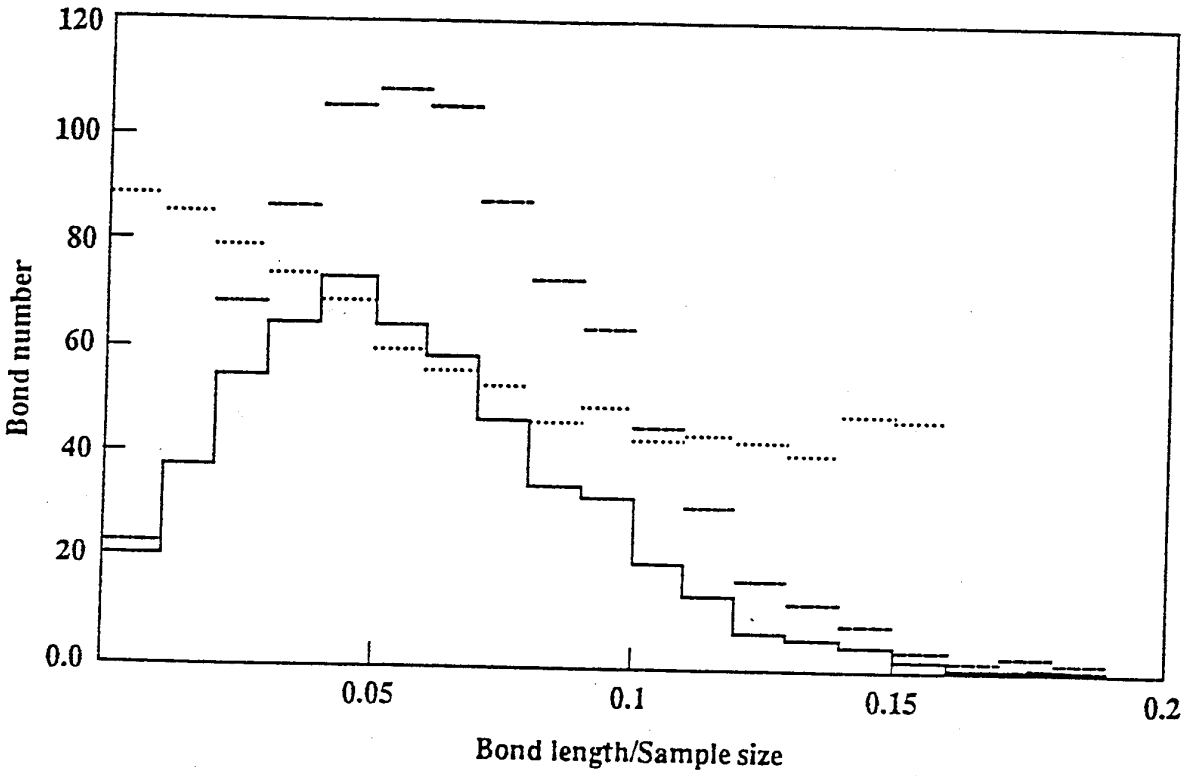
120
100
80
60
40
20
0.0
Bond number
0.05
0.1
0.15
0.2
Bond length/Sample size

Figure 3

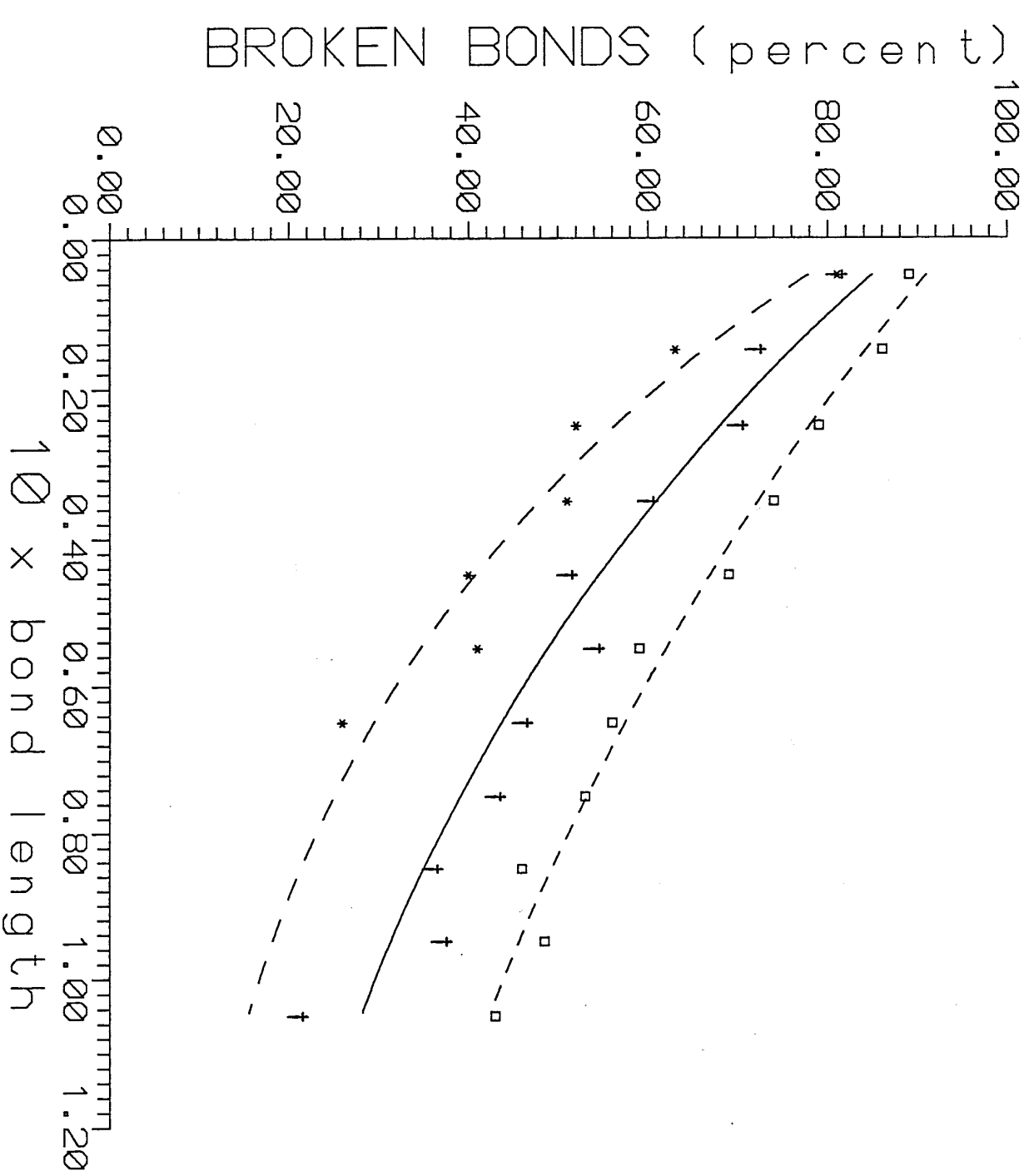
BROKEN BONDS (percent)
0.00
20.00
40.00
60.00
80.00
100.00
0.00
0.20
0.40
0.60
0.80
1.00
1.20
10 x bond length

Figure 4

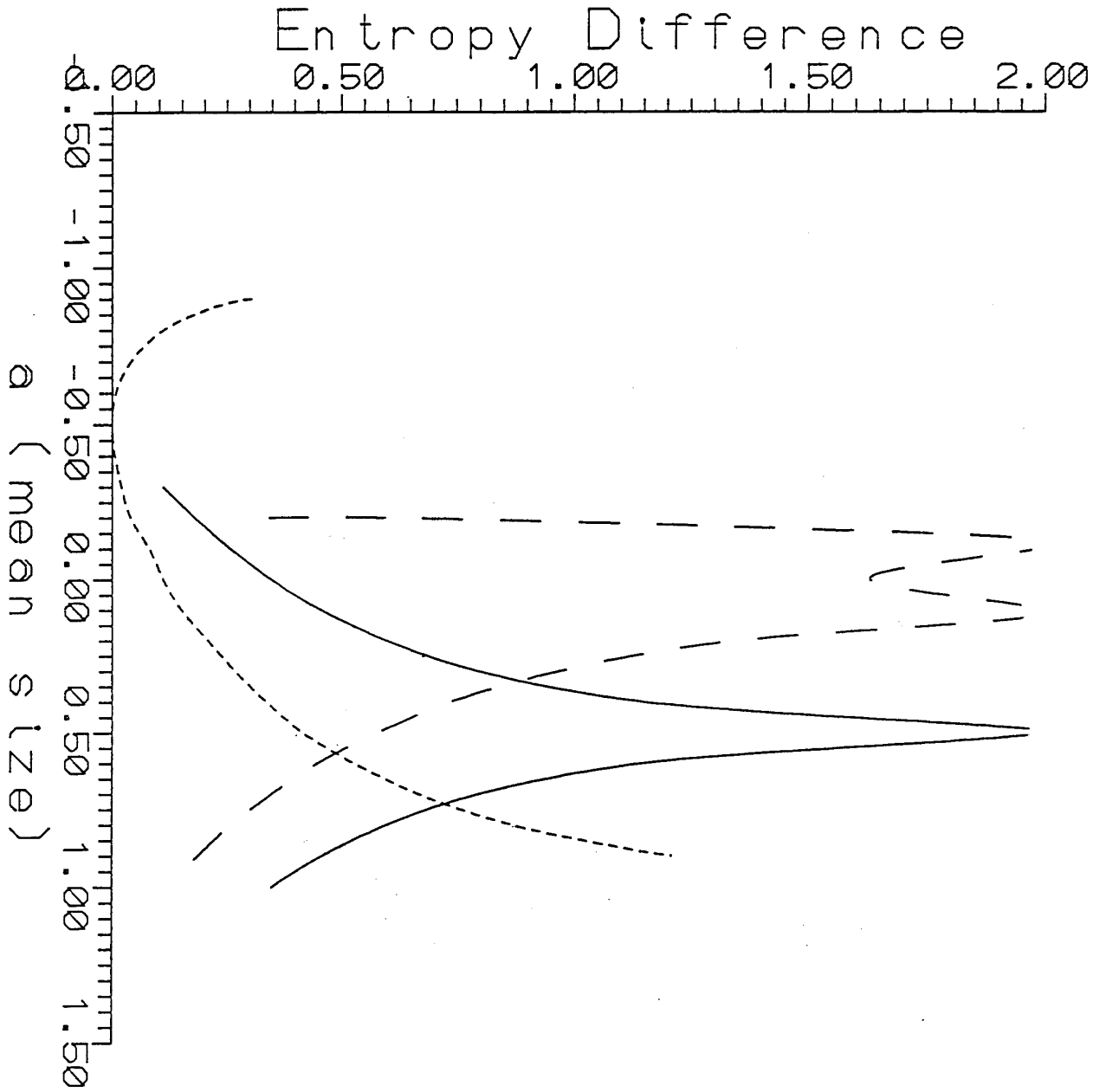
Entropy Difference
0.00
0.50
1.00
1.50
2.00
-1.50
-1.00
-0.50
0.00
0.50
1.00
1.50
a (mean s(Ze))

Figure 5

Transport Treatment of Crack Population In Finite Medium Part II : Damage Behavior in Different Zones.

M.Lemanska, R. Englman and Z. Jaeger
Soreq Nuclear Research Center, Yavne 81800, Israel

Abstract

Extensive graphical results are given of a non-linear transport equation approach (derived and described in part I of this work) for crack population in a spherical medium surrounding a charged borehole. The central quantity numerically computed by time integration is the "damage" or the total volume associated with the cracks. Typically, intensive cracking (large damage) appears near the borehole and close to the surface (spalling), where the detonation pulse becomes (upon reflection) tensile. The extents and quantities of damage in these two zones are given as functions of the sample size, initial crack distribution, attenuation length and the form of the pulse.
An interesting result arising from this non-linear method is the disappearance of the spall zone in spite of the relatively strong tensile part of the wave. This phenomenon is caused by the increased attenuation of the tensile pulse (on its way to the surface) due to the large number of cracks (either initially present or formed later).

1. Introduction

This work is a continuation of the work [1], called here Part I, in which we have presented the motivation and aims of our research. The transport equation of interest [2,3] has been described there. The notations and definitions hold also here. In order to facilitate the reading of this paper we recall some of the basic equations in Sec.2.

The numerical simulation [4,5] is performed for spherical geometry as in Part I, but the model considered here is more complicated. In this work a spherical detonation source of small radius a_0 is assumed, which is concentric with the sample sphere of radius R_0. The outgoing pressure wave consists of compressive (c, positive) and tensile (t, negative) rectangular parts with variable amplitudes and lengths. The wave is moving from the center to the boundary and is reflected inwards to the center. The reflection turns the tensile and compressive parts into each other.

Both Part I and Part II of this work should be regarded as an attempt to apply a statistical-deterministic method, the transport equation, to the treatment of damage problems in a spherical medium. To test the usefulness of this method, we investigate here the dependence of the final damage on (i) the initial crack distribution, (ii) the sample size, (iii) the pressure wave and (iv) the

wave attenuation factor. We also examine the effect of the sample dimension on the extent of the crushed regions (around the borehole and near the surface).

2. Assumptions and Definitions

We work with a pressure wave of the form:

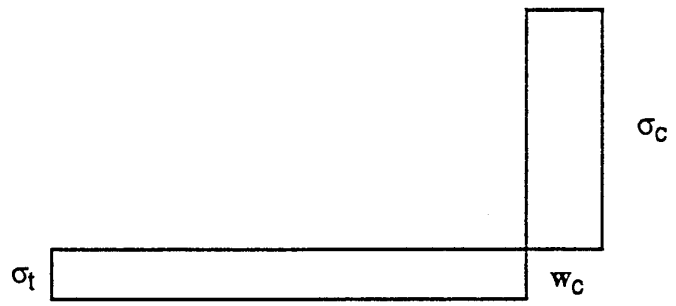

Fig.1. Depiction of the pressure wave. The symbols have the following meanings:

σ_c, σ_t : strength of compressive and tensile pressure respectively.

w_c, w_t: width of compressive and tensile parts of the pressure pulse.

Next, we recall some basic equations described in detail in Part I. Let r be the crack- tip position, ℓ its long dimension, v_ℓ is the crack velocity postulated to be isotropic and constant . The non-linear transport equation for crack-tips motion at time t is:

$$\frac{\partial T}{\partial t} + v_\ell \bar{\Omega} \text{ grad } T - P(r,\ell,t) - \int_{\ell'<\ell} K^+(\ell' \rightarrow \ell,\ r,t,T,T')\ d\ell' + \int_{\ell'>\ell} K^-(\ell \rightarrow \ell',\ r,t,T,T')\ d\ell' = 0 \quad (1)$$

where $T(r,\ell,t)\ dr\ d\ell$ is the number of crack-tips in the ranges $(r+dr,r)$, $(\ell+d\ell,\ell)$ at time t .

The source term P:

$$P(r,\ell,t) = \gamma_i \left| \sigma(r,t) - \sigma_i \right| e^{-\ell/\ell_o} (\sigma_o \tau_p \ell_o)^{-1} \quad (2)$$

where ℓ_o is the mean crack length, σ_o the amplitude of detonation pressure and τ_p stress-pulse time. They are assumed to be unity. γ_i is crack activation-rate coefficient (i=c,t),σ_i is a threshold pressure for crack growth, both are dependent on the stress type.

The scattering terms are similar to the source term. Explicitly

$$-\int_{\ell} K^{+}\, d\ell^{*} + \int_{\ell} K^{-}\, d\ell^{*} = \lambda_i \,|\,\sigma(r,t) - \sigma_i\,|\,(\sigma_o \tau_p \ell_o)^{-1} \left[-\int_{o}^{\ell} T(r,\ell^{*},t) e^{-(\ell-\ell^{*})/\ell_o}\, d\ell^{*} + \right. \tag{3}$$

$$\left. A \cdot T\,(r,\ell,t) \int_{\ell}^{\ell_{max}} e^{-(\ell^{*}-\ell)/\ell_o}\, d\ell^{*} \right]$$

where $\ell_{max} = R_o - a_o$ is the maximum length of cracks, λ_i is crack growth-rate coefficient (i=c,t) and

$$A = \int_{o}^{\ell_{max}} d\ell \int_{o}^{\ell} T(r,\ell^{*},t) e^{-(\ell-\ell^{*})/\ell_o}\, d\ell^{*} \Big/ \left[\ell_o \left(\int_{o}^{\ell_{max}} T(r,\ell',t)\, d\ell' \right. \right. \tag{4}$$

$$\left. \left. - e^{-\ell_{max}/\ell_o} \int_{o}^{\ell_{max}} T(r,\ell',t)\, e^{-\ell'/\ell_o}\, d\ell' \right) \right]$$

The pressure function $\sigma(r,t)$

$$\sigma\,(r,t) = \sigma^{*}\, F(r,t) \tag{5}$$

where $\sigma^{*} = \sigma_c \sigma_o$, $\sigma_t \sigma_o$ for a compression and tensile pressure respectively. The function F determines the attenuation process in term of the path integral of the local damage D(r,t).

$$F\,(r,t) = \frac{1}{r} \exp\left[-\int_{a_o}^{r} D(r',t)\, dr' (R_o\, \delta\, \ell_o^{3})^{-1} \right] \tag{6}$$

where δ is a medium dependent attenuation factor. The damage at point r and time t is defined by

$$D\,(r,t) = \int_{o}^{\ell_{max}} \ell^{3}\, T(r,\ell,t)\, d\ell \tag{7}$$

The final damage is also defined by Eq.(7) with $T(r,\ell,t_{max})$, where t_{max} is the travelling time of the pulse from $r=a_o$ to the boundary and backward.

The initial crack distribution is assumed to be uniform in the medium and is given as a function of crack length ℓ :

$$T_o\,(r,\ell) = T\,(r,\ell,0) = \frac{\alpha}{\ell_o} e^{-\ell/\ell_o} \tag{8}$$

This presents the initial condition for our transport simulation.The parameter α may be varied, but in general in this work it is put $\alpha=1.0$.

The initial damage is denoted by D_o. Assuming the above uniform crack distribution, D_o is

constant . From Eqs.(7) and (8), it is obtained

$$D_o = \frac{\alpha}{\ell_o} \int_o^{\ell_{max}} \ell^3 e^{-\ell/\ell_o} \, d\ell \qquad (7')$$

The ultimate mean damage D_{mean} is defined as the ratio of total damage to the sample volume, V_{sample}.

$$D_{mean} = \int_{a_o}^{R_o} r^2 D(r) \, dr / V_{sample} \qquad (9)$$

where $D(r)$ is the final damage at the point r and time t_{max}.

We next characterize the spall as the damage near the external boundary by its depth R_o-r_2 and its peak value. Similarly, for the damage zone around the borehole. (For illustration we show Fig.2)

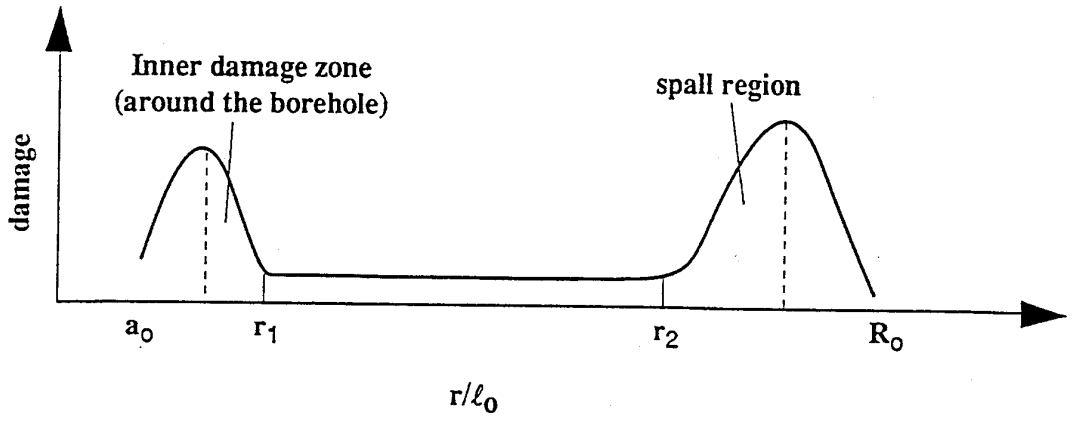

Fig. 2

For the study of items (i)-(iv) in the previous section, the wave parameter values are chosen after some preliminary computations, with a view of yielding results that compare well with observations, as follows:

$$\sigma_c = 10.0\sigma_o \quad w_c = 0.1 \, w_p$$

$$\sigma_t = 0.01 \, \sigma_o \quad w_t = 0.9 \, w_p$$

where σ_o is assumed to be unity, (see Table 1 of Part I).

The parameters in the above expressions were given the values:

$\ell_o = 1.0$, $\lambda_i = 1.0$, $\gamma_c = 1.0$ for compressive wave and $\gamma_t = 75.0$ for a tensile one.

3. Effect of The Initial Crack Distribution on The Final Damage.

The influence of the initial crack distribution on the final damage is examined for two values of the sample radius: $R_0 = 5.0\ell_0$ and $R_0 = 8.5\ell_0$. Troughout this work, the radius of the spherical charge is kept constant $a_0 = 0.5\ell_0$. The pressure pulse is also the same, with parameter values as in Sec.2.

The initial crack distribution is changed through variation of the parameter α, see Eq. (8). We used the following values: α=0.01, 0.1, 0.5, 1.0, 2.0, 5.0 and 10.0. Consequently the initial damage density D_0 varies from 0.03944 to 39.44 for $R_0=5.0\ell_0$ and from 0.0574 to 57.4 for $R_0=8.5\ell_0$ (See Eg.(7')).The range of α values is sufficiently large for discussing the question of interest.

Due to the similarity of the computational outcomes in both cases, only the ones for $R_0 = 5.0\ell_0$ are presented in Figs. 3,4,5. For better estimation of the obtained results, the differential damage produced by the explosion, which is defined by $D(r,t)-D_0$, is shown in Fig. 4 and the relative one $D(r,t)/D_0$ in Fig. 5.

The following conclusions can be drawn.The ratio $D(r,t)/D_0$ grows as the value of α decreases. In other words, a smaller initial damage results in getting later a relatively larger one. This is clear, because the presence of cracks causes the attenuation of the outgoing pulse. Indeed, it is found, that for sufficiently large α ($\geq$5), for both $R_0/\ell_0 = 5$ and 8.5 cases, the spall zone does not exist.

For sufficiently small α ($\leq$0.1), the peak and the depth of the spall are independent of α. The same result is observed for the inner damage zone. See Fig.3. That is clear, because the initial value of the function F(r), [see Eqs.(6) and (7')] is small and has no influence on the computational results. In the limit, as $\alpha \to 0$, the peak of the damage near the center reaches a minimal value and the peak of the spall attains a maximal one.

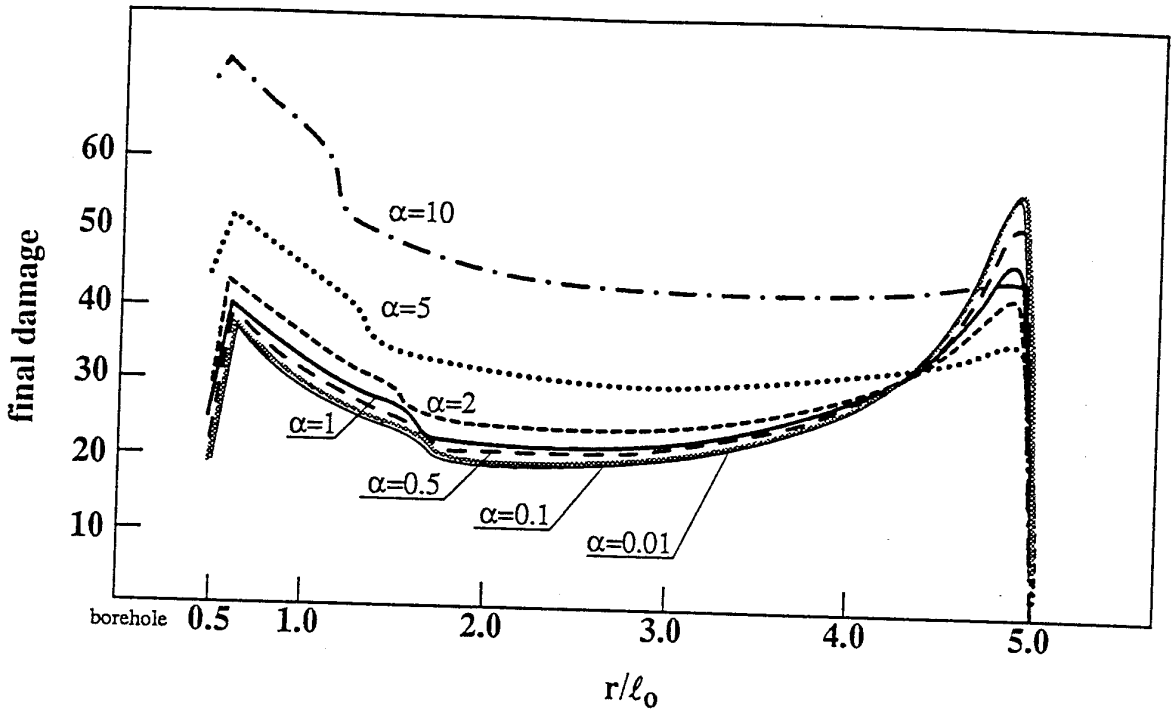

Fig. 3. Final damage for various initial crack distributions.

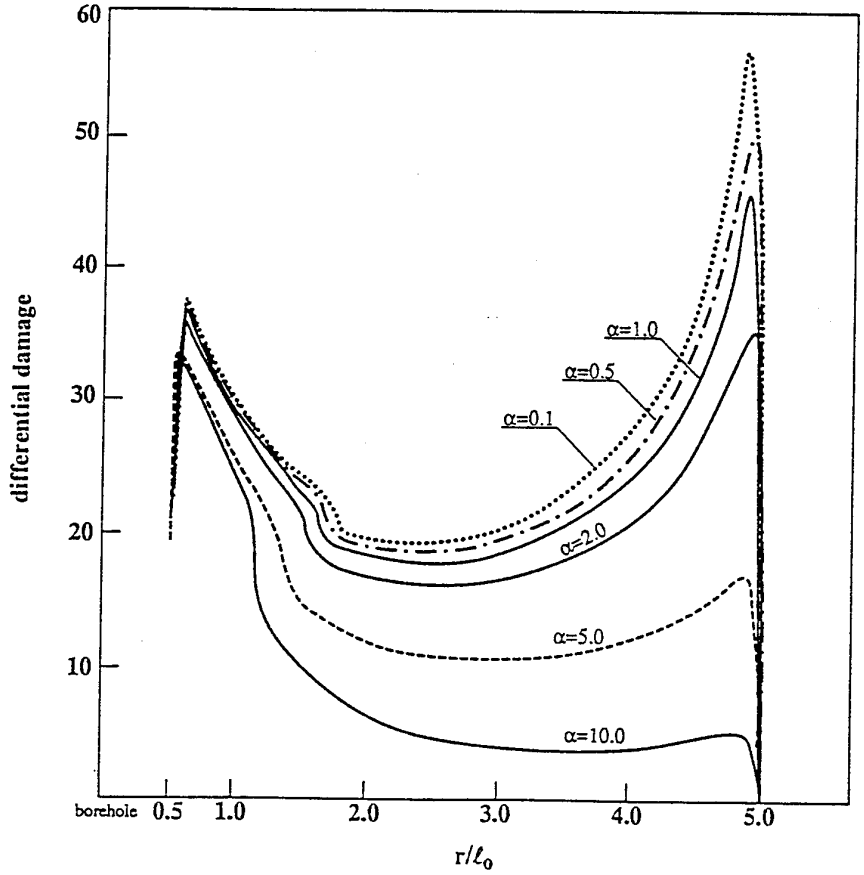

Fig. 4. Differential damage for various initial crack distributions.

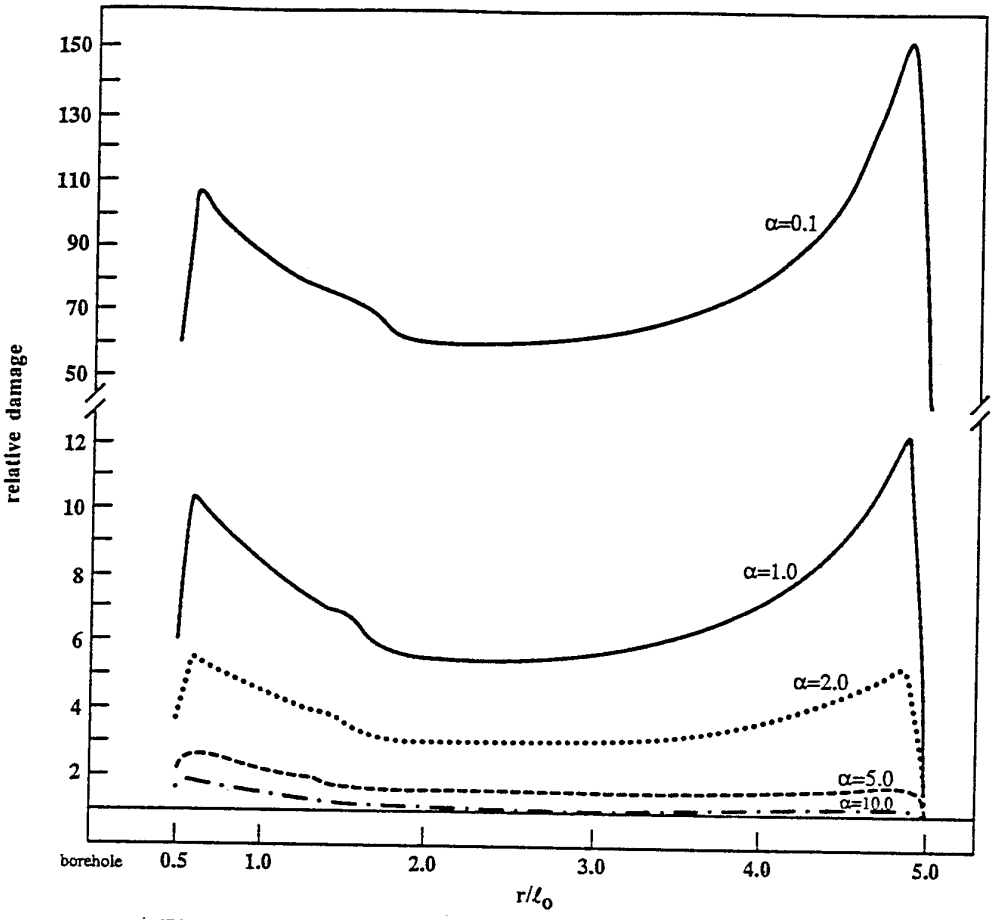

Fig. 5. Relative damage for various initial crack distributions.

4. Effect of the Sample Size on the Final Damage Distribution

In this section the radial behaviour of the final damage for various sample sizes will be considered. To investigate this quantity, R_0 is varied between $1.0\ell_0$ and $10.5\ell_0$. Other parameters are kept fixed and have the values as in Eqs.(10) and (11). The parameter α is also fixed and assumed α=1.0. The results are presented in Figs. 6,7,8.

First, we consider the damage caused by the outward pulse, as shown in Fig.6. The outward pulse near the boundary is weak, and its contribution to the damage is small. In this figure the spall does not appear because it is created only by a strong enough reflected (inward) pulse.

The damage peak near the charge increases as R_0 grows, but levels off for sufficiently large R_0, to become independent of the sample radius. This may be explained by Eq. (7').

Writing for simplicity, α,ℓ_0=1 in (7') and noting that the maximum crack length $\ell_{max}=R_0-a_0$ we obtain:

$$D_0 = \int_0^{\ell_{max}} \ell^3 e^{-\ell} \, d\ell = 6 - \int_{R_0 - a_0}^{\infty} \ell^3 e^{-\ell} \, d\ell \to 6 \qquad \text{for } R_0 \to \infty \tag{7"}$$

That means, for sufficiently large R_0, the value of the function F(r), Eq.(6), is independent of the sample size.

The final damage plotted in Figs.7 and 8 is caused both by the outward and returning pulses. For $1\ell_0 \le R_0 < 2.5\ell_0$, the width and the peak of the inner damage zone rise quickly. An interplay of two factors influences this phenomenon. One is the behavior of the initial damage explained above. Generally speaking, the second one is the ratio of the pulse length to the sample size. For $R_0 = 1.0\,\ell_0$, the two lengths are equal .The outward and the reflected pulses act simultaneously at all points r, and the contribution of the returning wave is small, because, in fact, only $\sigma_{out} + \sigma_{refl}$ is effective. Note, that these σ differ in sign. If the pulse length is smaller than the sample radius, the two pulses act simultaneously only in a limited region of points, r, near the boundary and the contribution of the returning pulse is important.

For sufficiently large R_0, $R_0 \ge 4.5\ell_0$, the peak and width of the inner damage zone are independent of the sample size. This may be explained by an interplay between two factors. The one is the behavior of the outward pulse considered above and the second one is that, the reflected pulse is weak for large R_0 and therefore its contribution is small.

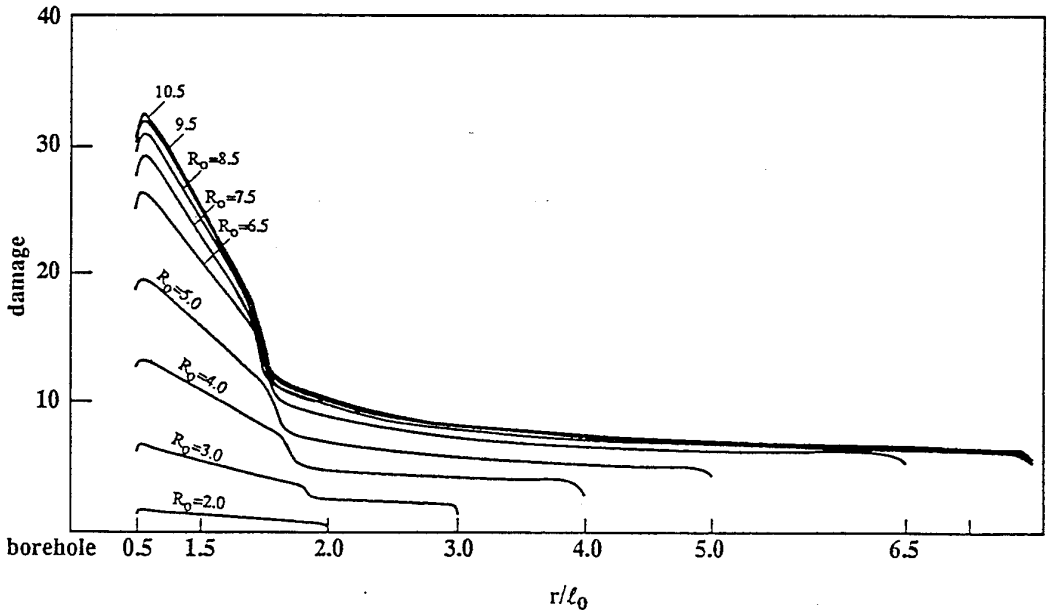

Fig. 6. Radial behaviour of the damage produced by the outward pulse for various sample sizes. For R_0=8.5,9.5,10.5 only the damage region around the borehole is depicted.

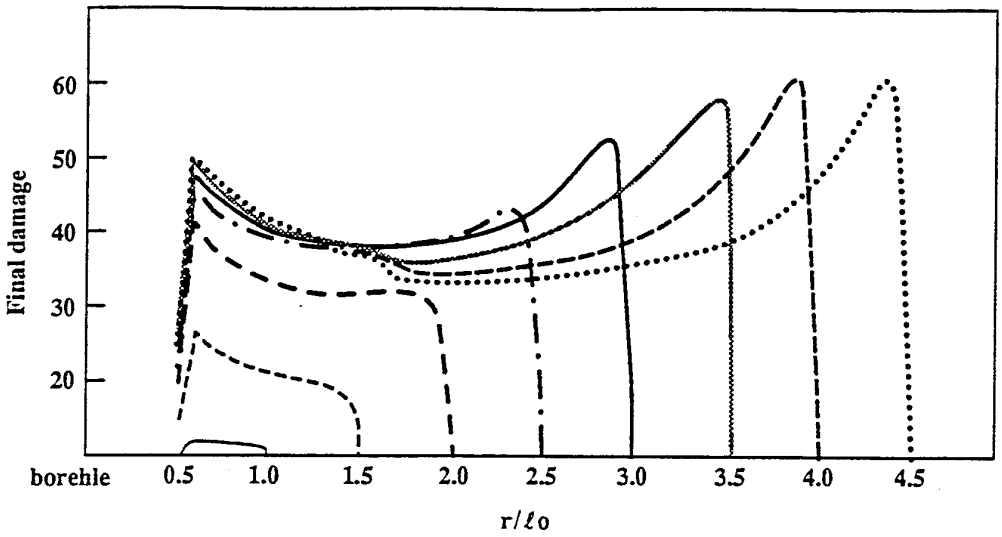

Fig. 7. The final damage distribution as a function of the sample size.

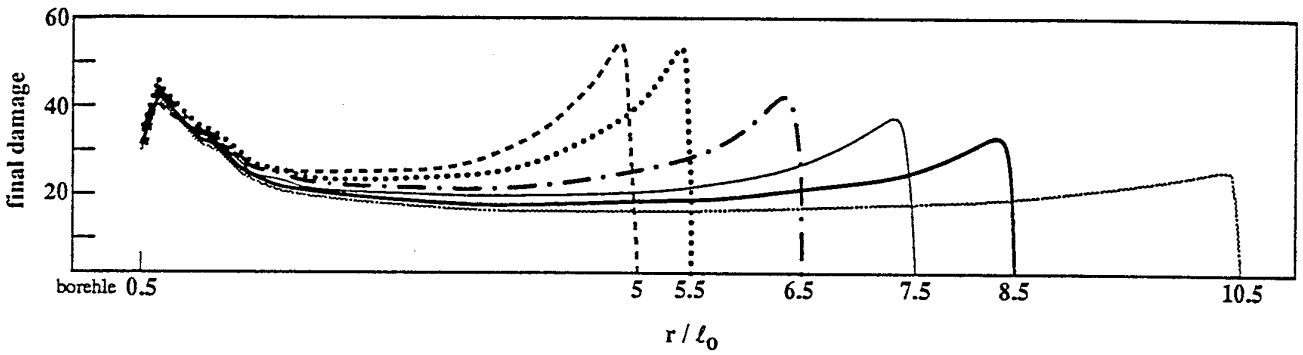

Fig. 8. The final damage distribution as a function of the sample size.

The behavior of the peak and width of the spall is different from the above. The peak spall, D_s, dependence on the sample size R_0 may be approximated as a parabola $D_s=4.73R_0^2+41.61R_0-39.76$, in the range $2.5 \le R_0 5.5$. It rises quickly, when R_0 increases from $1.0\ell_0$ to about $4.5\ell_0$, and attains its maximal value for $R_0 \sim 4.4\ell_0$. For $R_0 > 4.4\ell_0$, the peak decreases and for sufficiently large R_0, the spall does not exist. This is caused by the pulse behavior, which becomes attenuated during its passage due to material damage.

In most cases considered above, two damage zones are observed, One exists near the borehole and the other near the boundary. Between these two zones there is a region of low, almost constant damage. When is this value of damage equal to the initial one? What are the relations between the extent of the region of constant damage, the inner damage zone and the sample size R_0 ? In order to answer these questions, we let R_0 vary between $1.5\ell_0$ to $13.0\ell_0$. The parameters ℓ_0,λ,γ and σ are

given by Eqs.(10) and (11). The value of the parameter δ, see Eg.(6) is chosen to assure the existence of these three seperate zones as δ=4.225. The results of many computations are collected in Fig.9. For $0<R_0 \leq 4.25\ell_0$, the damage at any point r is greater than the initial one, curve (a), For $4.25\ell_0 < R_0 < 5.0\ell_0$, two seperated damage zones (internal and spalled) and a region of initial damage are observed. For this value of δ and when $R_0 \geq 5.0\ell_0$ two damage zones are obtained: an inner damage zone and an initial one. (The spall disappears). According to the above results, the curve (c) indicates, that the width of the inner damage zone is indifferent to the R_0 values for sufficiently large samples. Of course the ranges of R_0 cited above are dependent on the value of δ. Similar provisos may be made in connection with the effects of other parameters, as, for example, the pulse ones.

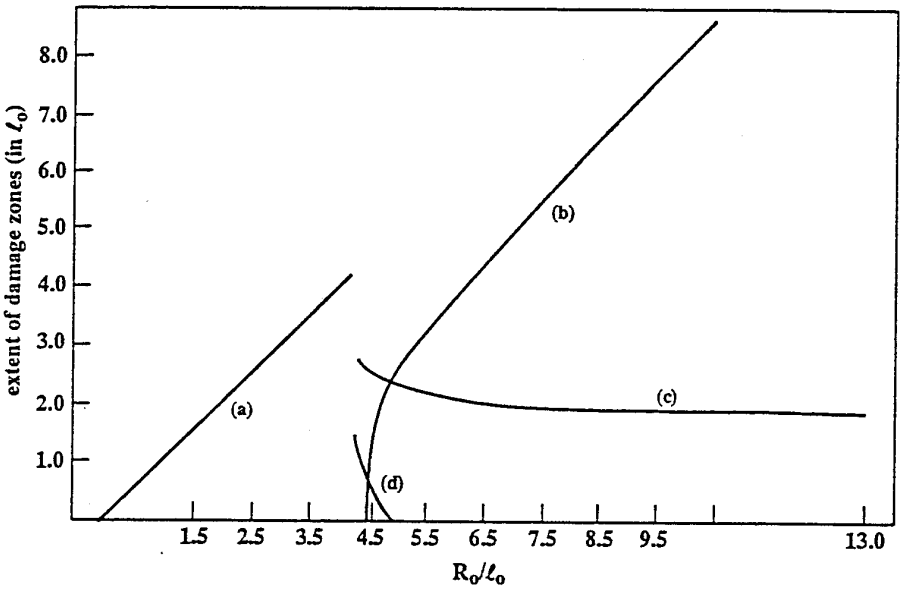

Fig.9. The extent of the damage zones versus the sample size. Curve (a): the damage at any point is greater than the initial one, D_0, the extent of the damage zone is equal to R_0.Curve (b): the extent of D_0 region versus R_0. Curve (c): the width of the inner damage zone near the borehole versus R_0. Curve (d): the width of the spall versus R_0.

5. Width and Volume of Spalled Regions for Samples of Various Size

During the study of this problem the sample radius, R_0, is varied and other parameters are fixed as in Eqs (10) and (11). The spall zone consists of regions of various damage value. Their widths for various R_0 are depicted on Fig.10. In Fig.11 the spall zone volume and in Fig.12 the mean damage, D_{mean}, versus R_0 are drawn.

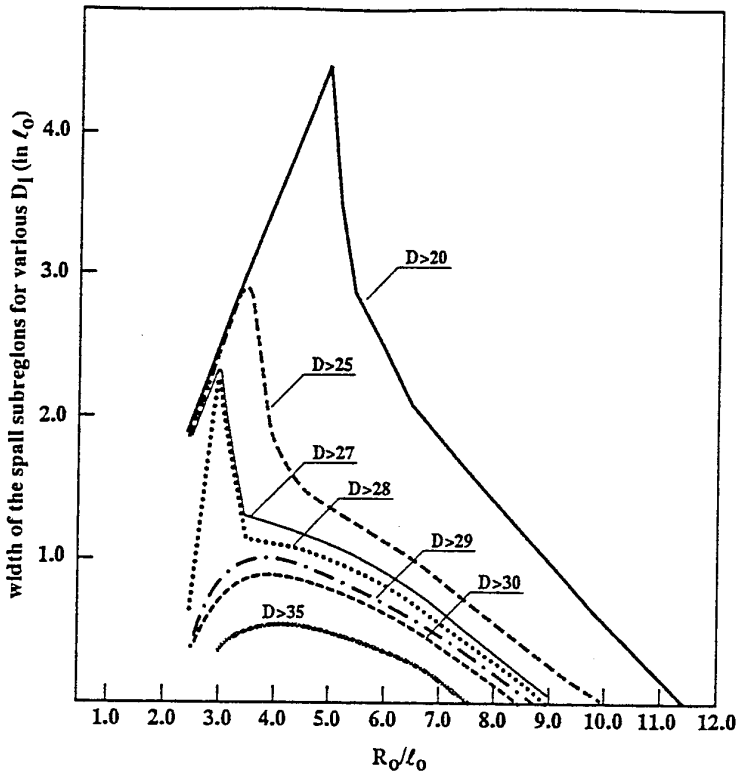

Fig. 10. Width of the subregions of the spall zone, having damage greater than D_i(D_i= 20,25,27,28,29,30,35) versus the sample size R_o. For example: for R_o=4.5 ℓ_o the width of the spall subregion of D>35 is 0.52 ℓ_o, the width of subregion of D>25 is1.5 ℓ_o. In the case of R_o=8.0 ℓ_o there does not exist a spall subregion of damage greater than 35.

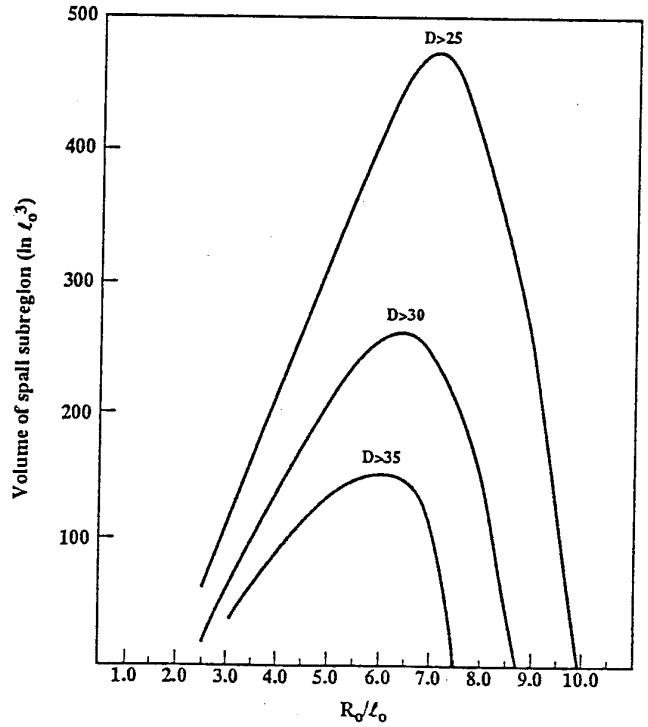

Fig 11 The volume of the spall zone subregions versus R_o, for D_i=25,30,35.

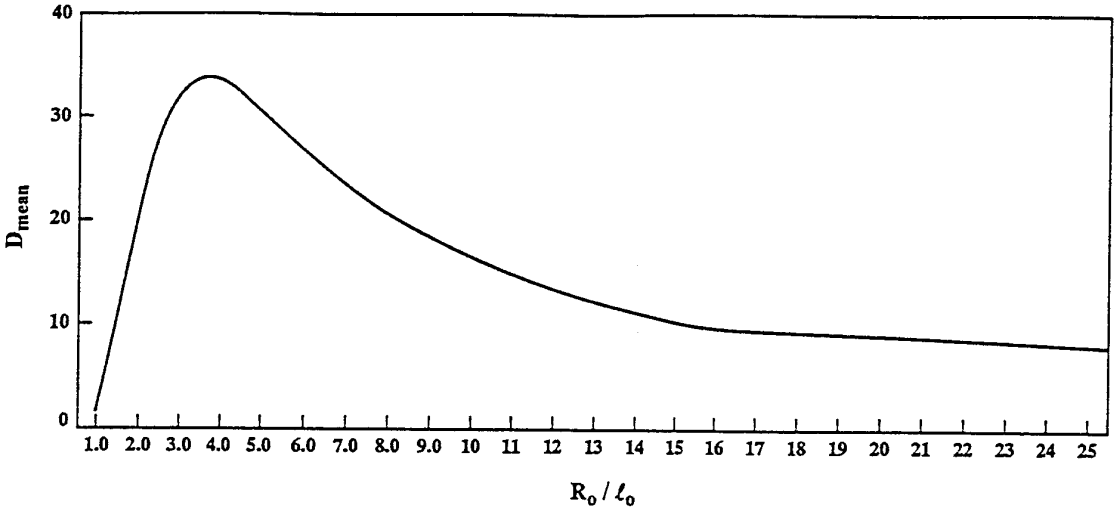

Fig. 12. The mean damage, D_{mean}, versus sample radius R_o.

D_{mean} attains a maximum value at $R_o \approx 3,5$, then it decreases and converges to a constant value.

6. Effect of Pulse Parameter Values

In this section the pressure wave remains rectangular and consists of a compresion and tensile parts, but the value of the parameters σ and τ are varied in order to examine their influence on the final damage. The sample size is $R_o=5.0\ell_o$ and $a_o=0.5\ell_o$. Three cases will be considered below.

a) The values of the parameters σ_c, τ_p and the length w_c, w_t of the compression and tensile, parts of pulse remain as in Eqs.(10), (11). The amplitude of the tensile wave varies. σ_t takes the values: $-0.001\sigma_o$,$-0.01\sigma_o$,$-0.1\sigma_o$ r and - $1.0\sigma_o$. It is noteworthy that the role of the tensile wave in the damage process is more significant than that of compressive one. Moreover in the returning phase of the wave the roles of σ_c and τ_t are changed, $\sigma_t \rightarrow \sigma_c$ and $\sigma_c \rightarrow \sigma_t$. In the light of these remarks, the results plotted on Fig.13 are easily understood. The large peak of the damage near the borehole, in the case of $\sigma_t = 1.0\sigma_o$, is caused by the outward pulse. During the passage to the boundary this pulse becomes so weak (due to the created large damage), that the reflected one is unable to form a spall. For considerably smaller value of σ_t, the effect of the outward pulse is weak and the contribution of the returning one is more important.

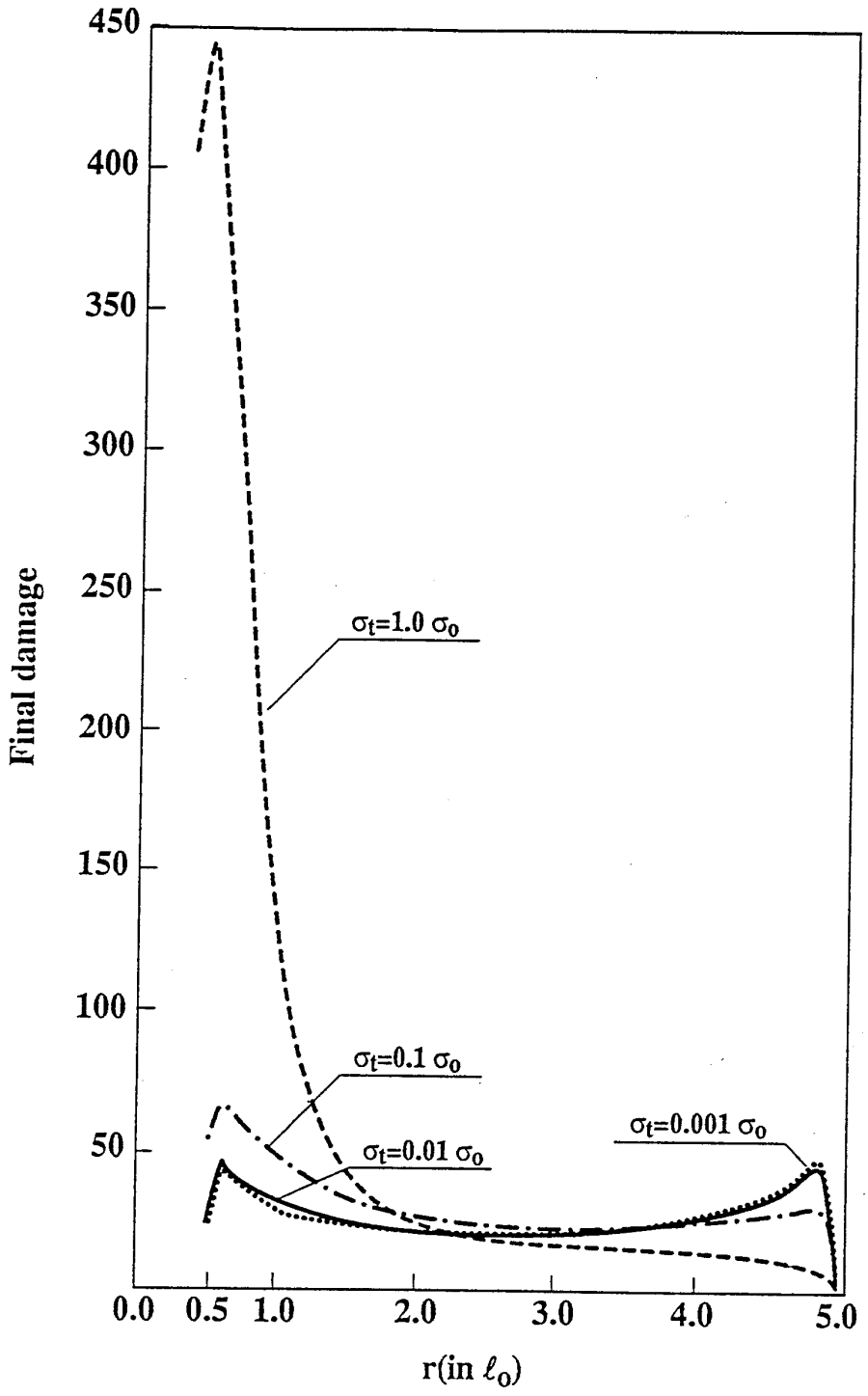

Fig. 13. Final damage for various σ_t values.

b) In the second case the values of the w_p, w_c, w_t remain as in (a). But here, σ_t is fixed and its value is $\sigma_t=0.01\sigma_o$. σ_c varies and takes the values: $\sigma_c=1.0\sigma_o$, $5.0\sigma_o$, $10.0\sigma_o$ and $20.0\sigma_o$. The obtained results are shown in Fig 14.

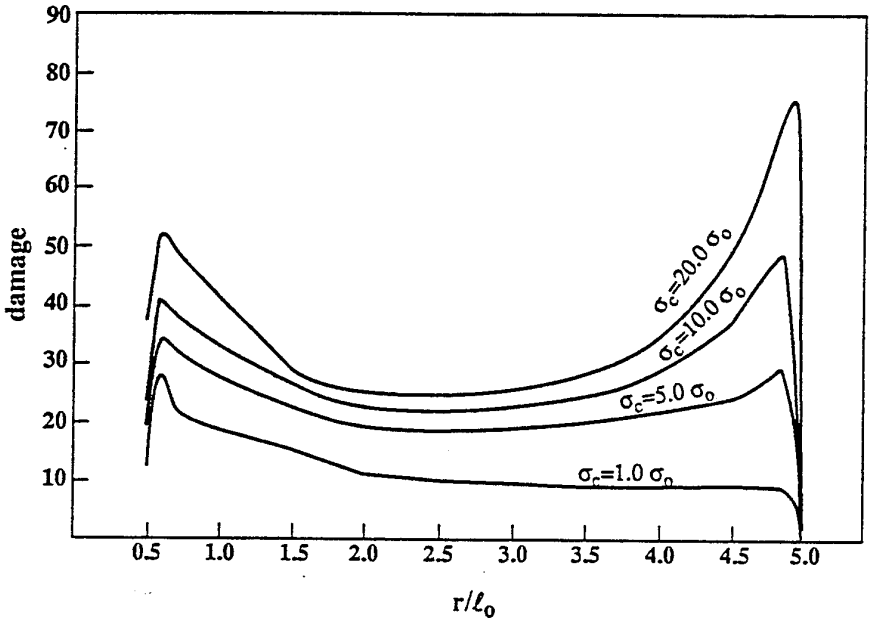

Fig. 14. Final damage for various σ_c values.

c) In this case the parameters σ_c, σ_t, w_c / w_p and w_t / w_p are kept fixed and their values are as in Eqs (10) and (11). The parameter τ_p, the pulse time, varies. Note that since the pulse velocity is constant, the pulse length varies accordingly with τ_p values, $w_p=0.5\,\ell_o$, $1.0\ell_o$ and $2.0\ell_o$. For larges τ_p both τ_c and τ_t are large, which explains the results given in Fig.15.

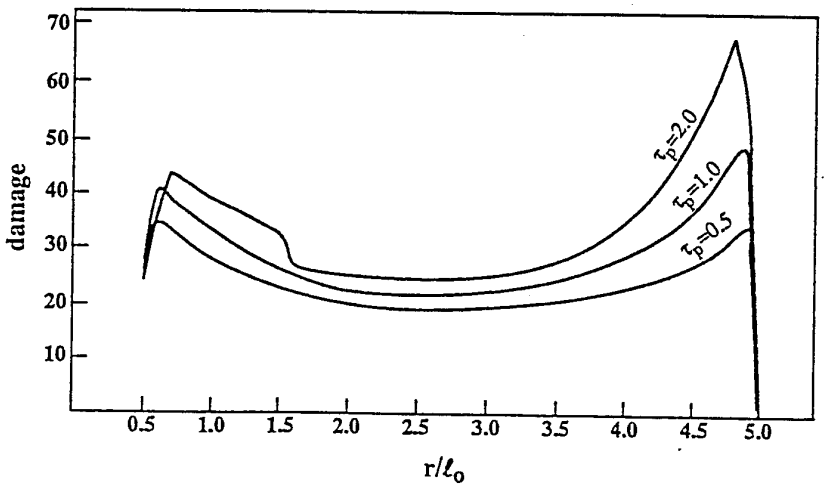

Fig. 15. Final damage for various wave length.

From the results of the cases (a) and (b) it may be concluded, that the ratio σ_c/σ_t plays an important role in the spall - formation. As was observed in our computations for spalling, this ratio should be sufficiently large, $\sigma_c / \sigma_t > 100$. It is clear, that the values σ_c / σ_t, which cause spalling depend on other parameters, especially on γ_t (crack growth) and δ (attenuation). On the basis of our computational experience, we found that even though $\sigma_c / \sigma_t < 100$ a large enough γ_t creates a spall. Same questions remain still open, such as whether there exist a value - range of σ_c / σ_t generating a spall ? Whether there exists an optimal value of σ_c / σ_t , for which the spall peak attains a maximum? In order to find answers, additional work should be performed. Similarly, it is anticipated, that there exists an optimal pulse length, for which the spall peak achieves a maximum.

7. Effect of the Attenuation Factor Value on the Final Damage

The attenuation constant δ, which appears in Eq (6), plays a remarkable role in decreasing of the pressure, $\sigma(r,t)$, during the pulse passage over the sample. The factor δ, characterizes a material property. It is important to examine its effect on the final damage.

In this section all parameters, except δ, have the values given by Eqs.(10) and (11).

First, we examine the effect of various δ values on the radial distribution of the final damage. The computations were performed for two samples having $R_0 = 3.0\,\ell_0$ and $R_0 = 5.0\ell_0$. For both samples $a_0 = 0.5\ell_0$. In the case of $R_0 = 3.0\ell_0$, δ is given the values: 75.0, 175.0, 250.0, 1000.0, 10000.0. In the limiting case, $\delta \rightarrow \infty$: $F(r) \rightarrow 1/r$. See Eq. (6). For $R_0 = 5.0\ell_0$, δ is given the values: 2.0, 10.0, 50.0, 200.0 and 2000.0. Furthermore, the limit case, $F(r) = 1/r$, is also considered. The results obtained for both two cases are similar and therefore only the one, for, $R_0 = 3.0\ell_0$ are depicted in Fig.16.

The damage near the sample center rises, as the δ value grows. For sufficiently large δ, the damage decreases quickly as a function of the position and the spall does not exist. To understand these results, we note that the function F(r) increases with δ (See Eq. (6)). Therefore for larger δ, the pulse is only weakly attenuated near the borehole.

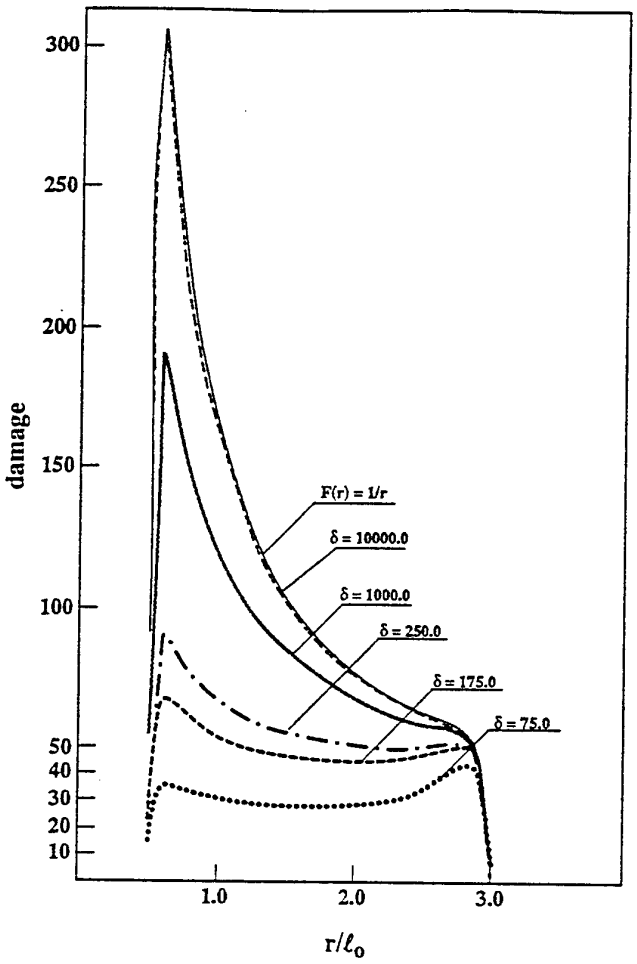

Fig. 16. Effect of δ value on final damage.

Now we shall examine, what are the relations beween the inner damage width, the spall width, the extent of the initial damage region and the value of the δ parameter. δ will be varied and all other parameters will be kept fixed at the values given by Egs.(10), (11). Three sample sizes were considered, $R_o = 5.0\ell_o$, $3.0\ell_o$ and $R_o = 8.5\ell_o$. The case of $R_o = 5.0\ell_o$ will only be discussed in detail, because the results obtained for other values of R_o are similar.

To estimate the influence of the initial damage, the parameter α takes the values 2.0, 1.0 and 0.1. The results for α=1.0 are ploted in Fig.17, where three curves, are drawn. Curve (a) gives extents of initial damage regions. On the curve (a') are shown the cases, for which a spall does not exist. On curve (a'') the case with spall. Curve (b) gives extents of the inner damage zones and curve (c) the spall widths. For example, for δ=4.5 the extent of D_o region is $0.45\ \ell_o$(A), the width of spall is $1.25\ \ell_o$ (B) and of inner damage is $2.8\ \ell_o$(C). The sum of these extents is $4.5\ \ell_o$. Note: $R_o - a_o = 4.5$. For $0 < \delta \leq 4.75$ the inner damage zone and the region of the initial damage are observed. The spall

exists only for $3.65<\delta\leq 4.75$. For $\delta=4.75$ the extent of the initial damage region is equal to zero. The inner damage zone and spall zone are coupled and their widths achieve a maximum. The damage distribution for this situation may be sketched as in Fig. 18.

For $\delta>4.75$ the damage at any point r of the sample is greater than the initial one, and its behavior was discussed at the beginning of this section. Another interesting point is the limit, $\delta\rightarrow o$. Then $F(r)\rightarrow 0$, see Eq.(6), and the pulse is inactive .

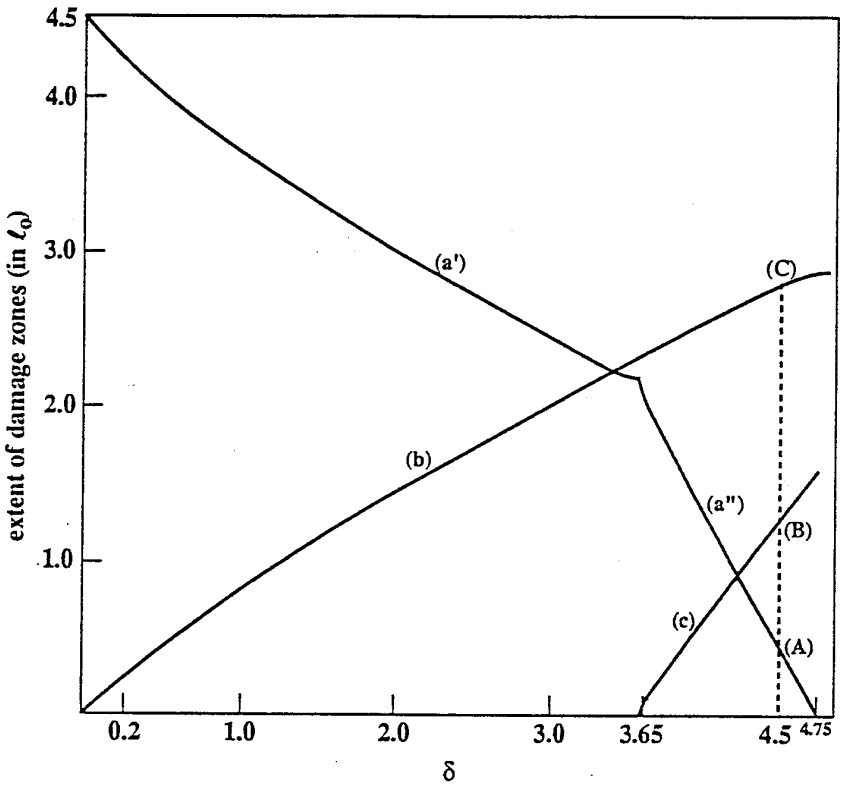

Fig. 17. Extent of damage zones as a function of δ value for $\alpha=1.0$.

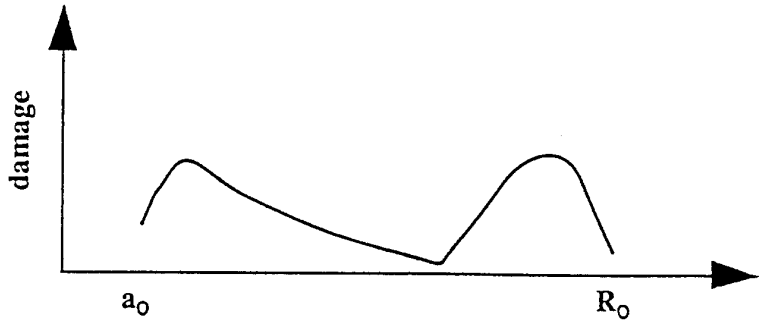

Fig. 18.

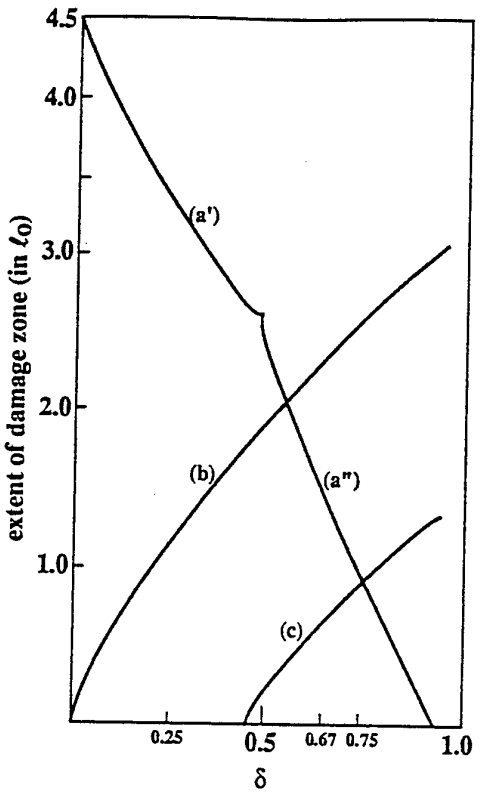

Fig.19. Extent of damage zones as a function of δ value, for α=0.1. The interpretation of curves (a), (b) and (c) is as in Fig. 17.

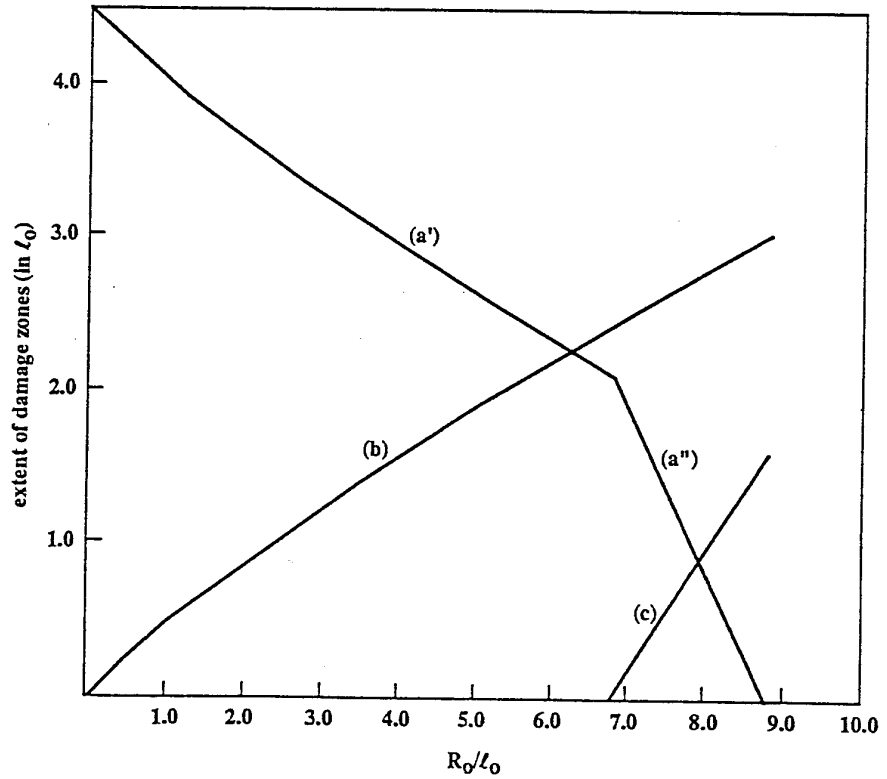

Fig.20. Extent of damage zones as a function of δ values for α = 2.0 . The interpretation of curves(a), (b) and (c) is as in Fig. 17.

At last we should note, that the curves on Fig.17 are approximately straight lines. This fact is remarkable, because our transport equation (see Sec.2) is not linear and the δ parameter is included in an exponential term.

On Figs.19 and 20 the results for α=0.1 and α=2.0 are given. They indicate, that the value of δ, for which a spall exists, increase, as α grows. Similar results are obtained for $R_o=3.0\ell_o$ and $R_o=8.5\ell_o$.

Additional results shown in Fig.21 are worthy of note. Each curve in this figure presents a scaling relation between those values of α and δ, that causes a spall of given width. The curves on Fig.21 refer to the spall width equal to $0.2\ell_o$, $0.5\ell_o$, $1.0\ell_o$ and $1.2\ell_o$ for sample size $R_o=5.0\ell_o$ and $a_o=0.5\ell_o$. The relation is linear. Similar results are obtained for $R_o=3.0\ell_o$.

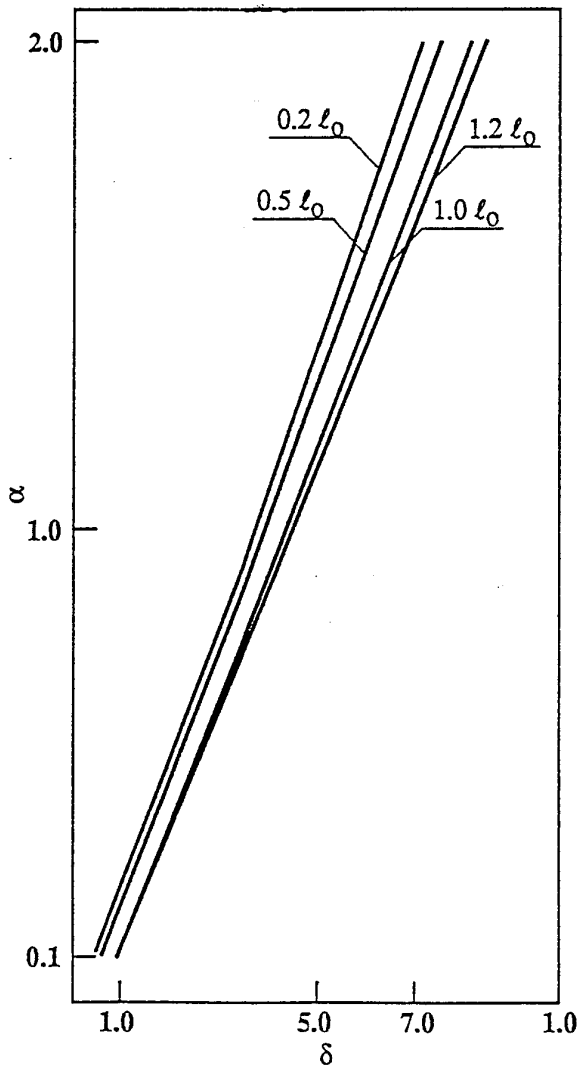

Fig. 21. Relation between α and δ for given spall widths, which are denoted on the curves.

8. Conclusions

The great number of graphical data in this article arises from the extensive computational work carried out throughout several years (on an IBM machine). Occasional repetitiveness is excused by the need to show that the results are systematic and what are the tendencies in the results.

The transport equation approach to crack population growth is only one of the possible treatments of a complicated stochastic problem: to us it appears neither less nor more justified than any other, and for a space and time-dependent description it may be uniquely workable. There are, admittedly, a great number of free parameters in the approach, whose values are not easily fixed in any concrete situation. Our aim was to elucidate the wide range of phenomena that can occur with some (not unphysical) choice of the parameters. Yet more parameters can be varied (as the crack velocity or introducing inhomogenity in the initial crack distribution).

Although the resultes presented in this paper are related to the samples defined in Secs. 3-7, it is possible to reach some conclusions, which seem to present the general behavior of damage systems.

(a) In a given sample, a pressure wave creates a spall zone, if the ratio σ_c/σ_t is larger than some threshold value.

(b) For a given pressure wave in a given medium, the damage peak in the spall zone increases for $R_o \leq R^*_o$ and decreases for $R_o \leq R^*_o$. For sufficiently large size of the sample R_o, the spall does not exist.(In the case of Sec.4, R^*_o=4.4)

(c) For a given pressure wave in a given medium, the damage peak and the width of the inner damage zone increases with the sample radius R_o. Both level off and became independent of the sample size for sufficiently large R_o. (See Sec.4)

(d) For a given pressure wave and sample size R_o, if $\alpha \geq \alpha^*$, where α^* is a sufficiently small number, the damage peak and the width of the inner damage zone and the spall region are independent of the α value. In the limit, as $\alpha \to 0$, the peak of the damage near the center reaches a minimal value, and the peak of the spall attains a maximal one. (See Sec.3)

(e) For a given pressure wave and sample size R_o, if $\alpha > \alpha^*$, where α^* is sufficiently large number, the spall zone does not exist. (See Sec.3)

(f) A pressure wave and a sample of radius R_o are given. For $\delta > \delta^*$, is a sufficiently large number, the spall zone does not exist and the damage peak of the inner damage zone increases with the δ value. In the limit, $\delta \to \infty$, the damage achieves a maximal value.

References

1. M. Lemanska, Z.Jaeger and R. Englman
Transport Treatment of Crack Population in Finite Medium , Annals of the Israel Physical Society, 8 (1986)

2. R.B. Stout and L.Thigpen , Modeling Microcrack Kinetics in Rocks , Report No. UCRL-83994(1980)

3. Davison, B., Neutron Transport Theory (Clarendon, Oxford 1957).

4. Carlson B.G., SN Method and the SNG Code, Report No. LAMS-2201(1959)

5. M.Lemanska and G.Szwarcbaum , SNG-TAC Code, Report No. IA-806(1963)